Homogeneous Test-bed for Cognitive Radio

ADNAN AHMAD CHEEMA

Homogeneous Test-bed for Cognitive Radio

by

Adnan Ahmad Cheema

2015

School of Engineering and Computing Sciences,

Durham University, UK

A thesis submitted for the degree of

Doctor of Philosophy

Abstract

In the current frequency allocation scheme, the radio spectrum is found to be heavily underutilized in time, frequency and space dimensions or any of their combination. To improve spectrum utilization, the unused contiguous or non-contiguous portion of the radio spectrum (spectrum hole) can be accessed opportunistically using cognitive radio technology provided it is interference free to the local users of the network.

To reliably detect the spectrum holes, which is necessary to limit the interference, cognitive radio is required to have high time and frequency resolutions to detect radio technologies (e.g. GSM 900, 2.4 GHz WLAN) at the packet level in the transmitted channel to avoid misinterpretation of occupancy states in time and frequency. In addition, having high sensitivity and instantaneous dynamic range can enable cognitive radio to detect weak received signals and their detection in the presence of strong received signals. Besides these requirements, a large sensing bandwidth can increase the chances to find spectrum holes in multiple radio technologies concurrently.

A chirp channel sounder receiver has been developed according to the aforementioned requirements with a bandwidth of 750 MHz to provide reliable detection of received signals in two frequency ranges; 1) 250 MHz to 1 GHz, 2) 2.2 GHz to 2.95 GHz. The developed receiver is capable of finding spectrum holes having a duration of 204.8 μs and a transmitted channel bandwidth up to 200 kHz. To explore the spectrum holes in the space dimensions, six chirp channel sounder receivers have been developed to form a homogeneous test-bed, which can be deployed and controlled independently.

To experimentally validate the ability of the built receiver, short term spectrum occupancy measurements have been conducted to monitor 2.4 GHz WLAN traffic from a real wireless network to quantify the spectrum utilization and duration of spectrum holes in the time domain. It has been found that the radio spectrum is underutilized and empirical distribution of the duration of the spectrum hole can be modelled using lognormal and gamma distributions for prediction using a two state continuous time semi-Markov model.

To experimentally validate the receiver's capabilities in both the supported frequency ranges, long term spectrum occupancy measurements with 750 MHz sensing bandwidth have been performed and received signals have been detected at frame or packet level to quantify spectrum utilization. It has been found that the radio spectrum is highly underutilized at the measurement location and exhibits significant amount of spectrum holes in both time and frequency.

To experimentally validate the functionalities of the homogeneous test-bed, short term spectrum occupancy have been performed to monitor 2.4 GHz WLAN traffic from a real wireless network. The experiment has been conducted using multiple receivers to quantify the amount of cooperation individual or multiple cognitive radio users can provide for reliable detection of spectrum holes in time, frequency and space. It has been found that the space dimension influences strongly the statistics of cooperation parameters.

Declaration

No part of the work described in this thesis has been submitted in support of an application for another degree or qualification to this or any other university or institute of learning.

Dedication

To my family, specially my life and science companion, *Fareena*

Acknowledgments

I would like to thank Professor Sana Salous for giving me the opportunity to work on this exciting research theme, guidance and providing financial support for this PhD.

I would like to thank Dr. Stuart Feeney for the design of analogue circuits, Nasouruddin for helping in the PCB design, Xavier for discussions and suggestions on different ideas relating cognitive radio, Odiri for giving updates on world politics and issues during lunch time, Francesco for discussions on triggering issues and Gao for always giving big smile. Last but not least, thanks for your long lasting friendship, cooperation and assistance during the measurement campaigns.

I would like to thank Ian, Neil and Colin from the electronics workshop and Colin from the mechanical workshop for their support during the hardware development.

I would like to thank the School of Engineering and Computing Sciences, Durham University, UK for providing partial financial support for this PhD.

In the end, I would like to thank my family for their support and constant encouragement to complete the voyage of discovery.

List of Abbreviation

CR	Cognitive Radio
IDR	Instantaneous Dynamic Range
UMTS	Universal Mobile Telecommunication system
TV	Television
TETRA	Terrestrial Trunked Radio
GSM	Global System for Mobile
WLAN	Wireless Local Area Network
LTE	Long Term Evolution
ISM	Industrial, Scientific and Medical
CIR	Channel Impulse Response
CRN	Cognitive Radio Network
FMCW	Frequency Modulated Continuous Wave
LOS	Line of Sight
PRBS	Pseudo Random Binary Sequence
SNR	Signal to Noise ratio
STDCC	Swept Time Delay Cross Correlation
SAW	Surface Acoustic Wave
FFT	Fast Fourier Transform
IF	Intermediate Frequency
CW	Continuous Wave
LO	Local Oscillator
ADC	Analog to Digital Converter
NI	National Instrument
USRP	Universal Software Radio Peripheral
VSA	Vector Signal Analyzer
BPF	Band Pass Filter

SA	Spectrum Analyzer
LPF	Low Pass Filter
PPS	Pulse per Second
GPS	Global Positioning System
DDS	Direct Digital Synthesiser
UC	UP-Converter
EMI	Electromagnetic Interference
IR	Integrated Receiver
LNA	Low Noise Amplifier
FPGA	Field Programmable Gate Array
SC	Signal Conditioning
PCB	Printed Circuit Board
PFI	Programmable Function Interface
NF	Noise Figure
SE	Sensing Engine
CDF	Cumulative Distributed Function
GP	Generalized Pareto Distribution
WB	Weibull Distribution
EX	Exponential Distribution
GM	Gamma Distribution
LN	Log Normal Distribution
KS	Kolmogorov Smirnov
RFID	Radio Frequency Identification
DC	Duty Cycle
RF	Radio Frequency
FG	Function Generator

Table of Contents

List of Figures

List of Tables

1 Introduction

1.1 Motivation and Objective

The ever growing demand of radio spectrum for emerging radio technologies is becoming a challenging task to accommodate in the current frequency allocation scheme. The emerging radio technologies [1, 2] are looking to have radio spectrum in order of few MHz to few GHz to meet consumer demands in cellular, local area, medical and public safety wireless networks. These wireless networks are aiming to provide services like high data rate, connectivity, quality of service, security and interoperability with the drive to improve the radio spectrum utilization in current and upcoming frequency allocation schemes.

Over the last decade, it is well studied that most of the allocated radio spectrum is underutilized [3-9]. To improve utilization, the unused portions of the radio spectrum (spectrum holes) can be reutilized by assigning to emerging radio technologies. However, to do this, reliable spectrum occupancy measurements are required to find the spectrum holes in time, frequency and space dimensions or any of their combination. Moreover, these measurements can be beneficial to model the occupancy of the radio spectrum and to define protocols for *"when and how"* the spectrum holes can be reutilized.

The cognitive radio (CR) is an intelligent radio which can learn from the environment and adapt its parameters to provide reliable communication links and improve the spectrum utilization [10]. Broadly speaking, a cognitive radio technology is capable of finding spectrum holes reliably in the current frequency allocation scheme and also can access them efficiently by adding limited interference to local users of the network.

The reliable detection of spectrum holes depends on both the measuring system [11] and the detection algorithm [12] used by the CR users. Particularly, for the measuring system, it depends on the following factors:

- Time resolution: The ability to separate two consecutive transitions in the occupancy state (busy/idle) in a frequency or channel in the time domain at a given

location. If the time resolution is lower than the minimum occupancy transitions time, the time occupancy can be underestimated.

- Frequency resolution: The ability to separate two adjacent frequencies or channels in the frequency domain. If the frequency resolution is lower than the channel bandwidth, the frequency occupancy can be overestimated.
- Sensitivity and instantaneous dynamic range: The sensitivity is the ability to detect weak signals while the instantaneous dynamic range (IDR) refers to detection of weak signals in the presence of strong signals. Lower values of sensitivity and IDR can lead to underestimation of occupancy states in both time and frequency.
- Bandwidth: The ability to detect continuous portions of the radio spectrum in a given time resolution. The higher bandwidth enables the detection of spectrum holes over a wide frequency range, which can be aggregated in frequency to obtain a higher bandwidth or the CR user can switch to a different frequency to avoid interference to local users of the network.

A measuring system based on the chirp channel sounder receiver, designed at Durham University, UK, was used to monitor the occupancy states of the universal mobile telecommunication system (UMTS) 2100 band [13]. However, the system has limited bandwidth (250 MHz) with fixed time resolution of 4 ms. Moreover, it can only operate in the UMTS 2100 band. The primary objectives of this thesis are:

- Develop a new chirp channel sounder receiver which will have at least double the bandwidth compared to the previous system and also can provide high time-frequency resolutions for reliable detection of occupancy states. Moreover, it should have a programmable bandwidth, time resolution and frequency resolution to detect different radio technologies like television (TV), terrestrial trunked radio (TETRA), global system for mobile (GSM) 900, 2.4 GHz wireless local area network (WLAN), Bluetooth and Long Term Evolution (LTE) 2600 signals at packet or frame level.
- Develop a homogeneous test-bed based on chirp channel sounder receivers to provide a distributed proof of concept and experimental setup in real wireless networks for CR users.

1.2 Contributions

This thesis presents the following contributions:

- A chirp channel sounder receiver is developed which has 750 MHz bandwidth and supports a minimum time and frequency resolutions of 204.8 μs and 200 kHz respectively for occupancy measurements in two frequency ranges: 1) 250 MHz to 1 GHz and 2) 2.2 GHz to 2.95 GHz.
- A total of six chirp channel sounder receivers for homogeneous test-bed are developed, which are independent and can be deployed at different locations for distributed or cooperative scenarios.
- High time and frequency resolution measurements are performed in the 2.4 GHz industrial, scientific and medical (ISM) band where 2.4 GHz WLAN signal is detected at the packet level based on the received power in an indoor environment. The occupancy data are analysed to find spectrum utilization and further modelled to predict the duration of occupancy state (idle) i.e. idle time window, which the CR users can use to access the 2.4 GHz WLAN signal in the time domain. It is found that the empirical lognormal and gamma distributions can also be used to model the idle time window for a continuous time semi-Markov model. Further to this, the effect of low time resolution on the statistic of idle time window is investigated. It is found that a drop in the time resolution tends to produce misleading statistics i.e. longer idle time windows due to the measuring system is inability to detect occupancy transitions. Radio spectrum access in the time domain based on these statistics will increase the interference to local users of the network.
- High time and frequency resolutions wideband measurements are performed for 24 hours to study the spectrum utilization in Durham city, UK in indoor and outdoor environments. The measuring system was configured to sense 750 MHz bandwidth in two supported frequency ranges i.e. 250 MHz to 1 GHz and 2.2 GHz to 2.95 GHz at frame and packet levels respectively. It is found that the radio spectrum is highly underutilized in both time and frequency at the measurement location. Moreover, these measurements provide a valuable database for high resolution occupancy states in both time and frequency for spectrum utilization modelling and prediction.
- High time and frequency resolutions distributed occupancy measurements are performed in the 2.4 GHz ISM band to detect 2.4 GHz WLAN signal at the packet

level based on the received power in an indoor environment. The occupancy data are analysed to find the amount of new occupancy state information a sensing node can provide to the individual user or CR users for network cooperation to avoid the hidden node problem. It is found that the space dimension influences strongly the amount of new occupancy state information.

1.3 Organisation of Thesis

Chapter 2 provides the background on radio propagation mechanisms and associate propagation effects are explained. In addition, an overview of wideband channel measurement techniques is provided and a proposed channel measurement technique is explained with design parameters.

Chapter 3 provides the implementation details of the chirp channel sounder receiver at both the hardware and software levels and its extension to six receivers for the development of a homogeneous test-bed. The performance of the system is investigated with design parameters.

Chapter 4 provides the high time and frequency resolution measurements conducted to investigate the spectrum utilization and methods to access the spectrum holes in the time domain. Moreover, distributed high time and frequency resolution measurements are conducted and occupancy data are analysed for achievable network cooperation among CR users to avoid the hidden node problem in an indoor environment.

Chapter 5 summarizes the developed hardware, experiments and main outcomes of this thesis. In the end, future improvements in hardware and possible investigation required in occupancy data, collected as part of this project, are highlighted.

1.4 References

[1] W. Jianfeng, M. Ghosh, and K. Challapali, "Emerging cognitive radio applications: A survey," *Communications Magazine, IEEE,* vol. 49, pp. 74-81, 2011.

[2] T. S. Rappaport, S. Shu, R. Mayzus, Z. Hang, Y. Azar, K. Wang, *et al.*, "Millimeter Wave Mobile Communications for 5G Cellular: It Will Work!," *Access, IEEE,* vol. 1, pp. 335-349, 2013.

[3] M. H. Islam, C. L. Koh, O. Ser Wah, Q. Xianming, Y. Y. Lai, W. Cavin, *et al.*, "Spectrum Survey in Singapore: Occupancy Measurements and Analyses," in *Cognitive Radio Oriented Wireless Networks and Communications, 2008. CrownCom 2008. 3rd International Conference on*, 2008, pp. 1-7.

[4] T. Harrold, R. Cepeda, and M. Beach, "Long-term measurements of spectrum occupancy characteristics," in *New Frontiers in Dynamic Spectrum Access Networks (DySPAN), 2011 IEEE Symposium on*, 2011, pp. 83-89.

[5] J. Xue, Z. Feng, and P. Zhang, "Spectrum Occupancy Measurements and Analysis in Beijing," *IERI Procedia*, vol. 4, pp. 295-302, 2013.

[6] K. A. Qaraqe, H. Celebi, M. S. Alouini, A. El-Saigh, L. Abuhantash, M. M. Al-Mulla, *et al.*, "Measurement Analysis of Wideband Spectrum Utilization in Indoor Outdoor Environments," presented at the International Conference on Communications Technologies (ICCT 2010), 2010.

[7] M. Wellens, J. Wu, and P. Mahonen, "Evaluation of Spectrum Occupancy in Indoor and Outdoor Scenario in the Context of Cognitive Radio," in *Cognitive Radio Oriented Wireless Networks and Communications, 2007. CrownCom 2007. 2nd International Conference on*, 2007, pp. 420-427.

[8] M. Lopez-Benitez, A. Umbert, and F. Casadevall, "Evaluation of Spectrum Occupancy in Spain for Cognitive Radio Applications," in *Vehicular Technology Conference, 2009. VTC Spring 2009. IEEE 69th*, 2009, pp. 1-5.

[9] R. I. C. Chiang, G. B. Rowe, and K. W. Sowerby, "A Quantitative Analysis of Spectral Occupancy Measurements for Cognitive Radio," in *Vehicular Technology Conference, 2007. VTC2007-Spring. IEEE 65th*, 2007, pp. 3016-3020.

[10] S. Haykin, "Cognitive radio: brain-empowered wireless communications," *Selected Areas in Communications, IEEE Journal on,* vol. 23, pp. 201-220, 2005.

[11] D. Finn, J. C. Tallon, L. A. DaSilva, P. V. Wesemael, S. Pollin, W. Liu, *et al.*, "Experimental assessment of tradeoffs among spectrumsensing platforms," presented at the Proceedings of the 6th ACM international workshop on Wireless network testbeds, experimental evaluation and characterization, Las Vegas, Nevada, USA, 2011.

[12] T. Yucek and H. Arslan, "A survey of spectrum sensing algorithms for cognitive radio applications," *Communications Surveys & Tutorials, IEEE,* vol. 11, pp. 116-130, 2009.

[13] S. Salous, "Chirp sounder measurements for broadband wireless networks and cognitive radio," in *Communication Systems Networks and Digital Signal Processing (CSNDSP), 2010 7th International Symposium on*, 2010, pp. 846-851.

2 Radio Channel Wideband Measurement Techniques

This chapter provides a short introduction to the radio propagation channel, associated propagation effects and wideband measurement techniques. The wideband radio channel measurement techniques are explained and categorized into two types: 1) active, where the complex channel impulse response (CIR) is measured for radio channel characterization and modelling, 2) passive, where the received power is measured to find the occupancy state of the radio channel in time and frequency at any given location for applications in cognitive radio networks (CRN).

Primary focus is given to linear frequency modulated continuous wave (FMCW) based channel measurement techniques and their working principles are explained to perform both active and passive measurements. In the end, design parameters for the proposed measuring system, which will be based on linear FMCW, are listed particularly for CRN.

2.1 Radio Propagation Channel

The radio propagation channel provides a link between the transmitter and receiver antennas for the transfer of information with the cost of propagation impairments. These impairments can be studied by classifying the radio propagation mechanisms into two types [1]:

- Free space propagation
- Terrestrial propagation

In free space propagation, the transmitter and receiver antennas have non-obstructed or line of sight (LOS) link e.g. satellite or microwave links, where the received power changes as a function of their relative distance. The drop in received power is inversely proportional to the square of their relative distance and formally known as the free space path loss.

In terrestrial propagation, the transmitted signal can experience effects like obstruction, reflection from smooth surfaces, scattering from rough surfaces and diffraction around the obstructed object due to buildings, terrain, vehicles etc. Due to

these effects or any of their combination, multiple echoes of the transmitted signals having different values of amplitude, time delay and frequency (Doppler) can arrive at the receiver's antenna. These variations in the received power depend on three factors: 1) path loss due to relative distance between the transmitter and receiver antennas and locations, 2) shadowing due to obstructions when single or multiple echoes experience power absorption, and 3) multiple echoes due to their constructive or destructive self-interference. Factors 1 and 2 are generally referred to as large scale propagation effects while factor 3 is referred to as small scale propagation effects.

The large scale and small scale propagation effects produce randomness in the received power due to which it is possible that a CR cannot detect a local user of the network reliably. This phenomena is known as the hidden node problem [2]. Figure 2.1 shows an illustration of the hidden node problem where four CR users are used to detect the transmission of a local user of the network. CR user "1" can reliably detect the local user due to having LOS link. While, CR user "2" cannot detect the local user due to shadowing effect and can always consider the local user in the idle occupancy state. CR user "3" has received two echoes and in the case when both echoes have destructive self-interference, it can lead to strong attenuation due to which reliable detection of the local user is not possible. Another possibility is that path loss can also lead to the hidden node problem if the CR user (e.g. "4") is outside of the transmission region of the local user.

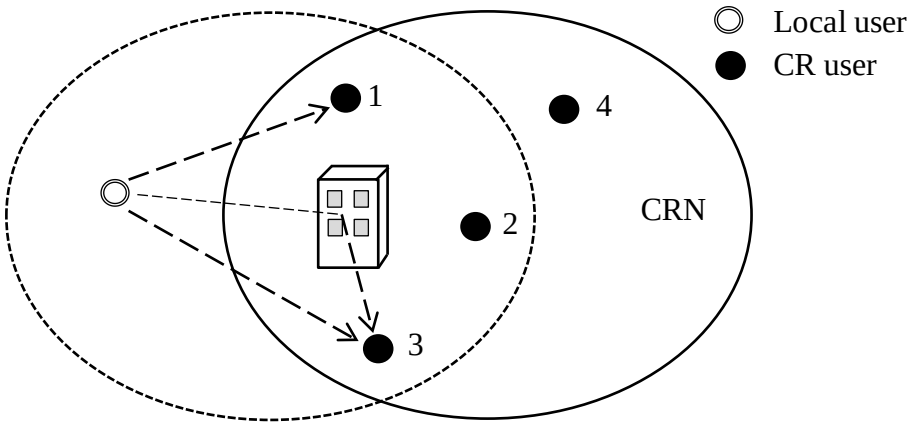

Figure 2.1 Hidden node problem in CRN

In order to study propagation effects, the radio channel can be estimated using two types of measurement techniques:

- Active
- Passive

In active measurement techniques, the radio channel is excited or sounded using a known signal and then variations in amplitude and phase are observed at the receiver to estimate the complex CIR, which can be further utilized to characterize and model the radio propagation channel. In addition in this technique, the location of transmitter and receiver are known and predefined. While in case of passive measurement techniques, the receiver at any given location is used to measure the received power of a transmitter or transmitters, which are transmitting from unknown locations, in order to quantify the occupancy state of the signal in time and frequency dimensions. By having knowledge of signal occupancy state at any given location, the spectrum holes can be reassigned in the time and frequency domains for applications in CRN. This will help to increase the spectrum utilization and will allow accommodating the emerging applications in CRN. The details of wideband active and passive measurement techniques are given in the following two sections.

2.2 Active Wideband Measurement Techniques

2.2.1 Pulse Technique

A high power short duration pulse with the duration of T_p is transmitted to excite the radio channel and which get convolved with the response of radio propagation channel as shown in figure 2.2. At the receiver, the amplitude of the response can be obtained by using the envelop detection method. However, to get phase variations in echoes for Doppler information, the received signal can be detected using quadrature detection.

The duration of T_p defines the time delay resolution i.e. the minimum time required to separate two consecutive echoes, and by reducing the pulse duration a higher value of time delay resolution can be obtained. To observe the time variant behaviour of the radio channel, the pulse can be transmitted periodically. However, careful consideration is required to select a suitable time period (T). The value of

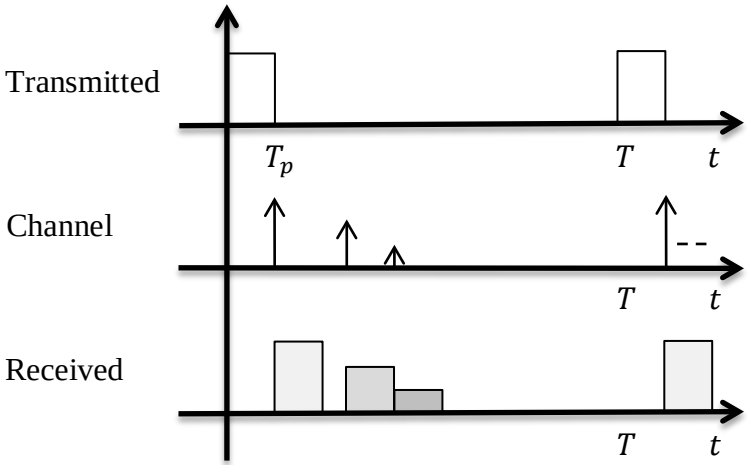

Figure 2.2 Principle of pulse technique

time period depends on the time delay spread of the CIR which is normally selected to accommodate the last arriving echo. Moreover, short time periods can be used to capture fast variations in CIR with measurable Doppler shift up to $\pm\frac{1}{2T}$. In [3, 4], a short duration pulse (0.5-10 ns) is used for channel measurements in the 2.4 GHz and 60 GHz bands respectively with a time period of 500 ns. In [5], a long duration pulse (500 ns) with time period of 100 µs is used for channel measurements at 450 MHz.

Although the implementation of pulse based channel estimation technique is simple however it requires high peak to average power ratio to obtain high time delay resolution as the required peak power is inversely proportional to pulse duration. Moreover, for high time delay resolution, the receiver is required to have wideband band pass filter (BPF), whose bandwidth is inversely proportional to the pulse duration, which makes it vulnerable to interference from other channel users or transmissions.

2.2.2 Pulse Compression Techniques

The high peak to average power ratio problem in the pulse based technique can be solved by increasing the duration of the pulse. However, by doing this, the time delay resolution will drop. To increase the resolution, the bandwidth of long duration pulse can be increased by modulating it in phase or frequency. This method is formally known as pulse compression. The pseudo random binary sequence (PRBS) is normally used for phase modulation and linear FMCW signal is widely used for frequency modulation.

At the receiver, the complex CIR can be obtained by two types of quadrature detectors which maximize the received signal to noise ratio (SNR) [6]: 1) matched filter detector and 2) correlation detector. In the matched filter detector, the received signal is convolved with a time reversed copy of the transmitted signal in order to get CIR. While in the correlation detector, the correlation is performed between the received signal and a copy of the transmitted signal at the receiver to get the amplitude and phase associated with an echo. In the PRBS technique, to detect multiple echoes, a parallel architecture can be employed where multiple time-delayed correlation detectors can be used to get the complex CIR. An improved practical method which eliminates the requirements for extra hardware and complexity for the parallel architecture is proposed in [7], where a single correlation detector is used and shifted across the time delay range to detect multiple echoes, formally known as swept time delay cross correlation (STDCC) detector.

The bit duration (T_b) of PBRS signal defines the time delay resolution and its duration (number of bits × T_b) or time period (T) limit the measurable range of delay spread of the complex CIR. A surface acoustic wave (SAW) matched filter based quadrature detector is used in [8, 9] where 127 bits long PRBS signal is transmitted to characterize the radio channel at 436.5 MHz with bit duration of 0.078 µs. The quadrature STDCC detector is used in [7, 10, 11] to characterize the radio channel at 910 MHz, 2 GHz, 5 GHz and 60 GHz bands where a time delay resolution of 0.1 µs, 0.01 µs, 0.01 µs and 0.0003 µs is obtained respectively.

The bandwidth of linear FMCW defines the time delay resolution while the time period or sweep time limits the measureable delay spread of the complex CIR. At the receiver, a correlation detector is used with a Fast Fourier Transform (FFT) algorithm to get the complex CIR [12]. The details of channel measurement techniques based on linear FMCW signal will be given in section 2.4. In both, PBRS and linear FMCW pulse compression techniques the Doppler shift is same as for the pulse based technique.

2.3 Passive Wideband Measurement Techniques

2.3.1 Homodyne Technique

In the homodyne technique, the received signal with bandwidth *B* is directly down converted to DC or zero intermediate frequency (IF) by mixing it with a

continuous wave (CW) local oscillator (LO) [13]. The down converted signal is digitized using an analog to digital converter (ADC) and further processed using the FFT algorithm to compute the received power over the sensed bandwidth. The frequency resolution (minimum frequency difference to separate two frequency components) is equal to the FFT bin size and time resolution is defined as the sum of time required to down convert the signal in observation and FFT processing time. Figure 2.3 shows the graphical representation of the homodyne technique where a received signal with bandwidth B centred at f_c is down converted to zero IF using CW LO.

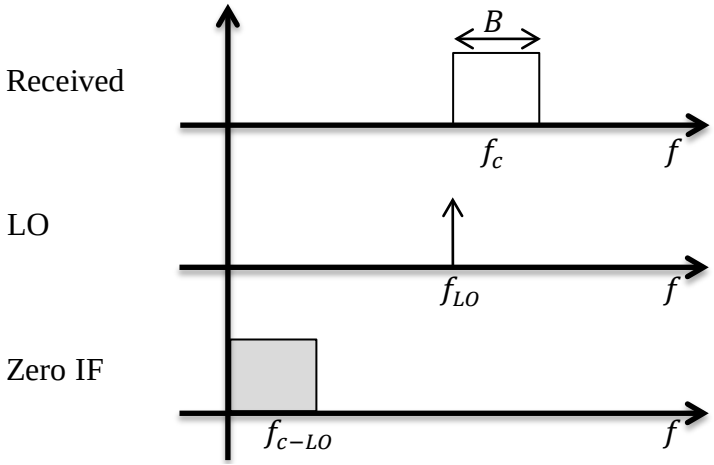

Figure 2.3 Principle of homodyne technique

The homodyne technique is mostly used by commercial measuring systems like vector signal analyzer, real time spectrum analyzer and national instrument (NI) universal software radio peripheral (USRP) [14]. These systems offer high time resolution however have limited bandwidth. Moreover, as in this technique, the sampling frequency is required to be at least double of B, which make them difficult to design for wideband applications [15]. For example, for 750 MHz sensed bandwidth, the sampling frequency is required to be at least 1.5 GHz for digitization.

In [16] spectrum occupancy measurements are taken over 24 hours using NI USRP and NI vector signal analyzer (VSA) in the 2.4 GHz ISM band. Different radio technologies (TV, TETRA, GSM 900, DCS 1800, UMTS 2100) are monitored individually over the duration of 20 minutes using NI USRP to quantify the spectrum occupancy and to predict the occupancy state [17]. Table 2.1 summarizes the time-frequency configuration parameters for both measurements where it can be observed

that the measuring systems are narrowband. In order to perform wideband measurements either multiple systems are required or the frequency of the LO can be changed in real time [18]. However, for wideband measurements, usage of multiple systems is not a cost effective solution and also requires high precision time synchronization among all if concurrent monitoring of all the bands is required. In addition, with a change in the LO's frequency, concurrent occupancy monitoring is not feasible and also increases the time resolution in proportion to the number of times a frequency is changed in the LO.

Table 2.1 Comparison of different configurations based on the homodyne technique

Ref.	Frequency Range (MHz)	Sensed Bandwidth (MHz)	Time Resolution (ms)	Frequency Resolution (kHz)	Platform
[16]	2400-2480	20	500	50	NI USRP
	2400-2480	50	30	50	NI VSA
[17]	Variable	Variable	0.128	Variable	NI USRP

2.3.2 Heterodyne Technique

Instead of using a CW LO, a swept LO is used to down convert the received signal with bandwidth *B* to low IF in the heterodyne technique [13]. The low IF signal is further passed through an IF BPF to obtain the required frequency resolution and then an envelope detector is used to get the received power over the sensed bandwidth. In this technique, the time resolution is equivalent to the time required to sweep the sensed bandwidth, alternatively it is also known as sweep time.

The heterodyne technique is widely used in spectrum analysers. Although a spectrum analyzer (SA) requires low sampling frequency for digitization of the low IF signal it has low time resolution [15]. Figure 2.4 shows the principle of the heterodyne technique used in SA where multiple IF stages are used for down conversion [19].

Table 2.2 provides a comparison of different configuration parameters for various occupancy measurements conducted around the globe where a SA is used to measure the received power to quantify spectrum utilization in indoor and outdoor environments. Although a SA can provide large sensed bandwidth, however it has low time resolution.

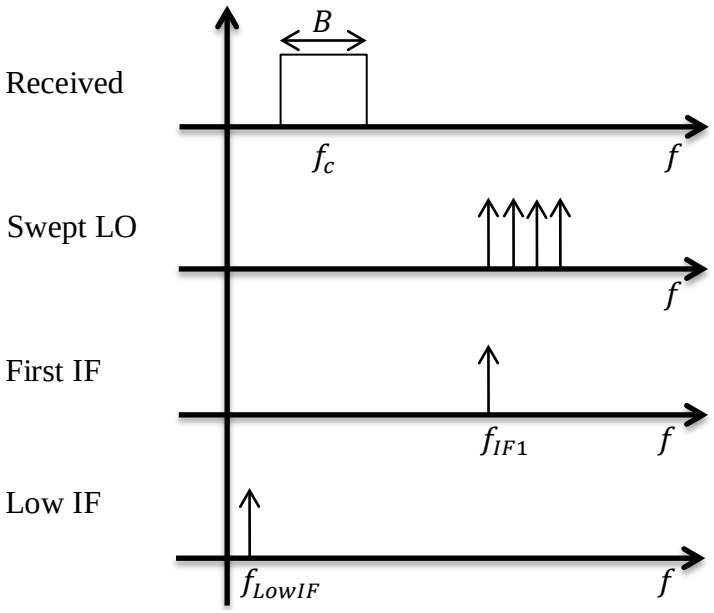

Figure 2.4 Principle of heterodyne technique in spectrum analyzer

Table 2.2 Comparison of different configurations based on the heterodyne technique

Ref.	Frequency Range (MHz)	Sensed Bandwidth (MHz)	Time Resolution (s)	Frequency Resolution (kHz)	Duration (Day)
[20]	80-5850	60	828	150	12
[21]	300-4900	20	360	300	153
[22]	450-2700	Variable	0.42	15/100/200	1
[23]	700-3000	2300	0.128	300	3
[24]	770-5250	1500	1	200	7
[25]	75-3000	500	12.5-15	10	2

The homodyne and super heterodyne techniques are used to get the received power of the signal. However, to find the occupancy in time and frequency at any given location, the received power is further processed using energy detection algorithm [26]. In this technique, the received power is compared with a decision threshold to find binary occupancy decision of signals, according to the following piecewise defined function as given in equation 2.1:

$$D_{t,f,l} = \begin{cases} 1, & P_{t,f,l} > decision\ threshold \\ 0, & otherwise \end{cases} \qquad \text{Equation 2.1}$$

where $P_{t,f,l}$ denotes the received power and $D_{t,f,l}$ denotes the binary occupancy decision at measurement time t, frequency f and location l. A signal is considered to be in the busy state i.e. $D_{t,f,l} = 1$, if the received power is higher than the decision threshold and otherwise is considered in the idle state.

2.4 Linear FMCW Technique

In active measurements, a linear FMCW signal or chirp signal with time resolution T and bandwidth B is transmitted to excite the radio channel. The received echoes are detected using a correlation detector by performing first heterodyne detection, where the received echoes are mixed with a locally generated reference chirp signal, and then by passing through a low pass filter (LPF) [6]. The filtered baseband signal is a composite signal which contains multiple sinusoids having different frequencies, phases and amplitudes. In the composite signal, the frequency of each echo is proportional to the time delay (τ) associated between the transmitter and receiver relative distance and can be computed using equation 2.2

$$f_k = \tau_k \left(\frac{B}{T}\right), k = 1, 2, 3, \ldots \qquad \text{Equation 2.2}$$

where f_k and τ_k are the frequency and time delay of the k^{th} echo. The filtered composite signal is digitized and stored for offline processing. The amplitude and Doppler information associated with each echo from the stored data can be found using the double FFT processing technique [12]. In addition, it is also important to note that a combination of correlation detection and double FFT processing for a chirp signal based channel sounding can provide complex CIR and hence does not require extra hardware to implement a quadrature detector as required by pulse or PRBS based techniques. Figure 2.5 shows the received echoes in time and frequency which are mixed with a reference chirp signal (LO) to get a composite beat note signal and then the FFT is applied to get the relevant time delay for each echo.

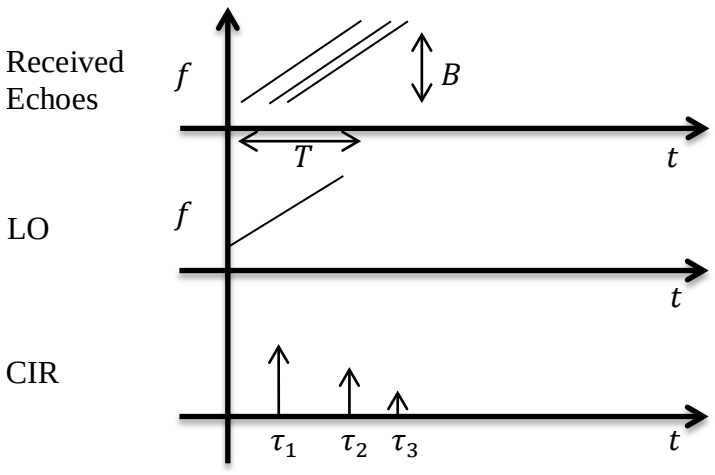

Figure 2.5 Principle of echo detection using chirp signal

In case of passive measurements, the received signal is mixed with a locally generated linear chirp signal and passed through a LPF to get a low IF signal and digitized for further offline processing. Generally, this LPF is very wide on the order of a few MHz, which is set in accordance to the highest detectable frequency in the beat note signal for active channel measurements. To get narrow frequency resolution for passive measurements, more filtering is required which can be achieved by applying digital filters during offline processing. Further to this, a Hilbert transform is used to get the envelope of the received signal and used to compute the received power over the sensed bandwidth. Figure 2.6 shows the graphical illustration of the down conversion process using a chirp signal.

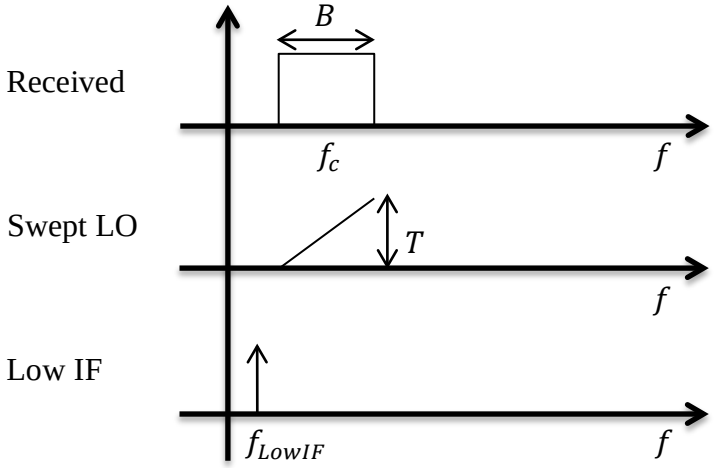

Figure 2.6 Principle of down conversion using chirp signal

For active measurements, a dual band chirp channel sounder is implemented in [27], which is used to characterize the radio channel in the UMTS 2100 uplink and downlinks bands. This sounder was further modified by adding eight parallel radio frequency (RF) chains in the receiver to characterize the radio channel in the angular dimensions [28]. In [29], a new chirp sounder was designed to characterize the radio channel in three bands simultaneously: 1) 2.5 GHz, 2) 3.4 GHz and 3) 5.7 GHz. Further to this, the sounding system was extended to the 60 GHz band. As, the primary function of the chirp channel sounder is to find the complex CIR, which can provide a knowledge base for radio channel characterization and modelling, limited amount of passive measurements have been performed using the chirp channel sounder receiver. In [30], the chirp channel sounder receiver presented in [28] is used to characterize the spectrum occupancy of the UMTS 2100 downlink band using

eight directional antennas for very short duration (400 ms). Table 2.3 summarizes the parameters of the aforementioned developed chirp channel sounders over the last decade.

Table 2.3 Summary of different chirp channel sounders

Ref.	Frequency Range (GHz)	Bandwidth (MHz)	Time Resolution (ms)	RF Chain (Tx/Rx)	Measurement Type
[27]	1.92-1.98	60	4	1/1	Active
	2.11-2.17	60	4	1/1	Active
[28]	1.92-1.98	60	4	1/8	Active/Passive
	2.11-2.17	60	4	1/8	Active/Passive
[29]	2.37-2.63	260	4	1/1	Active
	3.27-3.53	260	4	1/1	Active
	5.54-5.80	260	4	1/4	Active
	59.48-60.52	1040	4	1/1	Active

2.5 Proposed Channel Measurement Technique and Design Parameters

The chirp signal based channel measurement technique is chosen to develop a new wideband chirp channel sounder which will provide higher time and frequency resolutions compared to the previous sounding system developed at Durham University, UK [27-29]. It will also provide a base for extension in the mm-wave band for future work. The emphasis in this section is limited to its passive mode of operation for CRN and relevant design parameters are highlighted.

2.5.1 Time Resolution

Generally, higher values of time resolution are required to detect a signal at the packet or frame level based on the received power. The suitable choice of time resolution value depends on the specification of radio technology under observation. For instance, the 2.4 GHz WLAN signals are short in duration and have packet duration on the order of a few 100 μs so for reliable detection of packets, the time resolution is required to have less than or equal to a minimum acceptable packet duration. In case of low time resolution, the transmission packets or occupancy state (busy/idle) which are less than the time resolution cannot be detected and can lead to underestimation of the occupancy states.

2.5.2 Frequency Resolution

In the observation band, the frequency resolution depends on the minimum channel bandwidth of available radio technologies. For instance, the GSM 900 channel bandwidth is 200 kHz wide so for reliable detection of occupancy states in all channels, the frequency resolution is required to be less than or equal to 200 kHz. The lower frequency resolution compared to the channel bandwidth of radio technologies tends to lead to overestimation of the occupancy state since the signal is detected in one channel, it will be considered to be detected over the whole bandwidth of the frequency resolution.

2.5.3 Sensitivity and IDR

The sensitivity of measuring system is defined as the minimum detected received power which can be distinguished from the thermal noise floor with a desirable margin of SNR. A low value of sensitivity is required for reliable detection of weak transmissions which are due to propagation effects between the transmitter or transmitters and the measuring system.

The IDR is defined as the difference between the strongest and weakest received signal power. Mostly, in the case of wideband, this parameter is more of a concern as different radio technologies may experience different propagation effects and so may have high to low received power values. The highest value of IDR is required for reliable detection of weak signals in the presence of strong signals.

2.5.4 Bandwidth

The sensing bandwidth is the continuous portion of frequencies which are down converted to low IF for digitization. The high bandwidth of the measuring system is essential to observe occupancy states in different radio technologies which can enable the CR user to find spectrum holes in time and frequency.

2.6 Summary

Wideband radio channel measurement techniques are categorized into active and passive according to their mode of operation. The concept and principle of each wideband channel measurement technique is briefly discussed. The design parameters and requirements are listed for the proposed system based on linear FMCW signal particularly for passive channel measurements.

2.7 References

[1] S. Haykin and M. Moher, *Modern Wireless Communication*: Prentice-Hall, Inc., 2004.

[2] A. F. Molisch, L. J. Greenstein, and M. Shafi, "Propagation Issues for Cognitive Radio," *Proceedings of the IEEE*, vol. 97, pp. 787-804, 2009.

[3] K. Seong-Cheol, H. L. Bertoni, and M. Stern, "Pulse propagation characteristics at 2.4 GHz inside buildings," *Vehicular Technology, IEEE Transactions on*, vol. 45, pp. 579-592, 1996.

[4] N. Moraitis and P. Constantinou, "Measurements and characterization of wideband indoor radio channel at 60 GHz," *Wireless Communications, IEEE Transactions on*, vol. 5, pp. 880-889, 2006.

[5] W. R. Young, Jr. and L. Y. Lacy, "Echoes in Transmission at 450 Megacycles from Land-to-Car Radio Units," *Proceedings of the IRE*, vol. 38, pp. 255-258, 1950.

[6] S. Salous, *Radio Propagation Measurement and Channel Modelling*, 2013.

[7] D. Cox, "Delay Doppler characteristics of multipath propagation at 910 MHz in a suburban mobile radio environment," *Antennas and Propagation, IEEE Transactions on*, vol. 20, pp. 625-635, 1972.

[8] J. D. Parsons and A. S. Bajwa, "Wideband characterisation of fading mobile radio channels," *Communications, Radar and Signal Processing, IEE Proceedings F*, vol. 129, p. 95, 1982.

[9] A. S. Bajwa and J. D. Parsons, "Small-area characterisation of UHF urban and suburban mobile radio propagation," *Communications, Radar and Signal Processing, IEE Proceedings F*, vol. 129, pp. 102-109, 1982.

[10] A. G. Smithson and I. A. Glover, "High performance digital radio channel sounder for use at 2 and 5 GHz," in *Antennas and Propagation, 2003. (ICAP 2003). Twelfth International Conference on (Conf. Publ. No. 491)*, 2003, pp. 805-808 vol.2.

[11] A. P. Garcia, W. Kotterman, R. S. Thoma, U. Trautwein, D. Bruckner, W. Wirnitzer, *et al.*, "60 GHz in-cabin real-time channel sounding," in *Communications and Networking in China, 2009. ChinaCOM 2009. Fourth International Conference on*, 2009, pp. 1-5.

[12] D. Barrick, "FM/CW radar signals and digital processing," US Department of Commerce,1973.

[13] B. Razavi, *RF microelectronics*: Prentice-Hall, Inc., 1998.

[14] N. Instruments. *USRP*. Available: http://www.ni.com/sdr/usrp/

[15] S. Hongjian, A. Nallanathan, W. Cheng-Xiang, and C. Yunfei, "Wideband spectrum sensing for cognitive radio networks: a survey," *Wireless Communications, IEEE,* vol. 20, pp. 74-81, 2013.

[16] E. Najafzadeh, D. George, and G. Peter, "LabVIEW-Based Spectrum Occupancy Measurements in the 2.4 GHz ISM band using National Instruments USRP," presented at the Joint International Workshop on Applied Radio Systems Research and Smart Wireless Communications (ARSR/SWICOM), Manchester, UK, 2012.

[17] M. Lopez-Benitez, F. Casadevall, and C. Martella, "Performance of spectrum sensing for cognitive radio based on field measurements of various radio technologies," in *Wireless Conference (EW), 2010 European*, 2010, pp. 969-977.

[18] W. Liu, O. Yaron, I. Moerman, S. Bouckaert, B. Jooris, and P. Demeester, "Real-time wide-band spectrum sensing for cognitive radio," in *Communications and Vehicular Technology in the Benelux (SCVT), 2011 18th IEEE Symposium on*, 2011, pp. 1-6.

[19] Agilent, "Spectrum Analysis Basics Application Note 150."

[20] M. H. Islam, C. L. Koh, O. Ser Wah, Q. Xianming, Y. Y. Lai, W. Cavin, *et al.*, "Spectrum Survey in Singapore: Occupancy Measurements and Analyses," in *Cognitive Radio Oriented Wireless Networks and Communications, 2008. CrownCom 2008. 3rd International Conference on*, 2008, pp. 1-7.

[21] T. Harrold, R. Cepeda, and M. Beach, "Long-term measurements of spectrum occupancy characteristics," in *New Frontiers in Dynamic Spectrum Access Networks (DySPAN), 2011 IEEE Symposium on*, 2011, pp. 83-89.

[22] J. Xue, Z. Feng, and P. Zhang, "Spectrum Occupancy Measurements and Analysis in Beijing," *IERI Procedia,* vol. 4, pp. 295-302, 2013.

[23] K. A. Qaraqe, H. Celebi, M. S. Alouini, A. El-Saigh, L. Abuhantash, M. M. Al-Mulla, *et al.*, "Measurement Analysis of Wideband Spectrum Utilization in Indoor Outdoor Environments," presented at the International Conference on Communications Technologies (ICCT 2010), 2010.

[24] M. Wellens, J. Wu, and P. Mahonen, "Evaluation of Spectrum Occupancy in Indoor and Outdoor Scenario in the Context of Cognitive Radio," in *Cognitive Radio Oriented Wireless Networks and Communications, 2007. CrownCom 2007. 2nd International Conference on*, 2007, pp. 420-427.

[25] M. Lopez-Benitez, A. Umbert, and F. Casadevall, "Evaluation of Spectrum Occupancy in Spain for Cognitive Radio Applications," in *Vehicular Technology Conference, 2009. VTC Spring 2009. IEEE 69th*, 2009, pp. 1-5.

[26] H. Urkowitz, "Energy detection of unknown deterministic signals," *Proceedings of the IEEE*, vol. 55, pp. 523-531, 1967.

[27] S. Salous and H. Gokalp, "Dual-frequency sounder for UMTS frequency-division duplex channels," *Communications, IEE Proceedings-*, vol. 149, pp. 117-122, 2002.

[28] S. Salous, P. Filippidis, R. Lewenz, I. Hawkins, N. Razavi-Ghods, and M. Abdallah, "Parallel receiver channel sounder for spatial and MIMO characterisation of the mobile radio channel," *Communications, IEE Proceedings-*, vol. 152, pp. 912-918, 2005.

[29] S. Feeney, "Wide-band channel sounding in the bands above 2GHz," PhD, ECS, Durham University, UK, 2007.

[30] S. Salous, "Chirp sounder measurements for broadband wireless networks and cognitive radio," in *Communication Systems Networks and Digital Signal Processing (CSNDSP), 2010 7th International Symposium on*, 2010, pp. 846-851.

3 Implementation of Wideband Chirp Receiver

This chapter provides the implementation details of the sounding system centred at 2.575 GHz and its extension to six independent receivers developed as part of this work, in both hardware and software aspects. The hardware part explains the components[1] level description, provides detail of interconnections and shows their performances using time and frequency responses. The software part provides detailed description of algorithms, their integration and methods to perform synchronization between a transmitter and a receiver or among receivers over the air. Moreover, it explains the algorithms for automatic gain adjustment, data fetching, monitoring and storing in real time.

Later in the chapter, the description of a receiver centred at 625 MHz will be given, which is developed as part of this work for passive measurements, to detect signals in TV and GSM 900 bands, to measure wideband spectrum utilization. The calibration and performance of the system is explained. Moreover, the summaries of system parameters and built hardware will be listed in the end.

3.1 Receiver

The wideband chirp channel sounder receiver consists of four main units as shown in figure 3.1: 1) Reference Clock and Distribution unit, 2) LO unit, 3) Down-converter unit, and 4) Command and Control unit. The details of each unit are given below.

3.1.1 Reference Clock and Distribution Unit

The reference clock and distribution unit generates multiple phase coherent reference clocks for the LO and command and control units.

The unit contains a commercial rubidium clock source which generates a 10 MHz sine wave [1], which is multiplied and amplified using a clock distribution circuit, to generate phase coherent reference clocks from 10 MHz to 80 MHz, as summarized in table 3.1. The unit can be operated from two types of power sources: 1) +220 V AC mains, 2) +12 V DC supply. The unit also contains a +12 V rechargeable battery, which provides about one hour of power backup for the

[1]*Most of the components described in this chapter, are designed here at Durham University, and any commercial components used in this work will be mentioned explicitly.*

rubidium, in order to keep it warm and maintain its locking status when none of the other power sources are available.

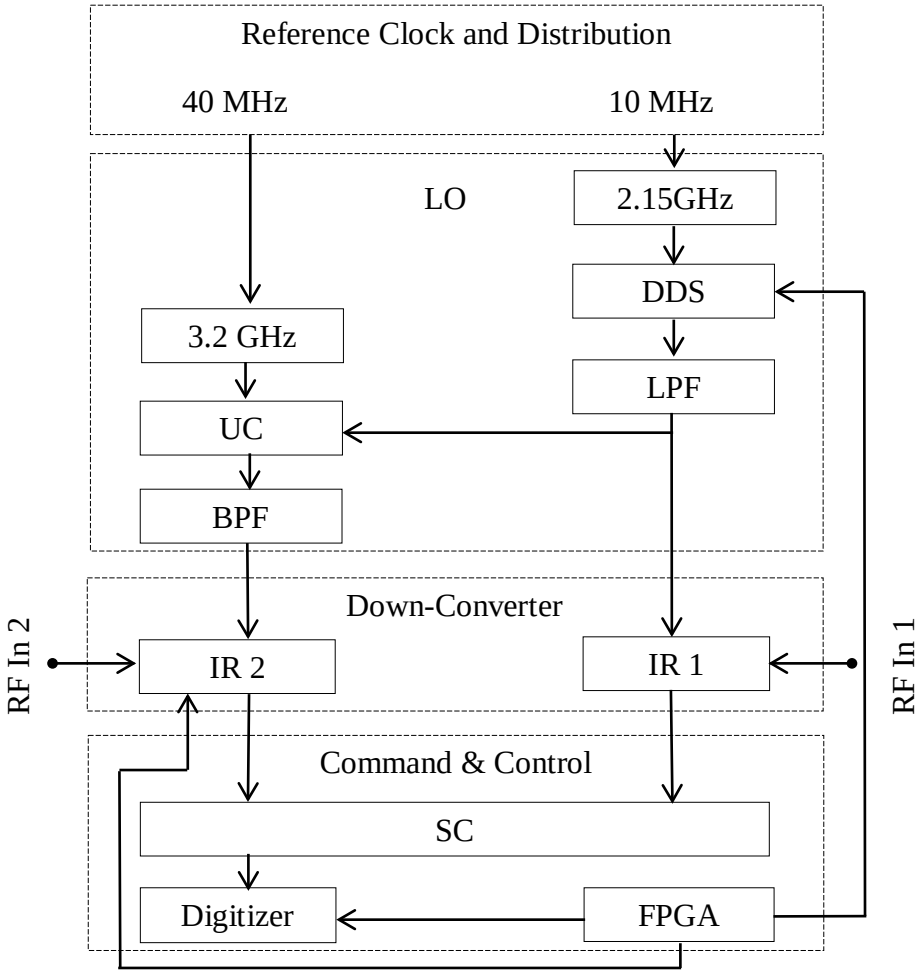

Figure 3.1 Block diagram of wideband chirp receiver

Table 3.1 Summary of reference clocks

Frequency (MHz)	Waveform Type	Voltage levels (max, min) (V)	Number of Outputs
10	Square	(+3.3, 0)	2
10	Sine	(+1.2, -1.2)	2
20	Sine	(+1.2, -1.2)	2
40	Sine	(+1.2, -1.2)	2
80	Sine	(+1.2, -1.2)	2

To perform passive time synchronized measurements using multiple receivers, the rubidium clock sources are required to be phase aligned with respect to each other or to a common reference. Additionally, for active measurements, where the relative time delay between the transmitter and receiver or receivers defines the position of multipath components in the time delay domain, any misaligned rubidium

clock source, which is drifting in time relative to the transmitter, can change the position of the multipath components during measurements and so can induce a Doppler offset. To mitigate these issues, clock sources are required to be phase aligned with the transmitter's clock source or any reference clock source in a considerable margin. To achieve this, the units are left on for 24 hours and phase aligned by adjusting their internal potentiometers and comparing their 80 MHz reference clocks on the oscilloscope. The 80 MHz output of unit labelled as "9" is considered as master reference clock and used to align other sources. A maximum drift between 0.2-0.4 ns is recorded over a minute i.e. 12-24 ns over an hour.

The components are assembled in a 3 U 42 HP rack. Figure 3.2 shows the labelled front panel of the unit. A switch is added on the front panel, which is used to select between two modes of operations: 1) in upward position, it allows the unit to run from the power source, 2) in downward position, it enables the battery charging circuit. The clock source can also be phase locked to an external reference signal i.e. pulse per second (PPS), which is generated by global positioning system (GPS).

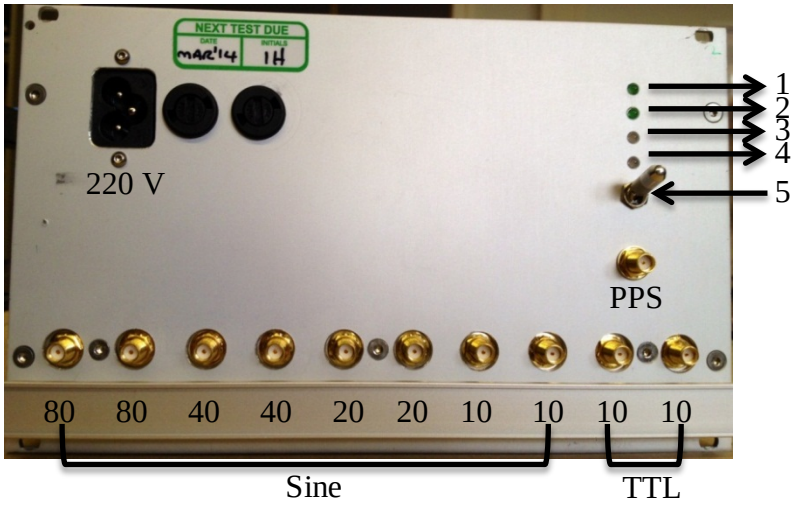

Figure 3.2 Front panel
1: Mains supply status, 2: +12 V DC supply[2] status, 3: Battery charging status, 4: clock source locking status, 5: switch for backup battery

3.1.2 LO Unit

The LO unit generates linearly increasing FMCW signals from DC to 1 GHz and from 2.2 GHz to 2.95 GHz frequency ranges simultaneously.

[2] The +12 V DC supply can be connected from back panel of the unit.

The unit contains two phase locked loop (PLL) clock sources. The 2.15 GHz PLL generates the sampling clock for the direct digital synthesiser (DDS) and the PLL at 3.2 GHz generates the carrier signal for the up-converter (UC) circuit.

The first PLL at 2.15 GHz is phase locked to 10 MHz (sine) reference clock and has ~8 dBm output power. The second PLL at 3.12 GHz is phase locked to 40 MHz reference clock and has ~7 dBm output power. Each clock source circuit operates at +12 V DC supply. Figure 3.3 shows the labelled top view of a clock source circuit.

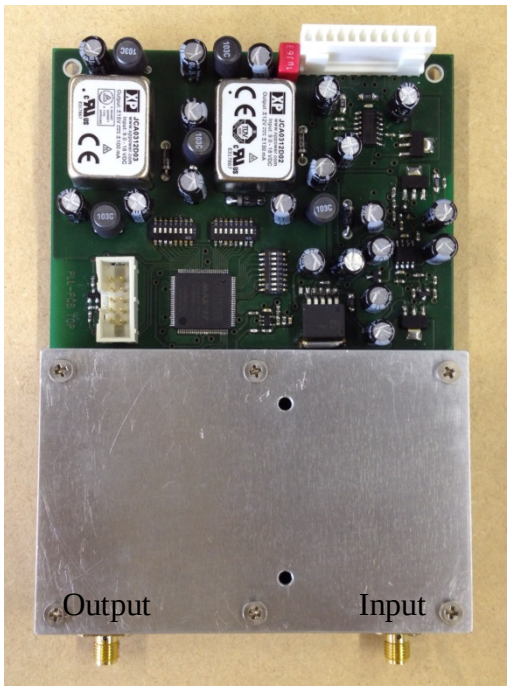

Figure 3.3 Top view of clock source circuit

The frequency sweep is generated with a commercial DDS [2], which can generate linear FMCW signals from DC to 1 GHz. In the current configuration, the DDS operates at 2.15 GHz sampling clock and requires 32 clock cycles (Δt) i.e. ~14.8837 ns, to update its frequency and has a minimum frequency resolution of 0.5006 Hz (Δf_{min}). The DDS parameters (start frequency, step frequency, stop frequency and sweep duration) can be configured via a USB interface. The DDS requires +12 V DC supply to operate.

The DDS generates stair case approximation of the linear FMCW signal by updating Δf frequency every Δt time as shown in figure 3.4. The time required to sweep a bandwidth ($f_{Stop} - f_{Start}$) is defined as sweep time T_s ($t_{Stop} - t_{Start}$).

Equation 3.1 gives the relationship between the sweep time (T_s) and the parameters of the DDS for the generation of phase coherent sweeps, where $8 * \Delta t$ unit time is a constant settling time required in the end of each sweep before the DDS can generate a new sweep. In adition to the settling time requirement, the DDS must also be configured in trigger mode, in which every sweep is generated on the positive edge of a transistor transistor logic (TTL) trigger signal.

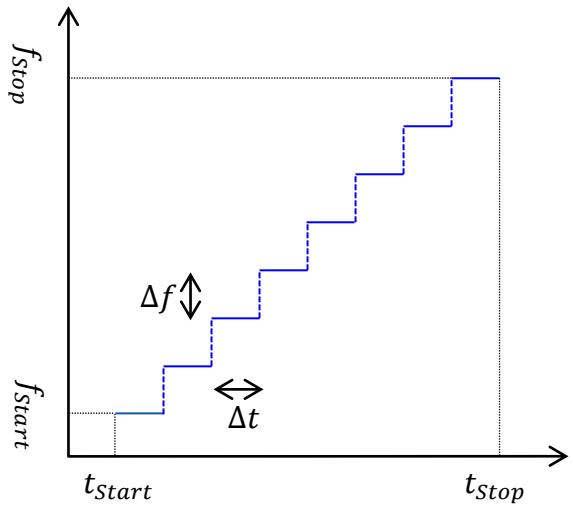

Figure 3.4 Stair case linear FMCW time-frequency approximation

$$T_s = \left(\frac{f_{Stop} - f_{Start}}{\Delta f} + 1\right) \times \Delta t + 8 \times \Delta t \qquad \text{Equation 3.1}$$

Due to design limitations of the DDS, an arbitrary trigger signal cannot be used to guarantee phase coherent generation of sweeps. Besides linear FMCW signal output, the DDS also generates a TTL reference signal referred to as “Refout” having a frequency of 1.0498 MHz i.e. sampling clock / 2048 and must be utilized to solve the aforementioned problem. Details of the trigger signal generation will be discussed in section 3.1.4. A program is written in C++ to control the parameters of the DDS and to calculate the clock dividing factor using equation 3.1. This factor will be used to divide the frequency of “Refout” signal so that various sweep durations of the trigger signal can be obtained. Details of the program will be given later in this section. Figure 3.5 shows the labelled top view of the DDS.

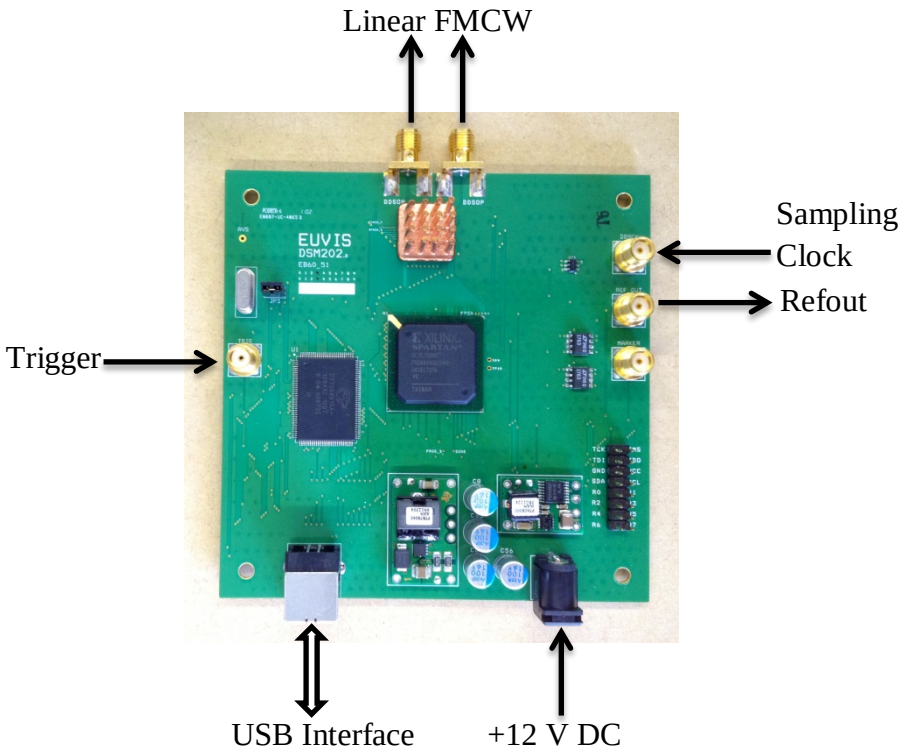

Figure 3.5 Top view of DDS

To remove high frequency components due to the digital to analog conversion process in the DDS, a reconstruction LPF is used at the output of the DDS having a cut off frequency of 1 GHz to suppress the aliasing components and the sampling clock. Figure 3.6 shows the magnitude response of the linear FMCW signal from DC to 1 GHz before and after passing through the LPF filter. The filtered signal has output power levels between 0 dBm and ~ -8dBm over 1 GHz swept bandwidth with less than 0.3 dB pass band ripples. Moreover, about +19 dB suppression is achieved for the sampling clock.

The filtered signal is further up converted using a UC circuit. The UC contains a mixer and requires +13 dBm LO drive power. It also contains an amplifier at the input of the LO which provides +13 dB gain and requires +5 V DC supply to operate. The carrier signal from the clock source is attenuated by adding a 6 dB attenuator at the input of the LO port so that the required drive power level can be maintained. The up converted signal is passed through a BPF to supress the carrier signal and the upper side band.

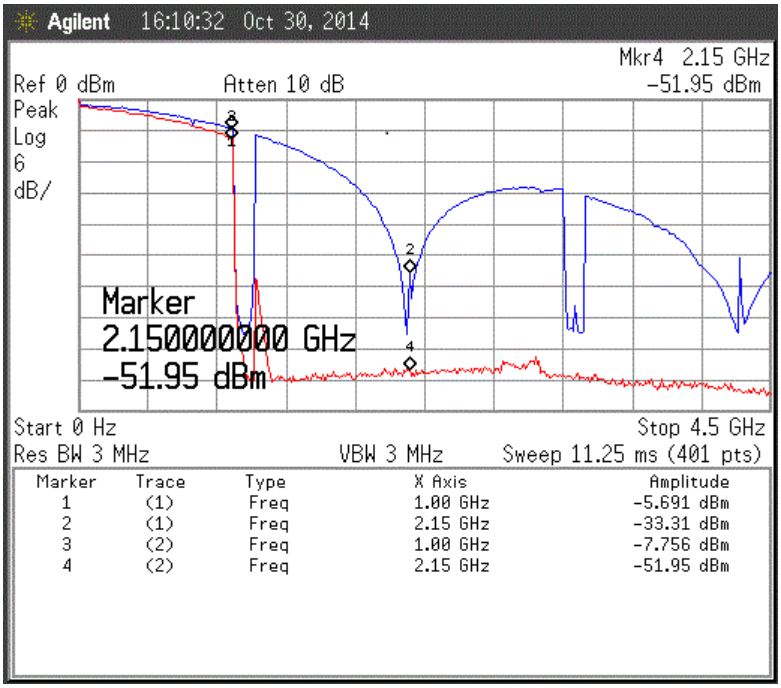

Figure 3.6 Magnitude response of linear FMCW signal before and after passing through LPF

The filter has 750 MHz pass band bandwidth, which restricts the swept bandwidth of the unit and only allows a signal from 2.2 GHz to 2.95 GHz, which is sufficient to detect 2.4 GHz ISM band and LTE 2600 signal concurrently. Figure 3.7 shows the up converted signal before and after the BPF. The filtered signal has power

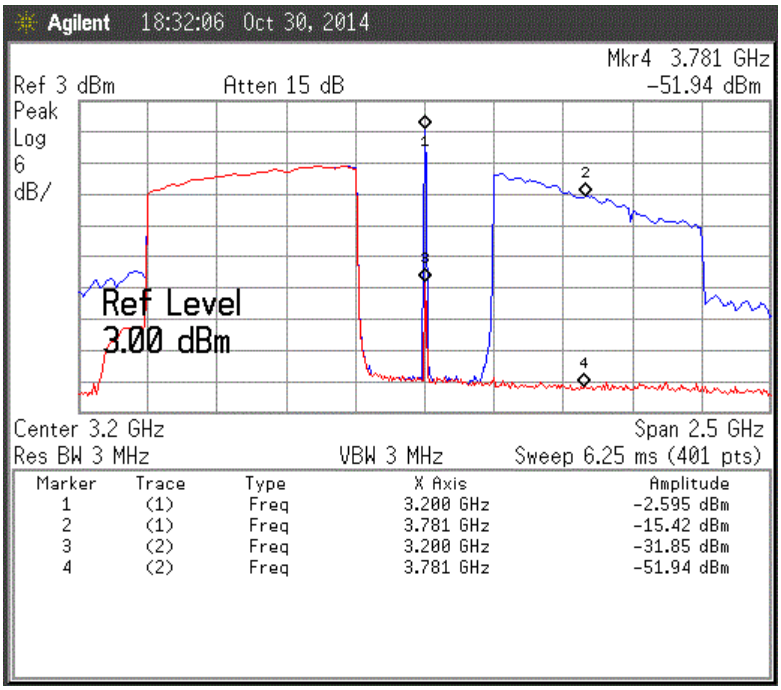

Figure 3.7 Magnitude response of up-converted signal before and after passing through BPF

levels between ~-15 dBm to ~-10 dBm over the frequency range of 2.2-2.95 GHz, having less than 0.5 dB pass band ripples. A suppression of ~+29 dB is achieved on the carrier frequency and ~+37 dB for the upper sideband.

All the components are tested against their expected performance before assembling them together. The components such as filters, clock sources and UC are shielded to avoid electromagnetic interference (EMI). The components are assembled in a 3 U 21 HP rack and an additional metallic plate is added to provide extra space to accommodate the components.

The unit contains a power supply circuit which takes external +12 V DC and produces + 12 V DC with regulated current for the PLL, DDS and power source status LED, which is further regulated to produce +5 V DC, using a L7805ACV regulator which provides power supply to UC circuit. The digital to analog converter chip in the DDS produces excessive heat while operating at room temperature, so to overcome this, a fan is added at the back panel of the unit, which operates with +12 V DC supply. Figures 3.8-3.11 shows the labelled front panel, back panel and internal design of the unit.

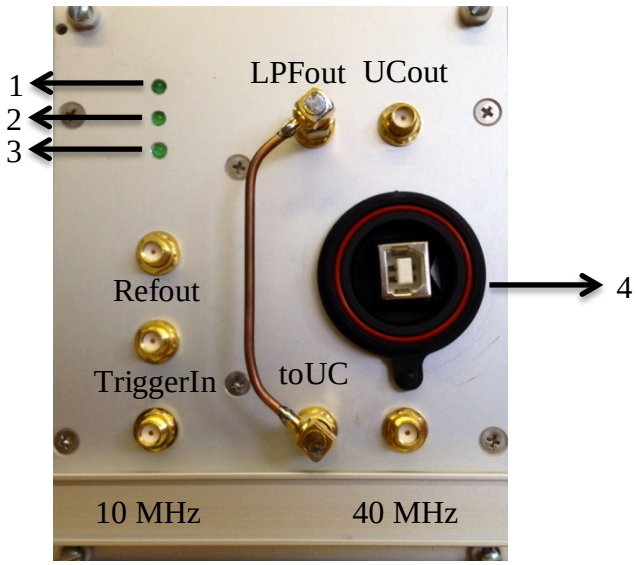

Figure 3.8 Front panel of LO unit

1: Power supply circuit status, 2: 2.15 GHz clock source locking status, 3: 3.2 GHz clock source locking status, 4: USB interface to program DDS

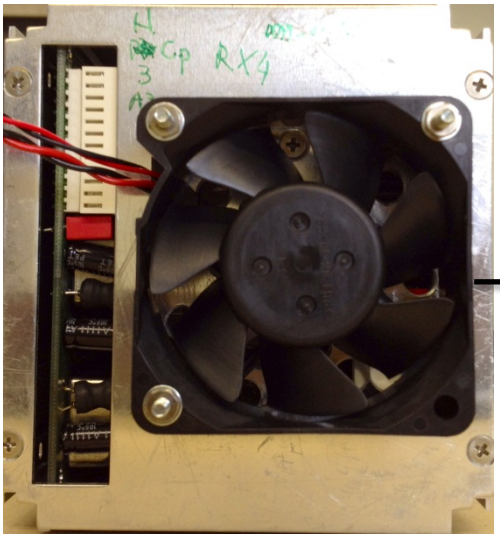

Figure 3.9 Back panel of LO unit

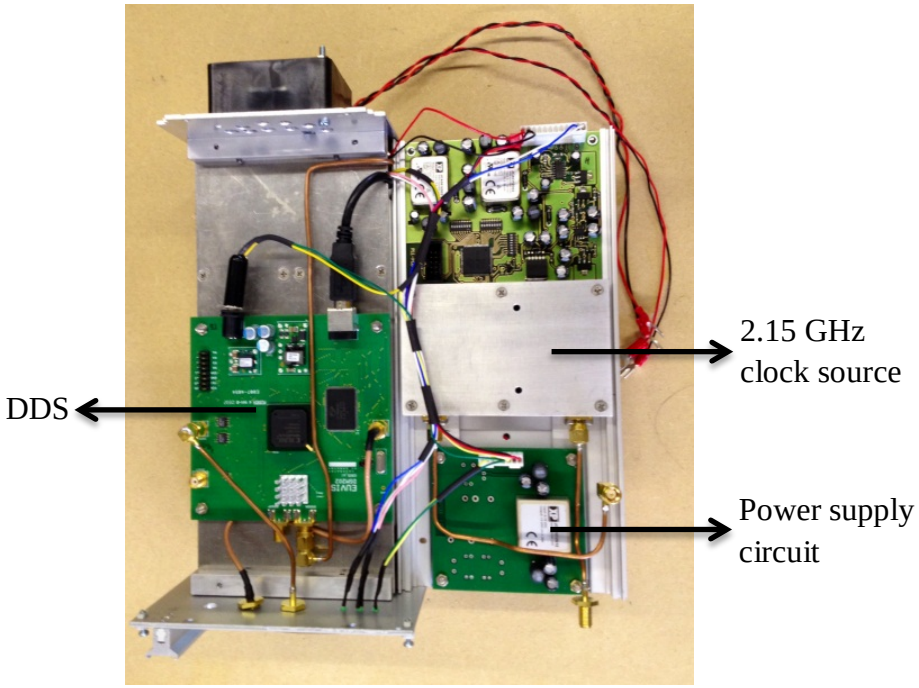

Figure 3.10 Top view of internal design of LO unit (left hand side of central metallic plate)

The software to programme the DDS is written in C++ on Microsoft Visual Studio 2010 express software package. Mainly, it allows the user to control the parameters of the DDS i.e. start, stop and step frequencies, configure its mode of operation i.e. free run or trigger, compute clock dividing factor and write this factor to a text file on the hard disk. The implementation details of the code are given in appendix A.

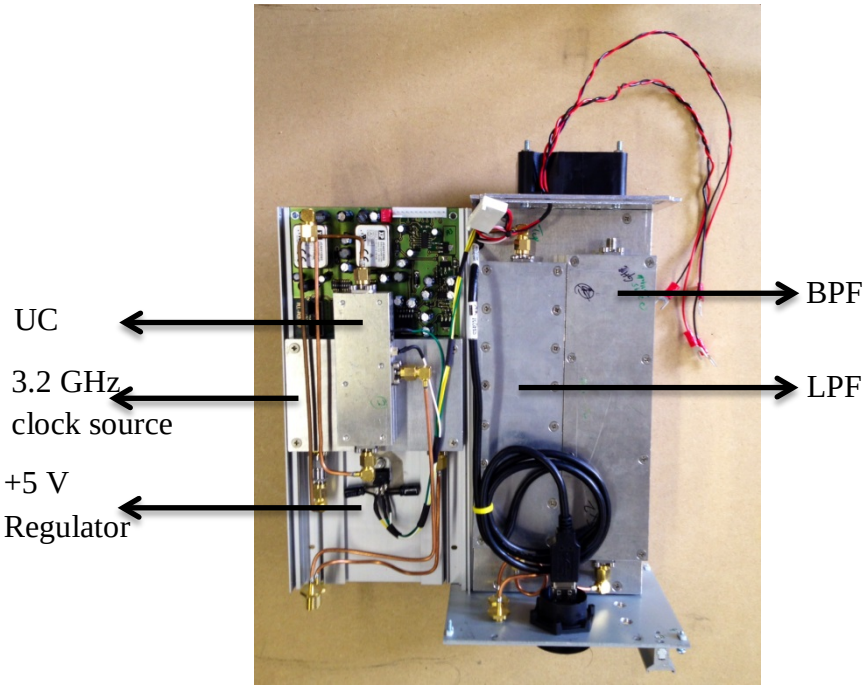

Figure 3.11 Top view of internal design of LO unit (right side of central metallic plate)

3.1.3 Down-converter Unit

The down-converter unit translates the RF signal to baseband from two frequency ranges: 1) 250 MHz to 1 GHz 2) 2.2-2.95 GHz.

The down-converter unit has two independent integrated receivers (IR), which contains a low noise amplifier (LNA), RF attenuator and a mixer to get the baseband signal. The IR '1' contains a programmable 30 dB LNA while IR '2' contains fixed gain 23 dB LNA with a programmable RF attenuator which can provide attenuation up to 31 dB. The RF attenuator prevents over driving of the mixer in the presence of strong received signals.

3.1.3.1 Down-converter for 250 MHz to 1 GHz

The IR '1' is developed by using commercial components. The RF signal is amplified in two steps: 1) a programmable amplification is obtained by passing through Jim M-75 LNA, 2) a fixed amplification of +13 dB is obtained by passing through Hittite HMC636ST89 evaluation board [3]. A Mini-Circuit ZEM-4300 [4] mixer is used to get a baseband signal which requires +7 dBm LO drive power. The low pass filtered signal (LPFout) from the LO unit is used to drive this mixer. The filtered signal from 250 MHz to 1 GHz has power levels from ~-3 dBm to ~-8 dBm over its bandwidth, which is much lower than the required power level to drive mixer and requires amplification. A Mini-Circuit ZFL-2000 amplifier is used to provide

+20 dB gain and attenuated by 6 dB to obtain the required drive power level for the mixer. The Jim M-75, HMC636ST89 and ZFL-2000 require +12 V, +5 V and +15 V DC supplies respectively. The total RF gain of IR '1' is +30 dB and is not assembled in the unit and developed as a prototype to perform only passive measurements. The block diagram of IR '1' is shown in figure 3.12.

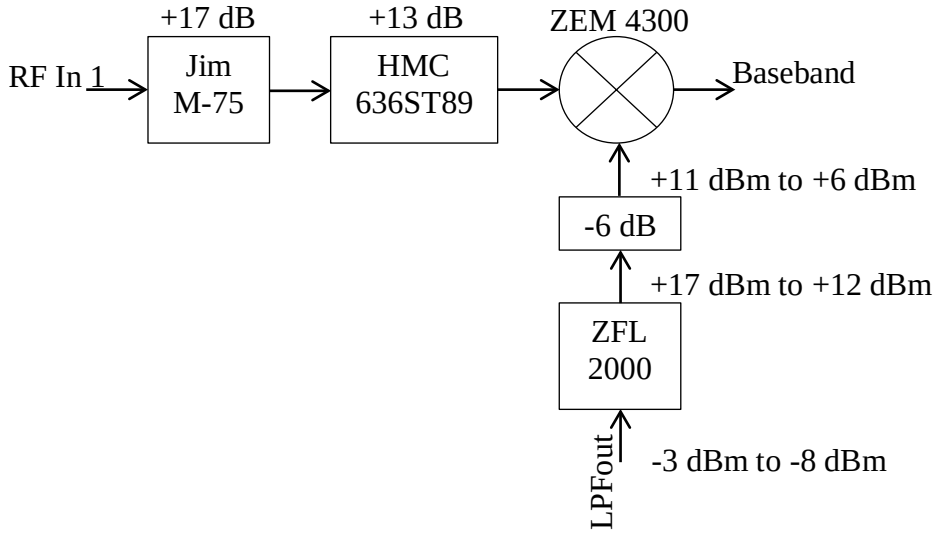

Figure 3.12 Block diagram of IR '1'

3.1.3.2 Down-converter for 2.2 GHz to 2.95 GHz

The total RF gain of IR '2' is 31 dB which can be reduced to 0 dB by adding a maximum RF attenuation of 31 dB. The gains of the RF attenuator can be controlled by 3 bits as summarized in table 3.2 where '0' represents 0 V to -3 V voltage range and '1' represents -4.2 V to -5 V range. To control the gains from the TTL levels, a level conversion circuit is added which maps 0 to -3 voltage range to TTL high and -4.2 to -5 volts range to TTL low. The layout of the PCB is given in appendix B. The IR '2' requires +5 V and -5 V DC supplies for the LNA and RF attenuator respectively.

The mixer in IR '2' requires +13 dBm LO drive power and has inbuilt +13 dB amplifiers at the input of the LO and RF ports respectively. In order to get sufficient drive power levels, the up-converted signal (UCout) from the LO unit is first split using a commercial Mini-Circuit ZX10-2-42-s+ power splitter having ~3.2 dB conversion loss [5] and then amplified using a commercial Mini-Circuit ZX60-5916M+ amplifier to get +17.7 dB gain [6] and obtain power levels between ~-0.5 dBm to ~4.5 dBm over the bandwidth. The amplified signal is amplified due to the in

Table 3.2 Bit combinations for RF attenuator

Bit2	Bit1	Bit0	RF Attenuation (dB)
0	0	0	0
0	0	1	5
0	1	0	10
0	1	1	15
1	0	1	21
1	1	0	26
1	1	1	31

built amplifier at the LO port of the mixer and hence provides the required drive power levels. The second output port of the splitter is terminated by adding a 50 Ω load which provides ~30 dB return loss. The terminated port can be utilized in the future for higher frequency translations to develop the channel sounder at higher frequency bands. The block diagram of IR '2' is shown in figure 3.13.

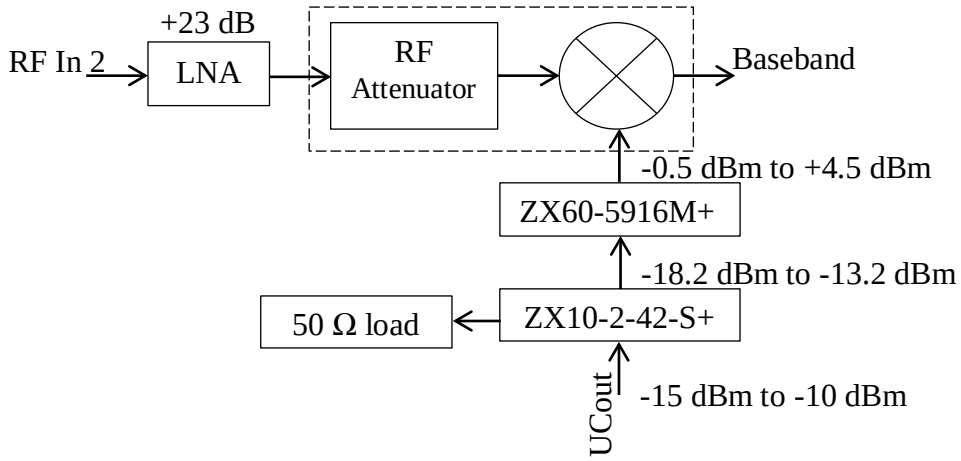

Figure 3.13 Block diagram of IR '2'

All the components are tested against their expected performance before assembling them together. The components of IR '2' are shielded to avoid any EMI. The components are assembled in a 3 U 21 HP rack and an additional metallic plate is added to provide extra space to accommodate the components. The unit contains a power supply circuit which takes external +12 V DC and produces + 12 V DC and -12 V DC with regulated current, which is further regulated to produce +5 V and -5V using regulators L7805ACV and LM7905CT respectively. Figures 3.14-3.16 show the front panel and the internal design of the unit, where unlabelled ports are left for future extensions.

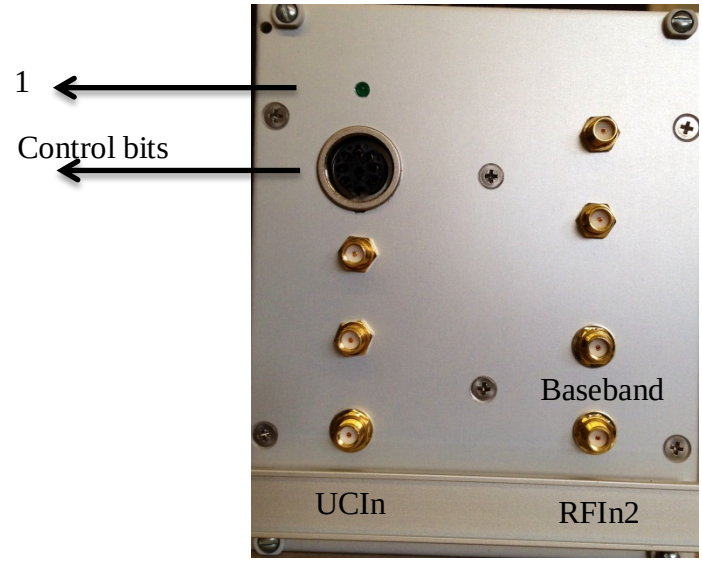

Figure 3.14 Front panel of down-converter unit
1: Power supply circuit status

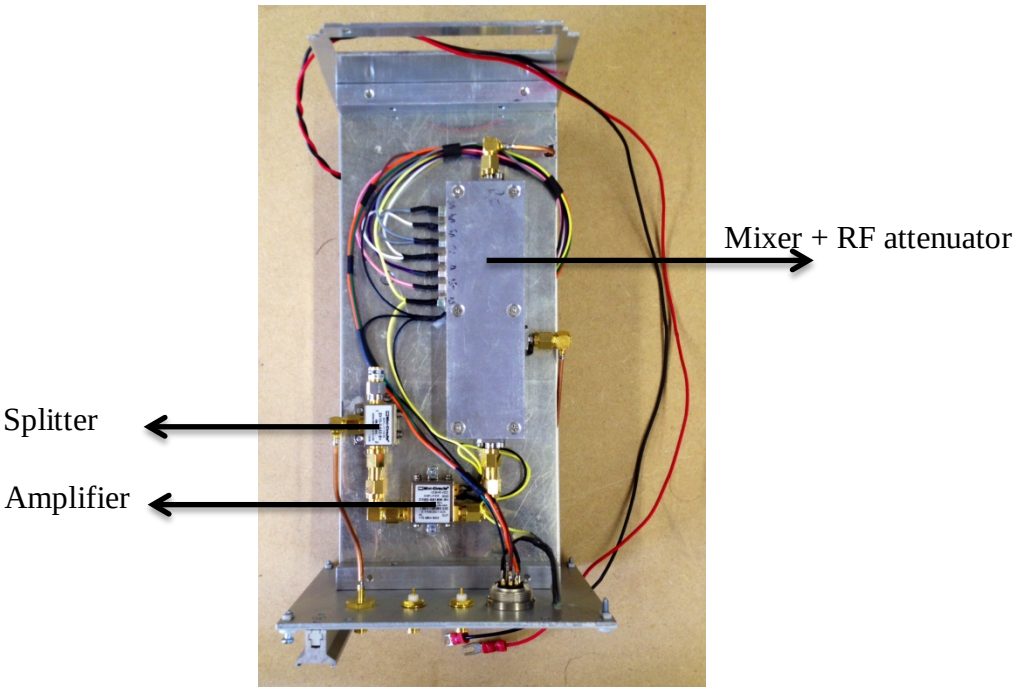

Figure 3.15 Top view of internal design of down-converter unit (left side of central metallic plate)

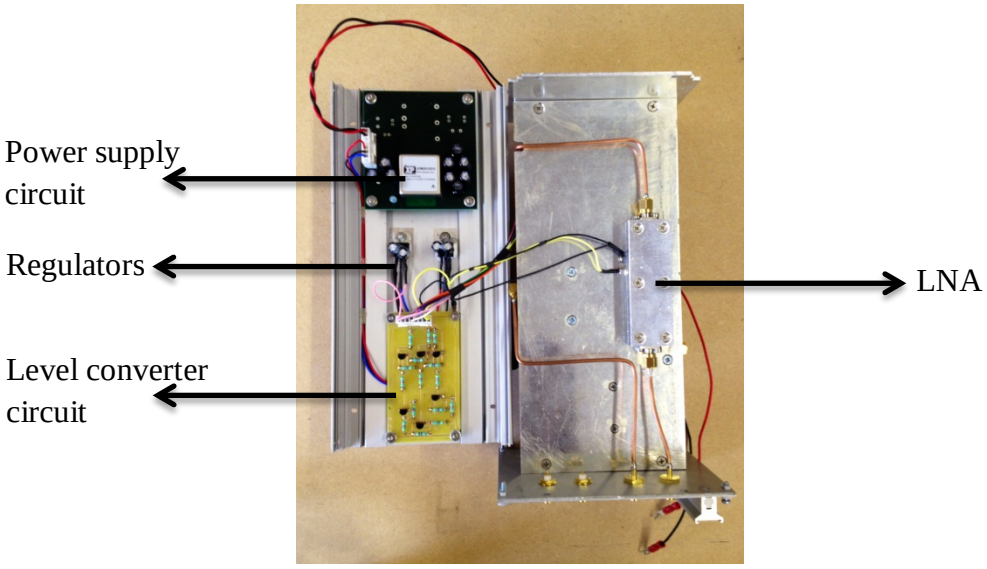

Figure 3.16 Top view of internal design of down-converter unit (right side of central metallic plate)

3.1.4 Command and Control Unit

The command and control unit consists of a field programmable gate array (FPGA) to generate control signals, a NI 6501 to provide full duplex communication link between the PC and the FPGA [7], a NI 5132 8 bit digitizer [8] and programmable signal conditioning (SC) circuit to provide amplification for the baseband signal.

The unit contains FPGA board, which is used to generate the trigger signals for the DDS and digitizer, provides control bits to the RF attenuator, SC and eight way antenna switch, allows the user to start the receiver either by triggering manually or from PPS signal and provides interface to PC via NI 6501. The “Refout” signal is used as sampling clock for FPGA so that all the tasks are executed coherently with the generation of sweeps on the positive edge of “Refout” signal. A dedicated FPGA printed circuit board (PCB) was designed, which contains Altera Cyclone II EPC20Q240C8 chip and all the I/Os are grouped in 5 bits or 8 bits ports according to the number of bits required for control signals. The board also provides free I/O lines for testing and for experimental purposes. The board requires +5V DC supply to operate. Figure 3.17 provides top view of the board. The design layout, netlist and ports legend are given in appendix C.

The NI 6501 is a commercial plug and play digital I/O product from NI, which provides USB to 24 parallel pins interface. It is used to perform read/write data

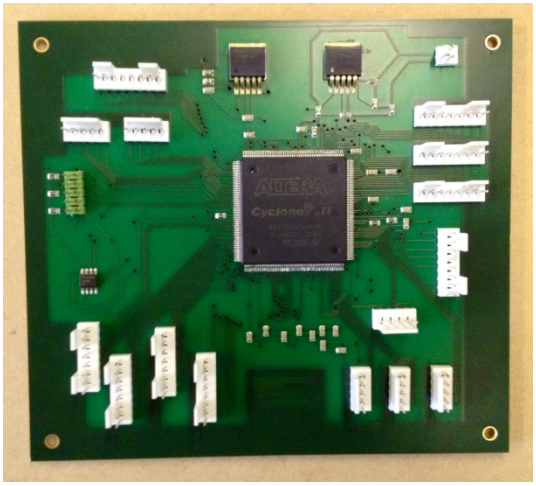

Figure 3.17 Top view of FPGA PCB

operations between the PC and the FPGA. The NI 5132 is a commercial plug and play USB 8 bit digitizer which is used to fetch, monitor and store baseband data in real time. It has two data channels with 32 MB memory per channel and a programmable function interface (PFI) channel which can be used for external trigger or sampling clock signal. The digitizer supports maximum sampling clock of 50 MHz. However, due to limited on board memory per channel, it is difficult to digitize long duration measurement data and also to transfer to the PC. The other limitation is, this digitizer cannot digitize and transfer data in parallel which add additional time delay for time sensitive measurements. To overcome these issues, Signatec PX14400 14 bits digitizer is also integrated in the unit for measurements, where long term data recording was required particularly for passive measurements. This digitizer has two data channels with 512 MB on board shared memory for both channels and has dedicated channels for external clock and trigger signal. The maximum supported sampling clock is 400 MHz. Moreover, it also minimizes the data transfer time from the digitizer to the PC due to high speed data transfer on the PCI express bus.

The SC circuit provides amplification in order to increase the dynamic range of the digitizer. It also has two BPF i.e. 5 MHz and 10 MHz, to remove DC and high frequency components from the baseband signal. The programmable gains of the SC are controllable by 7 bits control lines. Table 3.3 summarizes the bit combination and corresponding gains. The combination of offset gain and stage gain bits can provide an intermediate gain from -12 dB to 53 dB. The selection between filters can be selected by a control signal. The SC circuit requires +12 V and -12 V DC supplies to operate.

Table 3.3 Bits combinations for SC circuit

Stage Gain Bits			Offset Gain Bits				Gain
Bit6	Bit5	Bit4	Bit3	Bit2	Bit1	Bit0	dB
0	0	0	0	0	0	0	-12
0	0	0	0	0	0	1	-11
0	0	0	0	0	1	0	-10
0	0	0	0	0	1	1	-9
0	0	0	0	1	0	0	-8
0	0	0	0	1	0	1	-7
0	0	0	0	1	1	0	-6
0	0	0	0	1	1	1	-5
0	0	0	1	0	0	0	-4
0	0	0	1	0	0	1	-3
0	0	0	1	0	1	0	-2
0	0	0	1	0	1	1	-1
0	0	0	1	1	0	0	0
0	0	0	1	1	0	1	1
0	0	0	1	1	1	0	2
0	0	0	1	1	1	1	3
0	0	1	0	0	0	0	10
0	1	0	0	0	0	0	20
0	1	1	0	0	0	0	30
1	0	0	0	0	0	0	40
1	0	1	0	0	0	0	50

All the components are tested against their expected performance before assembling them together. The components are assembled in a 1 U 95 HP rack. The unit contains a power supply circuit which takes external +12 V DC and produces +12 V DC and -12 V DC with regulated current for the SC circuit and is further regulated to produce +5 V using L7805ACV regulators for the FPGA board and binary switches to provide control signal for filter selection, external reset of the unit and to start the unit manually by a user. Figures 3.18-3.19 show the front panel and internal view of the unit. The detail of components I/O interconnections and switching levels are given in appendix D, which also contains the details of the prototype unit which was designed at the beginning of this project for testing purposes.

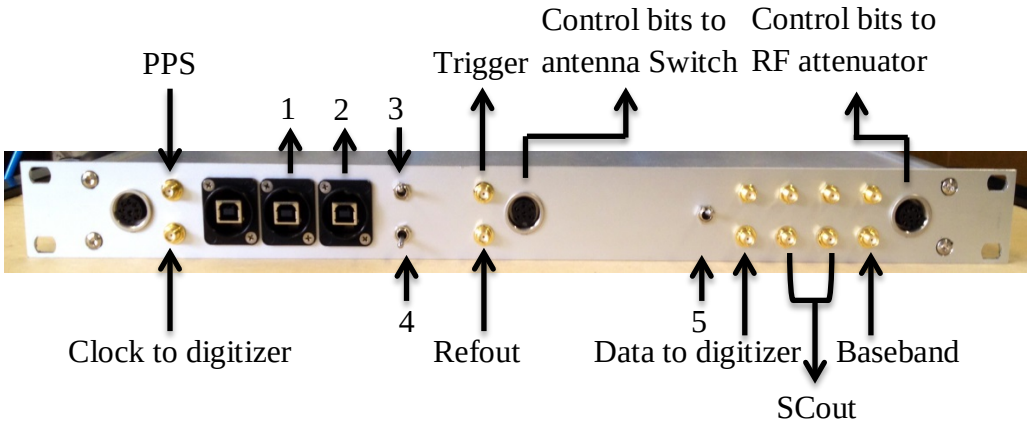

Figure 3.18 Front panel of command and control unit
1: USB interface to NI 5132, 2: USB interface to NI 6501, 3: Start switch, 4: Unit reset switch, 5: Filter selection switch

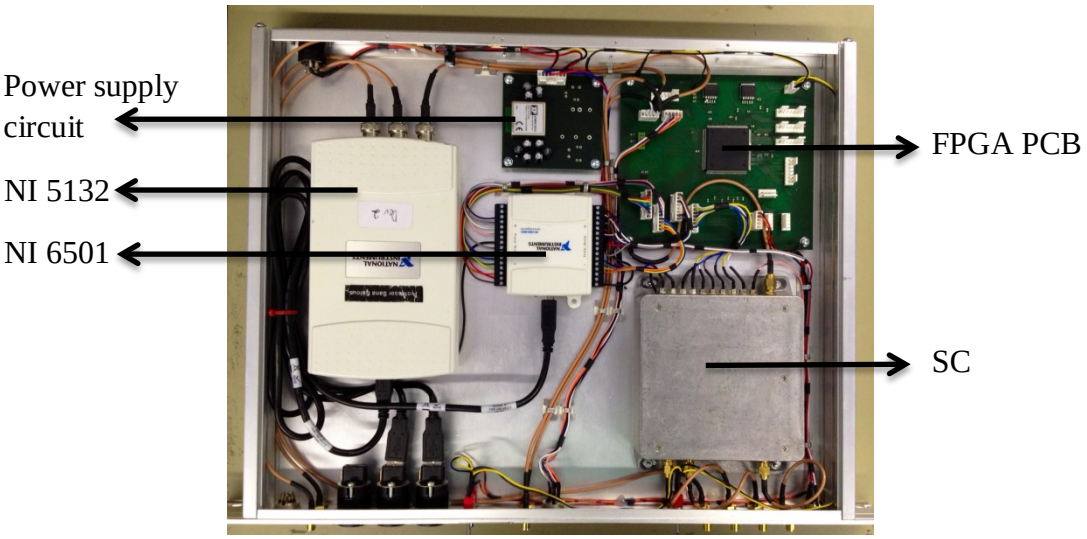

Figure 3.19 Top view of internal design of command and control unit

In order to operate the unit two software programmes are developed. The first software program is developed for users which allows them to control the gains of the receiver, provides baseband data analysis in the time-frequency domain and storage in real time. The second software program is developed for the FPGA chip to establish full duplex communication links between the PC and the FPGA and also to generate control signals. The software for users is written in NI Labveiw software package. It's a graphical programming tool which is normally used to design software involving NI products. The software provides integration of the following algorithms

- Initialization and configuration
- Data transfer and trigger generation

- Synchronization
- Gains calculation
- Data storage

In the initialization and configuration algorithm the I/O lines of NI 6501 and NI 5132 are reset and set to default values. The NI 6501 has 24 I/O lines, which are configured to write mode except for pin 2.6 which is configured in read mode to get acknowledgment signal from FPGA against read/write operations. The data channel '1' of NI 5132 is configured to sample the baseband signal and channel '0' is configured as a trigger channel. The PFI channel is configured to accept external TTL sampling clock for the digitizer.

The data transfer algorithm reads the 16 bits clock dividing factor from hard disk and transfers it to the FPGA byte by byte using NI 6501. Two flags are used for acknowledgment purposes to make sure the FPGA has received the 16 bits successfully in the correct order. The acknowledgment signal from the PC to the FPGA is sent on pin 2.7 referred to as "ByteWrite" and from the FPGA to the PC is sent on pin 2.6 referred to as "LabveiwFlag". The algorithm first writes the lower byte and set "ByteWrite" to high and waits for acknowledgment. As "ByteWrite" pin is high which defines that data are available to read, the FPGA will read it and set "LabveiwFlag" to high for acknowledgment. After receiving acknowledgment from the FPGA, the algorithm set "ByteWrite" to low which defines that second byte is available to read. After reading the second byte, the FPGA sets "LabveiwFlag" to zero for acknowledgment that both bytes have been received successfully. After that, the FPGA uses this number to divide the "Refout" signal and generate the trigger signal for the DDS and digitizer according to the desired sweep duration.

The synchronization algorithm consists of a delay routine which adds time delay in the trigger signal on the positive edge of "Refout" signal. As given in section 2.4 for active measurements, the frequency of the baseband signal is proportional to the relative time delay between the transmitter and receiver. Normally, the transmitter and receiver have arbitrary time delay at the beginning, which can make the beat note frequency outside the frequency range of the SC filter. In order to bring the baseband signal to the filter range, a time delay can be introduced in the trigger signal. Using this technique, the transmitter and receiver can be synchronized over the air.

However, in the passive mode, the trigger signals of multiple receivers can also be synchronized by introducing time delay in order to time align them with respect to a reference trigger signal. The value of the delay is programmable and can be set manually by the user. The relevant bits associated to the delay number are transferred to the FPGA using NI 6501 and this operation can be performed in real time.

The gain calculation algorithm gives the bits relevant to the RF attenuator and SC gains. The algorithm detects the maximum and minimum voltage levels received by the digitizer in time and compares it with the pre-defined vertical range of the digitizer. Here the vertical range defines the maximum and minimum voltage level that a digitizer can sample. The baseband signal is attenuated if the measured voltage levels are found to be higher than the digitizer set vertical range. On the other hand, weak signals where the voltage levels are small compared to the vertical range are amplified to the digitizer range to increase the dynamic range of the receiver. The relevant bits of the RF attenuator and SC are then transferred to the FPGA using NI 6501.

The data storage algorithm reads the data from on the board memory of the respective data channel and transfers it to the PC. The size of file depends upon the number of sweeps a user wants to store and the number of points contained in one sweep, which depends on the sampling clock of the digitizer and time resolution. Along with the data file, a parameters file is saved which contains the trigger signal frequency, number of samples per sweep, RF attenuator and SC gain values. These parameters are required for data processing and to get the received signal power. Each file consists of a fixed number of sweeps which are configurable manually by the user from the front panel of the software. It also allows the user to store multiple data files continuously or a single data file. Moreover, the baseband data can be seen in both the time and frequency domains in real time before saving and transferring to the hard disk. Figure 3.20-3.21 shows the flow diagram and front panel of the software. The details of the implemented software are given in appendix E.

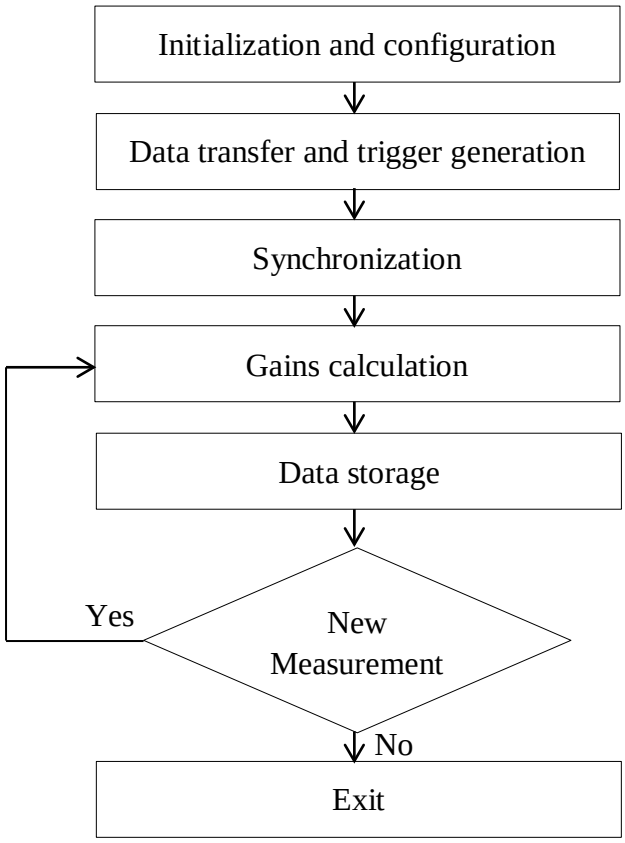

Figure 3.20 Flow diagram

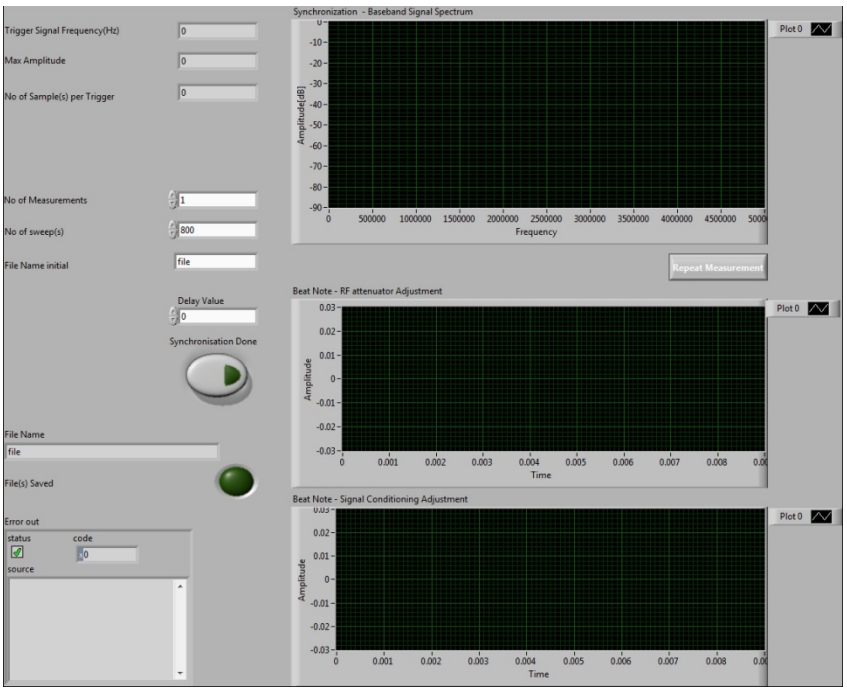

Figure 3.21 Front panel of software

The FPGA is responsible for generating control signals on the positive edge of “Refout” signal, which is used as a sampling clock of the FPGA. The program for FPGA is written in Quartus II v9.0 software package in Verilog HDL. It receives 16

bits clock diving factor from the PC, generates a trigger signal for the DDS and digitizer, set the RF attenuator and SC gains, define control bits for 8 way antenna switch and allows the user to start the unit manually or based on PPS signal. Figure 3.22 shows the timing diagram of all FPGA operations. The detailed description of the code written for the FPGA chip is given in appendix F.

Finally, all the units are assembled in a 3 U 95 HP rack, which contains a +12 V DC power supply to provide power to all the units. Figure 3.23 shows the front view of the receiver.

3.2 Transmitter

The transmitter is composed of four units: 1) reference clock and distribution unit, 2) LO unit, 3) Amplification unit, and 4) command and control unit. The design of reference clock and distribution unit and LO unit are similar to those as described in sections 3.1.1 and 3.1.2. The details of the amplification unit and dedicated command and control unit are given below.

3.2.1 Amplification Unit

The amplification unit takes the up converted signal (UCout) from the LO unit and amplifies it using a commercial Avantek SA-85-2583 amplifier. Figure 3.24 shows the amplified signal for transmission where about ~+36-32 dB gains is obtained over the bandwidth.

3.2.2 Command and Control Unit

The design of the transmitter's command and control unit is similar as explained in section 3.1.4 with limited functionalities. The unit is responsible to provide the following main functionalities

- Download the clock dividing factor in FPGA using NI 6501
- Generate the trigger signal for DDS and control signals for the antenna switch.
- Allow the user to start the unit manually with the help of start switch and PPS signal.

A prototype of the unit is developed and tested successfully. The internal design of the unit is shown in appendix D.

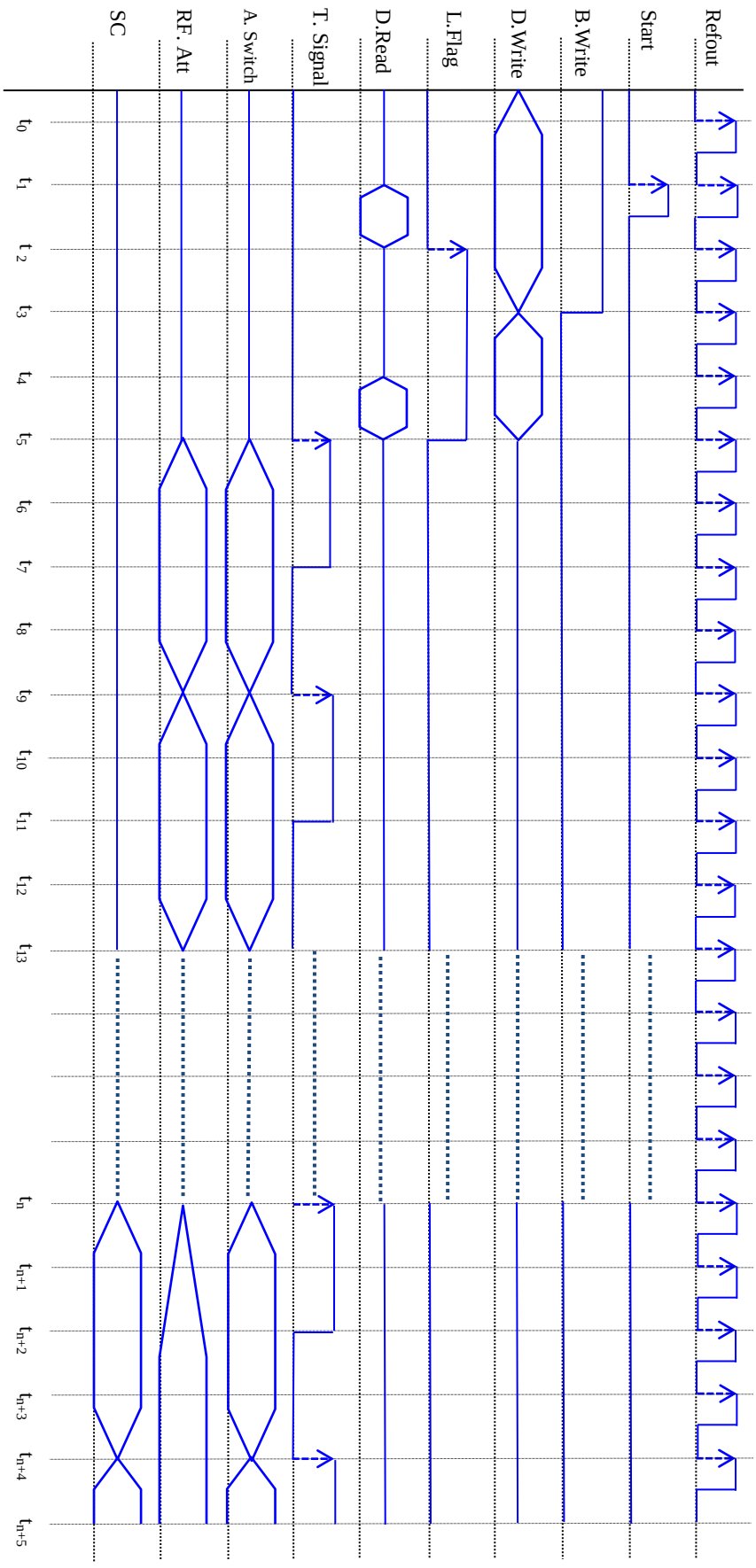

B.Write : Byte Write , D.Write:Data Write, L.Flag : LabveiwFlag, D.Read:Data Read, T.Signal:Trigger Signal, A.Switch:Antenna Switch, RF.Att:RF attenuator

Figure 3.22 Timing diagram

Figure 3.23 Front view of the receiver

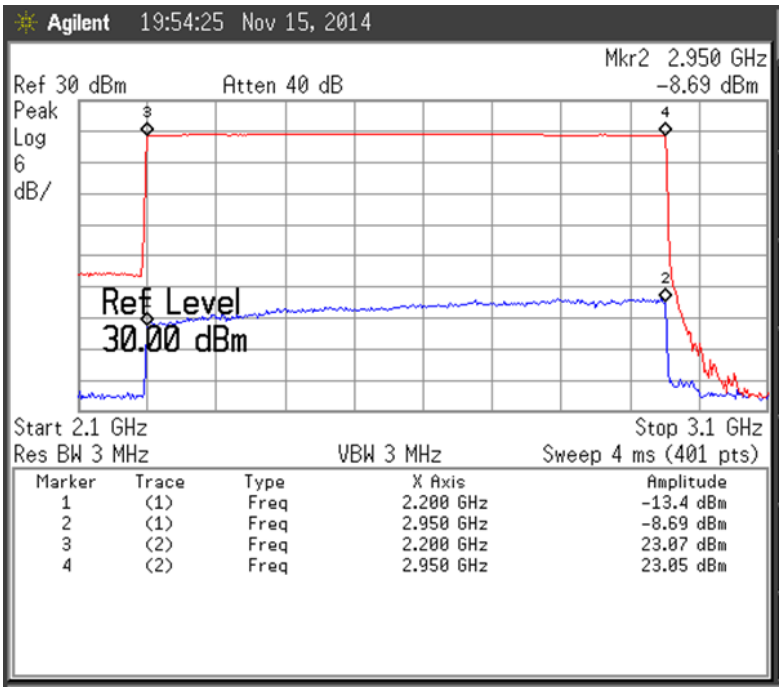

Figure 3.24 Magnitude response of amplified signal

3.3 Calibration and Performance

Before performing measurements, the receiver is calibrated for all gains and losses, which is essential to get the correct value of the received power. There are two types of variable gains which are present in the receiver: 1) RF attenuators, 2) SC, which requires calibration. Moreover, all the losses due to cables, connections, mixers etc will also be calculated in this section.

The performance of the receiver is evaluated based on two parameters: 1) sensitivity, 2) IDR. The sensitivity of the receiver is very important to detect weak primary user's signals in CRN, where higher values of sensitivity are essential to avoid the hidden node problem. The second parameter, IDR defines the ratio between

the highest to the weakest power levels which are detectable by a receiver. In order to reliably detect weak signals, in the presence of strong signals a higher value of IDR is required. Particularly, for a receiver to perform wideband spectrum sensing, where both weak and strong signals from different radio technologies are present, higher values of both sensitivity and IDR are desirable.

3.3.1 Experimental Setup and Processing

In order to perform calibration and measure the performance, a function generator (FG) is configured to generate a CW signal and fed to the receiver via attenuators. The received CW signal is mixed with a locally generated CW/FMCW signal to obtain the baseband signal.

To calibrate, the received CW signal at 2.765 GHz with -75 dBm is mixed with a locally generated CW signal at 2.764 GHz to get the baseband signal at 1 MHz. The received power levels of baseband signal are recorded for all combinations of RF attenuator in IR '2', to calculate the offset factor between the theoretical gain and measured gain. Similarly, to calibrate the SC gains, the baseband signal with 0 dB RF attenuation is fed to the SC and offset factor is calculated for all combinations.

To measure the sensitivity and IDR of the receiver, the attenuation between the function generator and receiver is increased with +5 dB steps until the received CW signal cannot be distinguished from the noise floor using parameters summarized in table 3.4. The amplified baseband signal from the SC circuit is digitized using the Signatec PX14400 digitizer and stored for offline processing in MATALB to get the received power. The details of the MATLAB code are given in appendix G.

Table 3.4 Summary of parameters for sensitivity and IDR test

	Parameter	I	II	III	IV
FG	CW frequency (MHz)	500	500	2765	2765
	Power (dBm)	-55	-55	-55	-55
Rx	Swept Bandwidth (MHz)	100	750	100	750
	Frequency range (GHz)	0.45-0.55	0.25-1	2.7-2.8	2.2-2.95
	Time resolution (µs)	204.8	204.8	204.8	204.8
	Frequency resolution (kHz)	400	1000	400	1000
	Vertical range (mV_{pp})	220	220	220	220
	Sampling clock (MHz)	80	80	80	80

3.3.2 Offset Factor

Figure 3.25 shows the measured offset factors in the RF attenuator gains where the highest offset of -2.2 dB is recorded for -31 dB RF attenuator gains. Figure 3.26 shows the measured offset factors in the SC circuit gains which have marginal variations up to 1 dB.

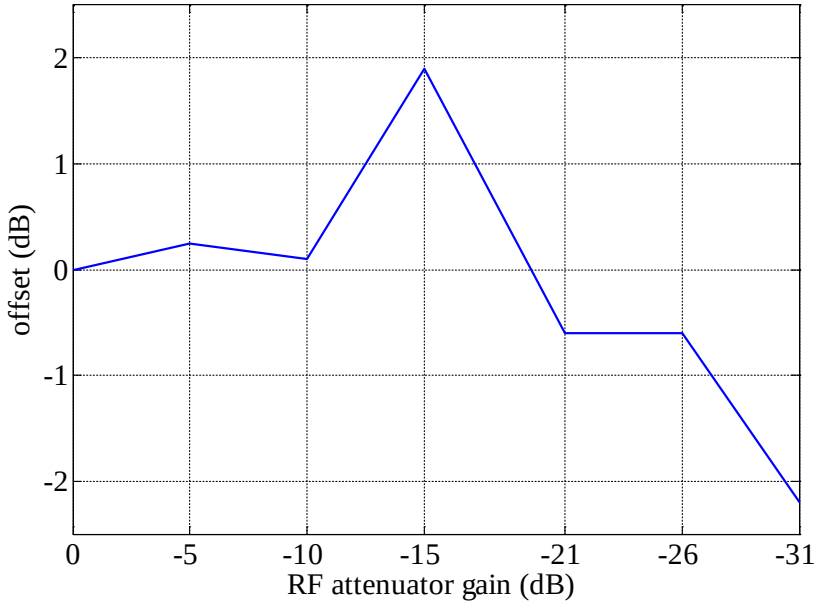

Figure 3.25 Offset in RF attenuator gain levels

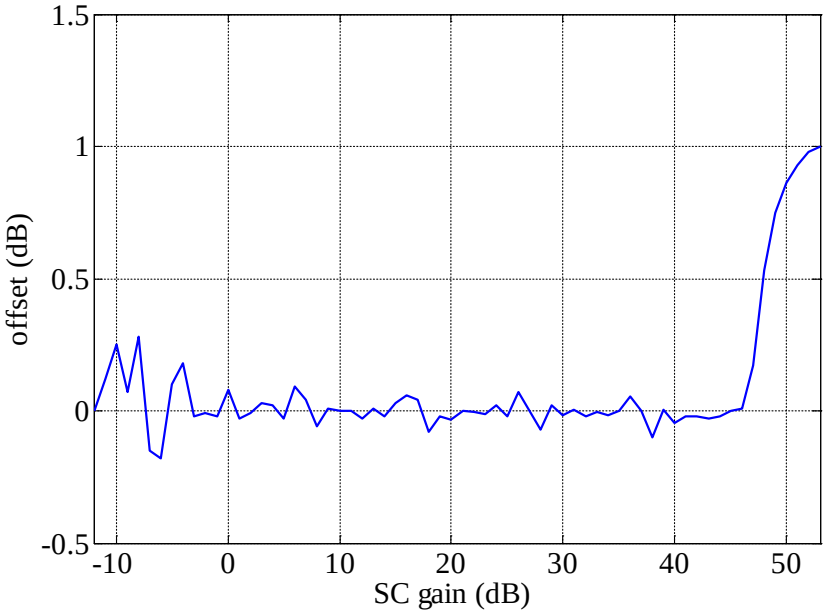

Figure 3.26 Offset in SC circuit gain levels

3.3.3 Sensitivity and Instantaneous Dynamic Range

The estimated CW power from offline processing is calibrated from all gains, offsets and system losses using the following equation

$$P_{receive}^{dBm} = P_{estimate}^{dBm} - IRgain^{dB} + RFattenuator^{dB} + RFattenuator_{offset}^{dB} - SC^{dB} - SC_{offset}^{dB} + losses_{system}^{dB} \quad \text{Equation 3.2}$$

where the value of $losses_{system}^{dB}$ is measured 7 dB for type I-II parameters and 4 dB for type III-IV parameters.

The SNR is calculated by finding the difference between the peak received power of CW signal and noise floor. Figure 3.27 shows the relationship between the SNR and the received power for type I-IV parameters, where the highest SNR i.e. IDR is found over 29 dB in all frequency ranges. Moreover, the sensitivity of the receiver is found below -90 dBm with at least 9 dB SNR criteria. The noise figure (NF) i.e. difference between theoretical noise floor and measured noise floor, is also calculated and found to be between ~11-14 dB. Table 3.5 summarizes all the performance parameters of the receiver.

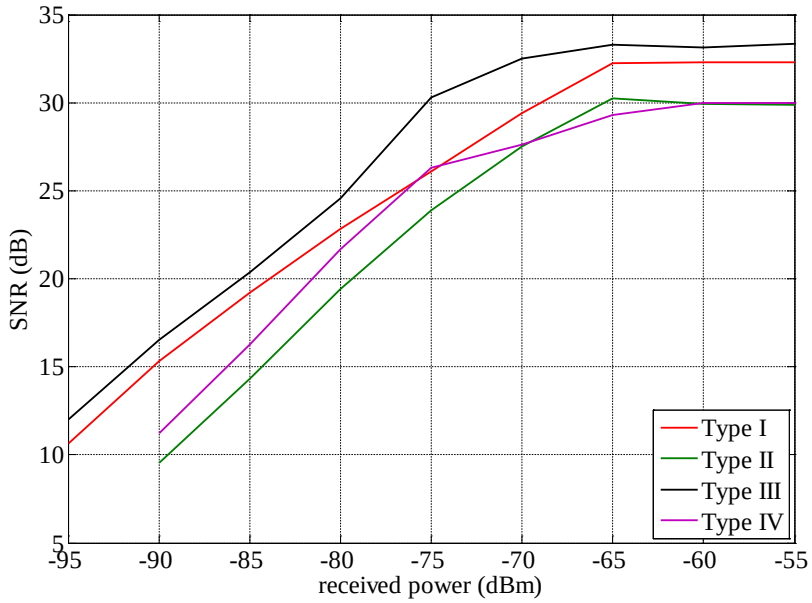

Figure 3.27 Received power versus measured SNR

Table 3.5 Performance parameters of receiver for type I-IV configurations

Type	Noise floor dBm	NF dB	Sensitivity dBm	Sensitivity SNR (dB)	IDR dB
I	-105.63	12.35	-95	10.63	32.31
II	-99.52	14.48	-90	9.52	29.89
III	-107.03	10.95	-95	12.03	33.32
IV	-101.21	12.79	-90	11.21	29.98

3.4 Extension to Multiple Receivers

This section covers the details of multiple receivers developed to create a homogenous test-bed to perform distributed channel measurements. Mainly, three units: 1) LO, 2) down-converter, 3) command and control, are developed for six independent receivers centred at 2.575 GHz.

The magnitude response of all LO units (UCout) are recorded on the SA as shown in figure 3.28. In order to calibrate the gains of the RF attenuator in the down-converter units and command and control unit, the experiment is repeated for all receivers as given in section 3.3.1. Figure 3.29-3.30 shows the comparison of the offset among all receivers. Table 3.6 summarizes the amount of hardware developed as part of this PhD and table 3.7 summarizes the specifications of the developed receiver.

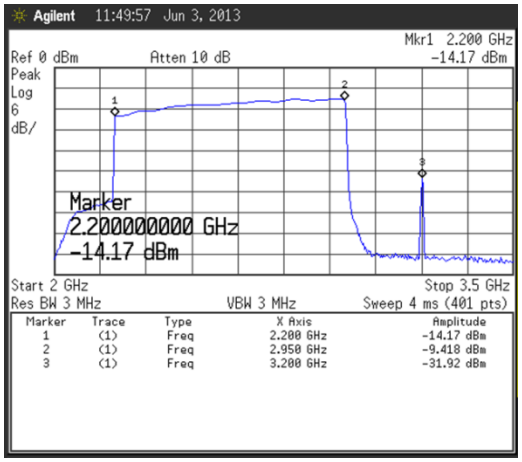

(a)

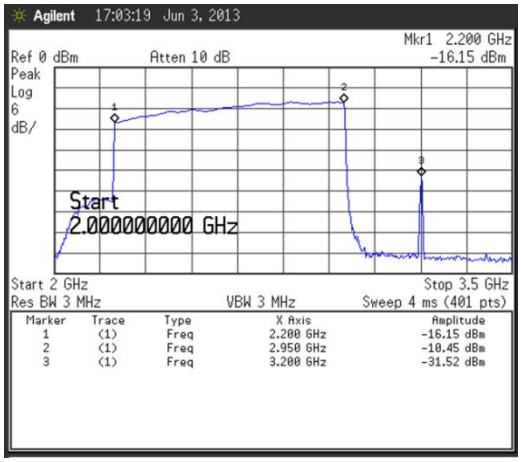

(b)

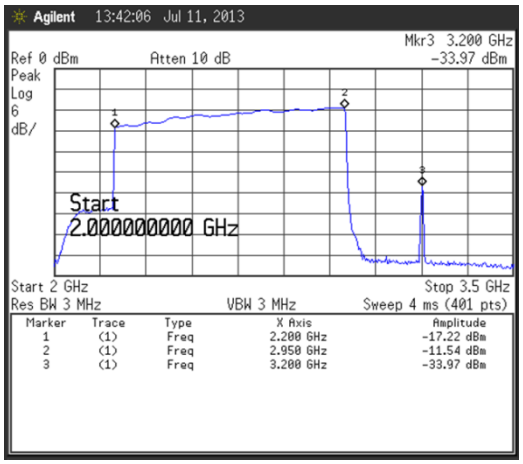

(c)

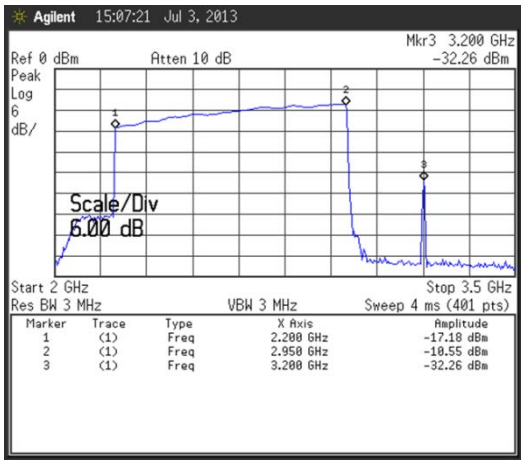

(d)

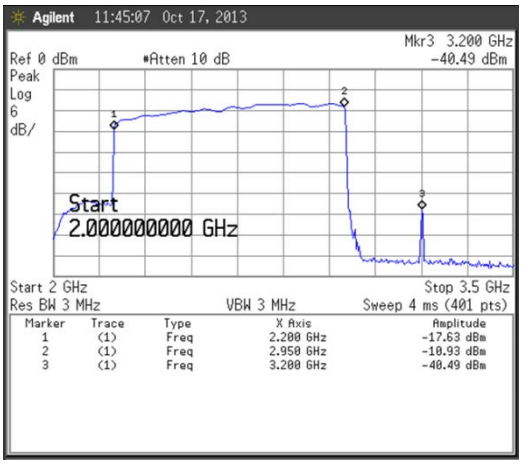

(e)

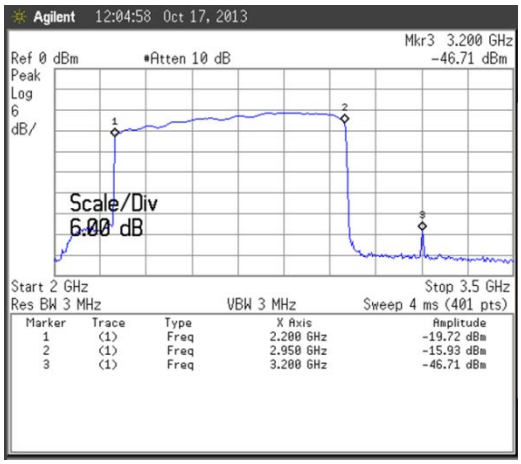

(f)

Figure 3.28 Magnitude response of LO unit installed in receiver (a) “1”, (b) “2”, (c) “3”, (d) “4”, (e) “5”, (f) “6”

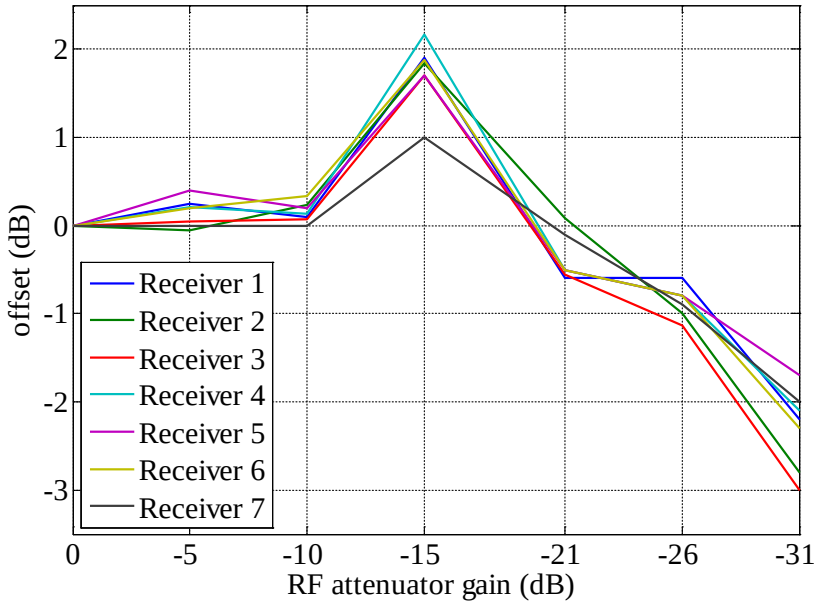

Figure 3.29 Offset in RF attenuator for all receiver

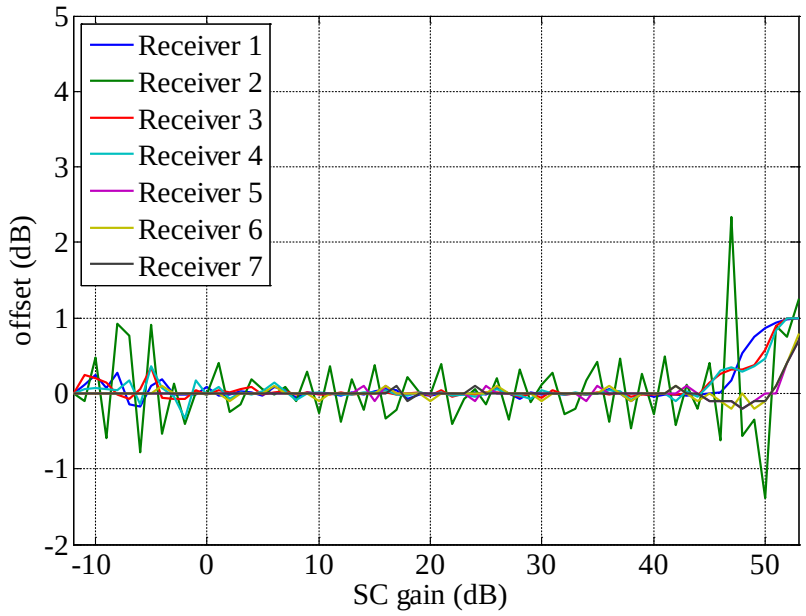

Figure 3.30 Offset in SC circuit for all receiver

Table 3.6 Summary of developed hardware

Unit	Quantity	Prototype	Tested and Validated
LO	6	0	Yes
Down-converter	7	0	Yes
Command and Control (receiver)	7	1	Yes
Command and Control (transmitter)	0	1	Yes
Receiver	6	0	Yes
Transmitter	0	1	Yes

Table 3.7 Specifications of developed chirp channel sounder receiver

Center frequency (MHz)	625	2575
Frequency Range (MHz)	250-1000	2200-2950
Bandwidth (MHz)	750	750
Minimum time resolution (μs)	204.8	204.8
Frequency resolution (kHz)	1000	1000
Instantaneous dynamic range (dB)	>29	>29
Sensitivity (dBm)	-90	-90
NF (dB)	14.48	12.79

3.5 References

[1] S. R. Systems. *PRS 10 Rubidium Oscillator*.
Available: http://www.thinksrs.com/products/PRS10.htm

[2] Euvis. *DSM202*.
Available: http://euvis.com/products/mod/dsm/dsm202/index.html

[3] Hittite. *HMC636ST89*.
Available: https://www.hittite.com/products/view.html/view/HMC636ST89

[4] Minicircuits. *ZEM-4300+*.
Available: http://194.75.38.69/pdfs/ZEM-4300+.pdf

[5] Minicircuits. *ZX10-2-42+*.
Available: http://194.75.38.69/pdfs/ZX10-2-42+.pdf

[6] Minicircuits. *ZX60-5916M+*.
Available: http://194.75.38.69/pdfs/ZX60-5916M+.pdf

[7] N. Instruments. *NI 6501*.
Available: http://sine.ni.com/nips/cds/view/p/lang/en/nid/201630

[8] N. Instruments. *NI 5132*.
Available: http://sine.ni.com/nips/cds/view/p/lang/en/nid/203719

4 Measurements

4.1 Opportunistic Spectrum Access in the 2.4 GHz ISM band

4.1.1 Background

CR is becoming a vital technology for enhancing spectrum utilization by accessing spectrum holes opportunistically in time, frequency and space, provided it is interference free to the local users of the network [1]-[2]. To avoid interference, a CR must be able to detect the spectrum holes reliably, which depends on the hardware used to sense the radio spectrum [3] and the detection algorithm used to detect the spectrum holes [4]-[5]. In this section, a CR module which can perform sensing and detection is referred to as a *"Sensing Engine"* (SE).

There are two commonly used techniques for the implementation of wideband SE which satisfy Nyquist sampling theorem: homodyne and heterodyne [5-7]. For large sensed bandwidths, the heterodyne technique has low time resolution but requires a low sampling rate to digitize the baseband signal. While, the homodyne technique provides high time resolution however needs higher sampling rates commensurate with the sensed bandwidth, which makes them difficult for practical implementation over a wide bandwidth. The advantages of both methods i.e. low sampling rate and high time resolution are taken to adopt a hybrid approach, where instead of using a CW LO to directly down convert a large sensed bandwidth to zero IF, the LO is swept across the sensed bandwidth so that each frequency of the LO down converts to low IF, which can be further digitized using a low sampling rate using a chirp channel sounder receiver [8]. Based on the hybrid approach, a SE was implemented and reported in [8], which has 250 MHz sensed bandwidth with a time resolution of 4 ms.

In terms of hardware, the performance of the SE is measured based on the time resolution and frequency resolution, sensitivity, IDR and sensed bandwidth [9]-[10]. The large sensed bandwidth is required to increase the chances of finding spectrum holes and possible bandwidth aggregation. To detect weak signals, a SE is required to have high sensitivity to overcome the hidden node problem and large dynamic range for reliable detection of weak signals in the presence of strong signals.

Similarly, higher values of the time resolution allow the SE to capture short duration signals. In order to detect narrow band signals present in the sensed bandwidth higher frequency resolution is required. For instance, the 2.4 GHz ISM band has a variety of power limited signals, which are short in duration on the order of a few 100 µsec and have a narrow bandwidth up to 1 MHz [11]. So, to detect signals in this band, a SE must have a time resolution to capture the signal at the packet level with at least 1 MHz frequency resolution. In this section the implemented SE i.e. chirp channel sounder receiver, is used to perform occupancy measurements from 2.2 GHz to 2.95 GHz band, which can sense large bandwidths up to 750 MHz and also provide high time and frequency resolutions.

To avoid interference, CR users access the spectrum holes in time, frequency and space or any of their combinations [2, 12, 13]. For opportunistic access in the time domain, measurements have been performed to characterize the idle time window (i.e. continuous fraction of time when the local users of the network are in the idle state) using high time resolution [14] and low time resolution SE [15]. Although low time resolution SE can sense multiple radio technologies or multiple channels of a radio technology over a wide bandwidth it cannot capture the signal at the packet level due to low time resolution. While, the high time resolution SE provides signal detection at the packet level, generally it covers a narrow bandwidth. For example, in [14] narrowband measurements with high time resolution SE were performed to characterize the idle time window for different radio technologies available up to 2 GHz. In [13, 16] a narrow band vector signal analyzer was used to perform high time resolution measurements to find the idle time window in a 2.4 GHz WLAN channel, where the data packets were generated artificially to stimulate network traffic in an interference controlled environment. This approach facilitates the identification of idle time window from a known pattern of transmitted data packets. In [17], four narrowband sensors were used to monitor the 2.4 GHz WLAN traffic. To sense all the WLAN channels, the span was divided into 16 channels and each channel was traversed sequentially after 8.192 s. Due to this long traversing time, concurrent and continuous real network traffic is not possible to monitor in all channels.

For opportunistic spectrum access in the time domain, a two state (busy/idle) continuous time semi-Markov model has been proposed in [13, 16, 17] where

empirical distribution of the idle time window in the 2.4 GHz WLAN band is fitted using distributions like exponential distribution, generalized pareto distribution and phase type distribution. Although, phase type distributions, which are complex to compute due to the high number of parameters, provide excellent fit, comparatively less complex distributions like the generalized pareto can also provide better fit. In [14] this analysis was further extended by modelling empirical distributions of radio technologies available up to 2 GHz using a wider set of numerically simple distributions. We will use these numerically simple distributions to model the statistics of idle time windows for signals available above the 2 GHz frequency range. Although, the implemented SE can monitor signals below 2 GHz; however in this section, the analysis is only focused for signals which are presents above 2 GHz. Moreover, the effect of using different time resolution on the statistics of idle window will also be investigated.

Directional antennas were used in [18-20] to find the effect of angular dimension on the spectrum occupancy. These measurements were conducted using considerably low time resolution per antenna or angle, ranging from 6 s to over a minute, which makes it difficult to capture signals at the packet level. We will also investigate the effect of angular dimension on the statistics of idle time window.

Although previous work used different SEs and distributions to model the statistics of idle windows; however they have the following shortcomings:

- The wideband SEs have low time resolution which makes it difficult to detect signals at the packet level [15]. The implemented SE is wideband and is capable of detecting signals at the packet level with 204.8 µsec time resolution.
- Single or multiple SEs were used to measure idle time window. However they can't detect multiple channels of a radio technology or multiple radio technologies concurrently due to having limited sensing bandwidth [13, 14, 16, 17]. The implemented SE supports 750 MHz swept bandwidth which allows it to detect multiple channels of a radio technology or multiple radio technologies concurrently at the packet level due to having low time resolution up to 204.8 µsec.
- The empirical distribution of idle time window was previously modelled using exponential, generalized pareto and phase type distributions for 2.4 GHz WLAN signals [13, 16, 17]. Moreover, the statistics of the idle time window were not presented for individual WLAN channels. In this work, in addition to the exponential

and generalized pareto distributions, Weibull, gamma and lognormal distributions are also tested and shown to provide appropriate fit to the idle time window under certain traffic load conditions. Moreover, analysis is presented for each of the concurrently measured WLAN channels.

- This work also investigates the effect of time resolution on the statistics of the idle time windows, which is vital to understand the accuracy of the width of the idle time windows in relation to the time resolution used during the measurement.
- Previous measurements were performed using omnidirectional antennas [13-17]. This work first investigates the effect of the angular dimension and time resolution per angle on the presence of signals at the packet level. Then, using the OR hard combining technique, a local user of network is considered as being in a busy state if it is detected in any of the angular dimensions, and combines their occupancy decisions in order to analyse the statistics of the idle time window per WLAN channel.

4.1.2 Experimental Setup

The implemented SE was configured with 750 MHz swept bandwidth with time resolution of 204.8 µsec to sense signals from 2.2 GHz to 2.95 GHz. It is placed to take measurements in an indoor environment to detect data packets based on the received power. The SE was used in conjunction with a custom designed wideband discone antenna, placed at 1.5 m above the ground on the 2nd floor of the School of Engineering and Computing Sciences at Durham University, UK. In the initial assessment measurement, only the 2.4 GHz WLAN signal was detected in the sensed bandwidth as shown in figure 4.1. To analyse the occupancy of the 2.4 GHz WLAN signal, the swept bandwidth of the SE was reconfigured to 100 MHz in the frequency range between 2.4 GHz to 2.5 GHz with a time resolution of 204.8 µsec. The measurements were taken on the 19th May, 2014 from 01:15 pm to 01:35 pm.

For the directional measurements from 2.4 GHz to 2.5 GHz, three commercial log periodic vertically polarized antennas were used with beam widths of 55 degrees [21]. The antennas were placed at 1.5 m above ground with angular separation of 90

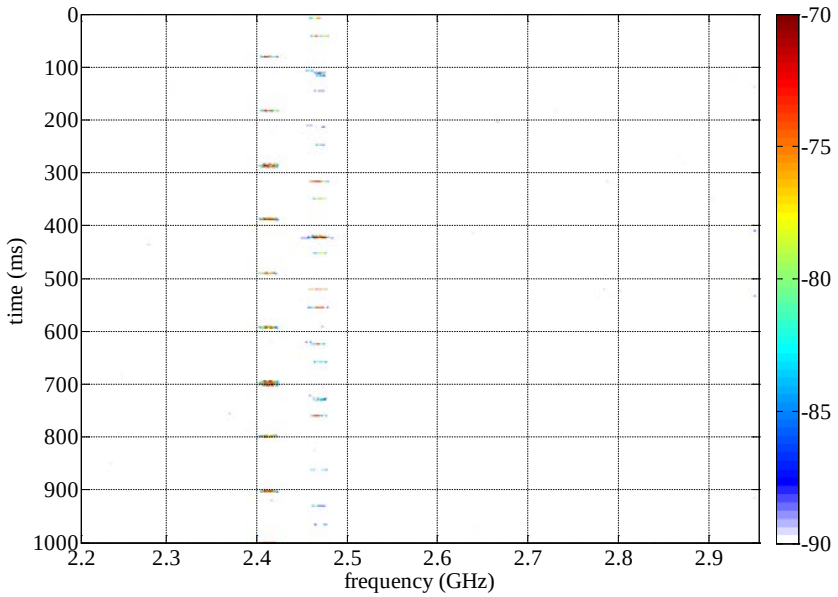

Figure 4.1 Time-frequency map from 2.2 GHz to 2.95 GHz

degrees. Due to having three antennas, which are switching at 204.8 µsec, the time resolution per antenna or direction is 819.2 µsec, which corresponds to the switching time between three antennas and an additional reference sweep is taken to get the correct antenna switching sequence in each data file. The measurements were performed on 23rd May, 2014 from 05:20 pm to 05:40 pm.

In both sets of measurements, the raw data were acquired with 80 MHz sampling rate in multiple files containing 2 seconds of data. For omnidirectional and directional measurements, 1171740 and 976080 snapshots were collected and processed with 400 kHz frequency resolution by applying a high order Gaussian window which is sufficient to detect 22 MHz wide WLAN channels.

4.1.3 Data Analysis Methodology

To compute the detection of signals in the sensed bandwidth the energy detection algorithm is used, where the received power is compared with a predefined threshold. Based on this, a binary time series is created in which “1” represents busy state and “0” represents idle state in a channel. Further to this, the duration of consecutive 0’s in a binary time series is computed to estimate the idle time window and its empirical cumulative distribution function (CDF) is computed.

The empirical distribution is fitted with generalized pareto distribution (GP), Weibull distribution (WB), exponential distribution (EX), gamma distribution (GM)

and log normal distribution (LN). The associated parameters (shape: k, scale: δ and location: μ) are found based on maximum likelihood techniques and used to compute the mean: M for the fitted distribution, table 4.1 summarizes the distribution functions along with the mean formula for the respective distribution.

Table 4.1 Distribution functions

t_w denotes idle time window ($t_w \geq 0$),exp(.) is exponential function, $\Gamma(.)$ is gamma function, $\gamma(.,.)$ is lower incomplete gamma function and erf(.) is complementary error function.

Distribution	Function and Mean
GP	$F(t_w) = 1 - \left(1 + k\left(\frac{t_w}{\delta}\right)\right)^{-\frac{1}{k}}$ $M = \frac{\delta}{1-k}$, $k < 1$
WB	$F(t_w) = 1 - \exp\left(-\frac{t_w}{\delta}\right)^k$ $M = \delta\Gamma\left(1 + \frac{1}{k}\right)$
EX	$F(t_w) = 1 - \exp\left(-\frac{t_w}{\delta}\right)$ $M = \delta$
GM	$F(t_w) = \frac{1}{\Gamma(k)}\gamma\left(k, \frac{t_w}{\delta}\right)$ $M = k\delta$
LN	$F(t_w) = \frac{1}{2}\left(1 + \text{erf}\left(\frac{ln\, t_w - \theta}{\sqrt{2}\delta}\right)\right)$ $M = \exp\left(\theta + \frac{\delta^2}{2}\right)$

In order to measure the goodness of fit between the empirical and used distributions, Kolmogorov Smirnov (KS) test is used and the distribution with minimum KS distance is chosen as the best representative of the empirical distribution.

4.1.4 Analysis

The analysis of both measurements taken using omnidirectional and directional antennas will be discussed in the following sub sections.

4.1.4.1 Omnidirectional Measurements

This section provides analysis of the measurements taken with the omnidirectional antenna in the frequency range from 2.4 GHz to 2.5 GHz. Figure 4.2

shows the time-frequency map of the WLAN traffic over the duration of 1000 ms, where -97 dBm is chosen as the decision threshold which is 10 dB above the noise floor level i.e. ~-107 dBm.

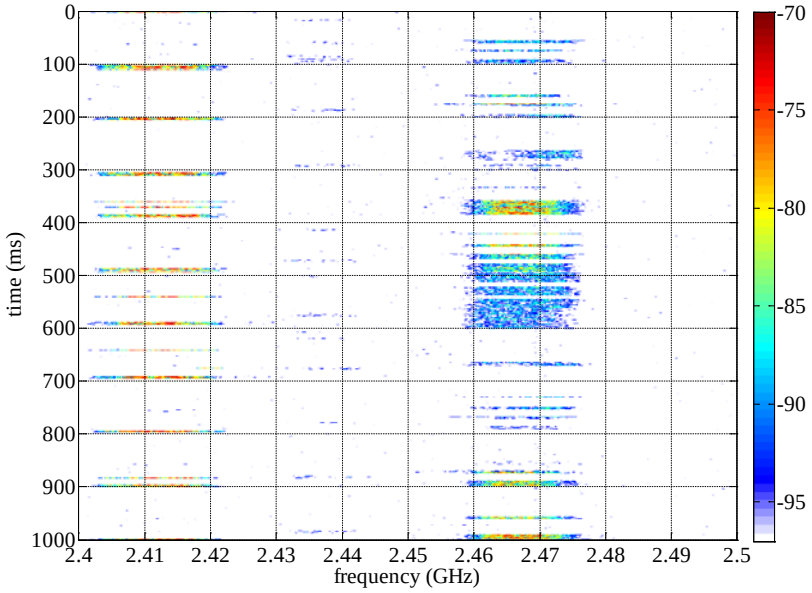

Figure 4.2 Time-frequency map from 2.4 GHz to 2.5 GHz

Figure 4.2 shows that most of the user's activity is present in the WLAN channels "1" and "12", which are used by the School's staff and students. There are different WLAN packets with different durations. For example, channel "1" does not remain in the busy state all the time. It remains in the idle state for various durations as represented by the 'white' colour in the time-frequency map thus by exploiting the idle state of the channel, it can be accessed in the time domain by the CR users. In order to find the statistics of the idle time window, both channels are further processed to get the binary time series as shown in figures 4.3-4.4.

Figure 4.4 shows the empirical CDF of the idle time window found in channel "1". The gamma distribution provides the best fit with minimum KS distance (D) and the estimated parameters are $k = 0.4898$, $\delta = 73.8318$ and the mean M = 36.1628 ms. Apart from this, the log normal distribution also provides second best fit.

It is also important to observe that the empirical CDF tends to increase rapidly in the interval (95 ms, 100 ms). The reason for such long windows is because the channel was in the idle state most of the time and the occupancy state was changing due to the arrival of the beacon packet which is observed to arrive every

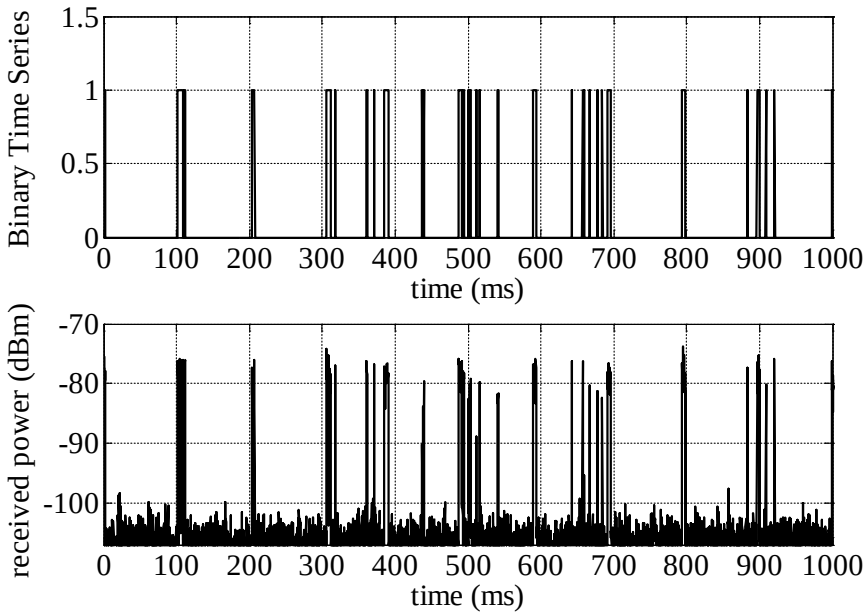

Figure 4.3 Mapping from received power to binary time series in channel "1"

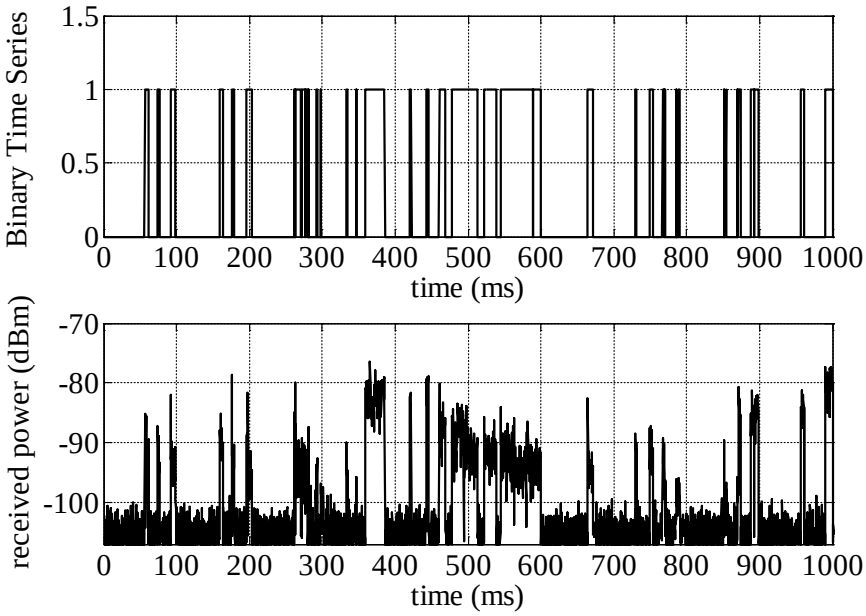

Figure 4.4 Mapping from received power to Binary Time Series in channel "12"

~100 ms. It can also be seen in figure 4.3 where the beacon packets are detected at t = 0, 100, 200, 700 and 800 ms. Figure 4.6 shows the empirical CDF of the idle time window in channel "12" where the generalized pareto distribution provides the best fit with estimated parameters $k = 1.1620$, $\delta = 3.285$. Although, it provides the best fit, since $k > 1$, the mean of the distribution is not finite. To calculate the mean value, the Weibull distribution parameters are used, which provide second best fit to the empirical CDF. The estimated parameters for this distribution are $k = 0.6255$,

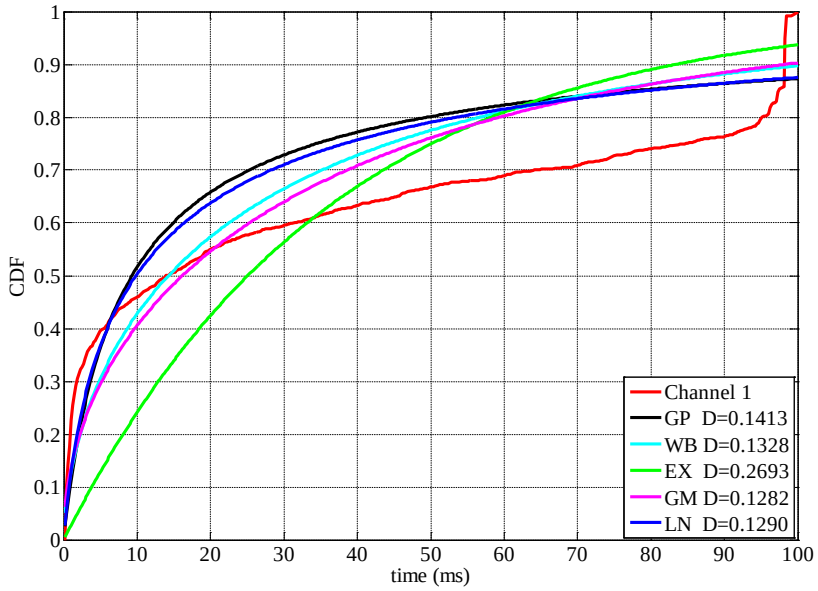

Figure 4.5 Empirical CDF versus fitted distribution of channel "1"

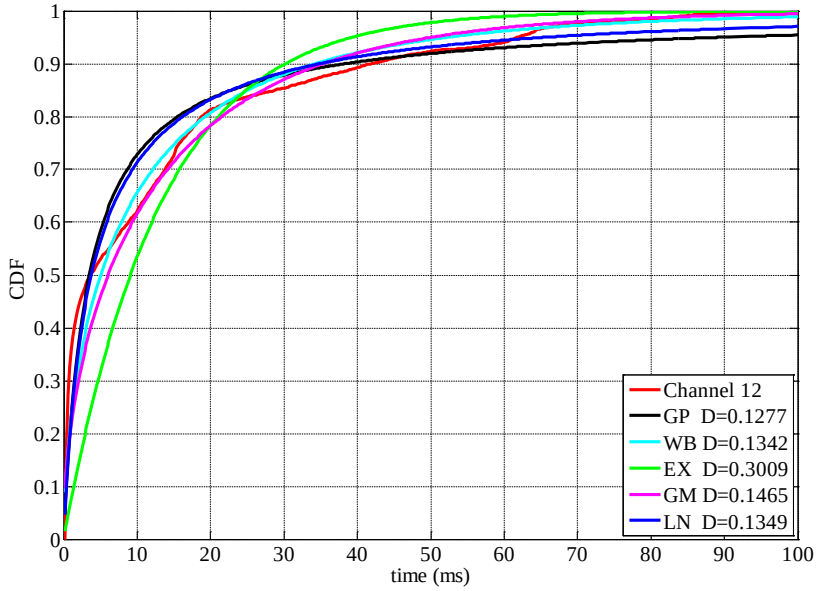

Figure 4.6 Empirical CDF versus fitted distribution of channel "12"

δ =9.0156 and the mean M = 12.8766 ms. By comparing both empirical CDFs, it is observed that channel "1" has less traffic load which provides larger idle time windows, so it is most suitable for CR users. Another key observation is that, it is not possible to have idle time window greater than 100 ms since the WLAN access point was periodically transmitting a beacon packet every ~100 ms. Beacon intervals can be extended when the traffic load is low on a channel. This can provide longer time

windows and allow multiple CR users to transmit/receive or a single CR user can transmit continuously.

During sensing, the SE is swept across the sensed bandwidth where each frequency point is traversed after the configured time resolution. To investigate the effect of low time resolution on the statistics of idle time window, the time series of both channels are resampled individually in the time domain with 1.6384 ms and 3.2768 ms time resolutions. This will help to illustrate the effect on the idle time window if network traffic is sensed using low time resolution SE. Figures 4.7-4.8 show the effect of different time resolutions on channels “1” and “12”, where reducing the time resolution tends to increase the duration of the idle time window. This apparent increase is due to the SE inability to detect packets with duration less than the time resolution. Thus, measurements performed using low time resolution SE do not provide reliable data for modelling time based radio spectrum access.

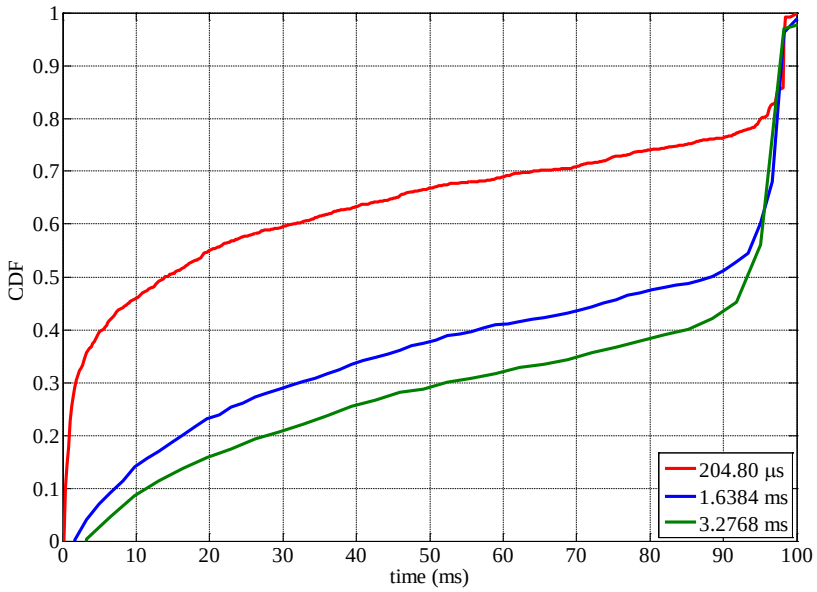

Figure 4.7 Effect of time resolution on empirical CDF of channel “1”

The empirical distributions can be further utilized to study how the variability of the load in a channel affects the fitted distributions and its parameters. Table 4.2 summarizes the KS distance between the empirical and fitted distributions. The generalized pareto distribution is found to have the best fit for channel “1” while the lognormal distribution provides the best fit for channel “12” for the time resolutions of 1.6384 ms and 3.2768 ms respectively.

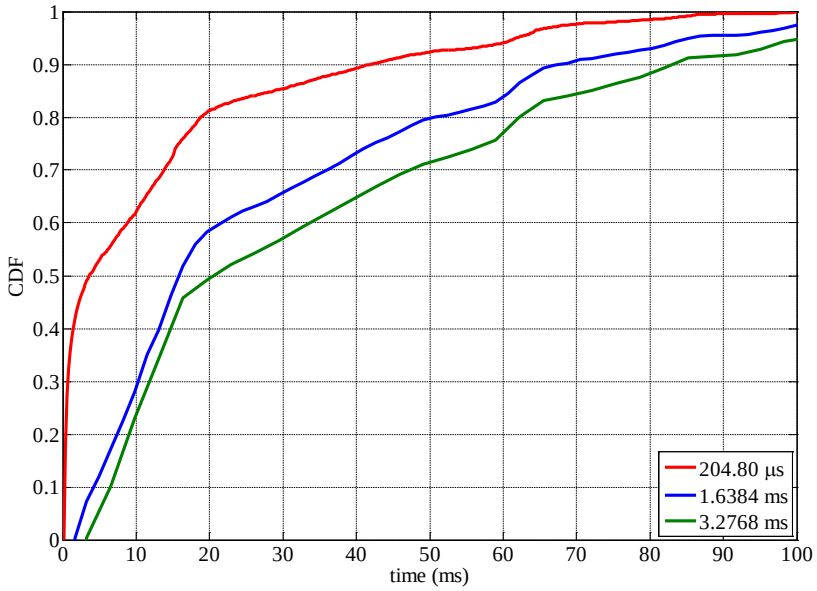

Figure 4.8 Effect of time resolution on empirical CDF of channel "12"

Table 4.2 KS distance for fitted distribution for different time resolutions

CDF	Channel 1			Channel 12		
	204.8 µs	1.6384 ms	3.2768 ms	204.8 µs	1.6384 ms	3.2768 ms
GP	0.1413	**0.2412**	**0.2741**	**0.1277**	0.1054	0.1507
WB	0.1328	0.2578	0.2879	0.1342	0.1321	0.1560
EX	0.2693	0.2492	0.2969	0.3009	0.1067	0.1522
GM	**0.1282**	0.2537	0.2900	0.1465	0.1408	0.1724
LN	0.1290	0.2449	0.2903	0.1349	**0.0796**	**0.1438**

For both channels, the mean idle time window was calculated for comparison with the exception for channel "12" for 204.8 µs time resolutions where the parameters of WB are used. Table 4.3 summarizes the parameters and the mean value for distributions which provide the best fit. The mean value tends to increase with the drop in traffic load as the channels remain in the idle state for longer time windows. These results show that previous work [16, 17], where the generalized pareto distribution was shown to provide the best fit or second best fit, the lognormal and gamma distributions can also be used to model the behaviour of the idle time window for different network traffic loads. Moreover, by having wideband detection capability, a CR user can monitor the traffic load on a particular or multiple channels and can concurrently exploit the idle state in multiple channels or radio technologies (e.g. WLAN, Bluetooth and LTE).

Table 4.3 Parameters for best fitted distribution

	Channel 1			Channel 12		
	204.8 µs	1.6384 ms	3.2768 ms	204.8 µs	1.6384 ms	3.2768 ms
k	0.4898	-0.4276	-0.4968	0.6255	-	-
δ	73.8318	87.5879	102.667	9.0156	0.9796	0.9142
μ	-	-	-	-	2.9397	3.2385
M	36.1628	61.3533	68.5910	12.8766	30.5544	38.7210

4.1.4.2 Directional Measurements

The directional measurements are presented in this section to find out how the angular dimension influences the statistics of idle time window. Three antennas (A1, A2 and A3) are used for this indoor measurement. Figure 4.9 shows the effect of different directions on the received power in channel "1" where it is observed that antenna A3 has a higher received power compared to the other two antennas. Similarly, antenna A1 has a higher received power for channel "12" as shown in

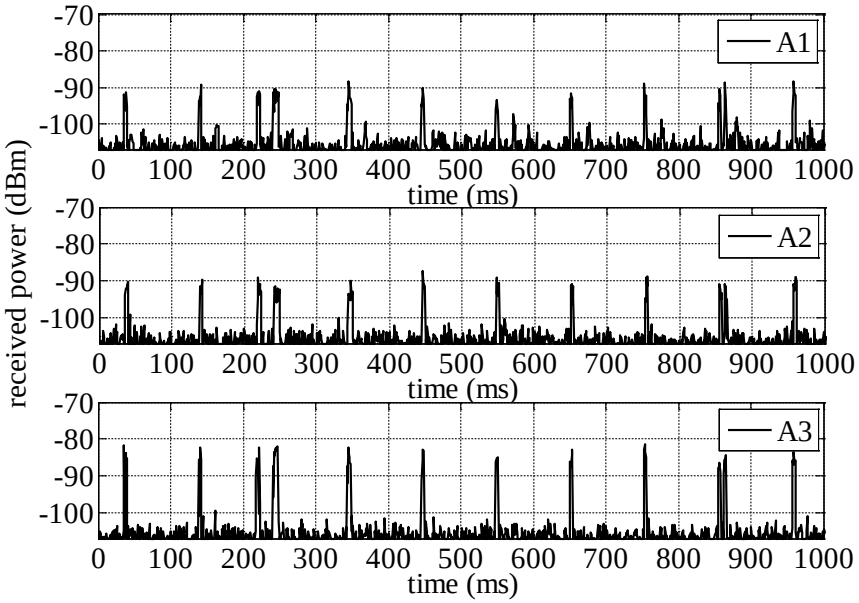

Figure 4.9 Effect of directional antennas on received power and short duration packets in channel "1"

figure 4.10. It is expected to have power level variations in different directions; however if at a certain direction the received power is lower than the decision threshold due to propagation effects, the channel may be considered in the idle state. Further to this, the time resolution per antenna also affects the state of the channel. For example, consider antenna A3 of channel "12" where the received power dropped by more than 10 dB and it cannot detect short duration packets.

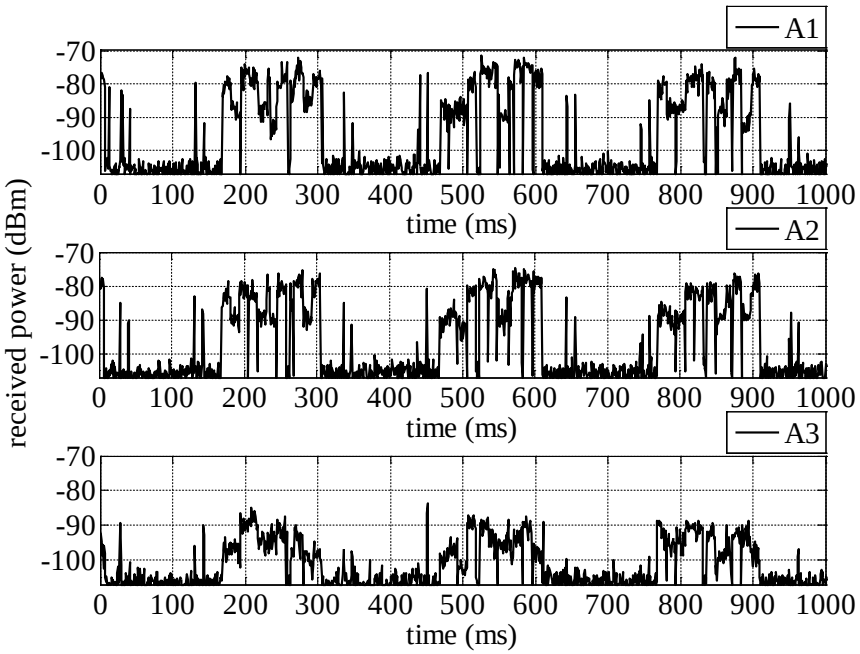

Figure 4.10 Effect of directional antennas on received power and short duration packets in channel "12"

A decision threshold of -97 dBm is used per direction to find the respective binary time series. In order to remove the uncertainty in the occupancy state due to the received power variations or the effect of time resolution per antenna, the binary time series are combined using the OR hard combining data fusion technique, where, a channel is considered in the busy state if it is detected in any of the directions. This series is used to compute the empirical CDF of the idle time window. Figure 4.11 shows the empirical CDF of both channels and table 4.4 summaries the KS distance for fitted distributions. The Weibull distribution provides the best fit for channel "1" with parameters k =1.1070 and δ = 51.7498. Channel "12" empirical CDF is fitted best with the lognormal distribution with parameters δ = 1.4980 and μ = 2.6644 with mean values equal to 49.8307 ms and 44.0975 ms. Thus the analysis shows that the angular dimension can influence the statistic of the idle window due to propagation effects and the time resolution per antenna used to acquire the data. In order to compensate for these effects, decisions can be made using the OR combining technique. However, the time domain based directional opportunistic spectrum access can be vital in the situation where communication links for a local user of a network are highly directional.

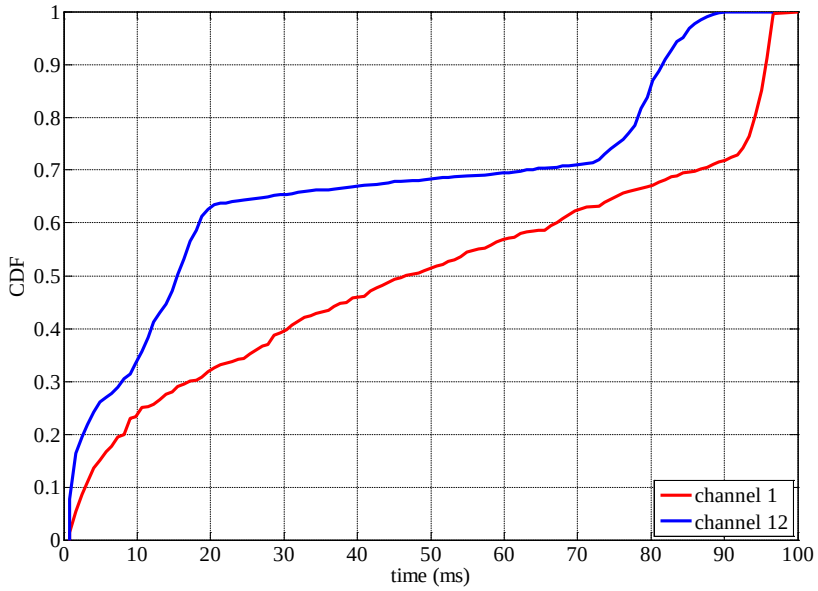

Figure 4.11 Empirical CDF of channels using OR combining technique

Table 4.4 KS distance for fitted distribution

CDF	Channel 1	Channel 12
GP	0.1610	0.1771
WB	**0.1459**	0.1654
EX	0.1480	0.1801
GM	0.1477	0.1651
LN	0.1751	**0.1473**

4.1.5 Summary

Both omnidirectional and directional high time resolution measurements were performed to model the distribution of the idle time window in the 2.4 GHz ISM band. It is found that distributions such as gamma, lognormal and Weibull can also be used to model the idle state of a 2.4 GHz WLAN channel. Moreover, previous reported measurements provide statistics of the idle time window over the full span of a radio technology which doesn't provide the statistics per channel. Here, analysis is performed per channel, which shows that different channels in a radio technology may have different idle time window statistics and their idle state can be modelled using different distributions.

In addition, previously reported high time resolution measurements are performed using narrow band SE thus they can only detect a specific radio technology. The presented SE has the capability to provide detection of various radio

technologies over a wide bandwidth which can increase the chances to find time based spectrum opportunities more efficiently in CRN.

4.2 Long Term Spectrum Occupancy Measurement

4.2.1 Background

The concept of CR is emerging rapidly and becoming a reality in order to improve the spectrum utilization. The reliable spectrum occupancy measurements are essential to understand spectrum utilization in time, frequency and space and also to provide a knowledge-base to model spectrum utilization. These empirical models are essential to define protocols for "*when and how*" the users of CR networks can access the spectrum holes and induce limited interference to the licensed users of the network.

To study spectrum utilization, several spectrum occupancy measurements have been performed worldwide in both indoor and outdoor environments using spectrum analyzers [22-27] or dedicated receivers [28]. These measurements were performed using different time and frequency resolutions for variable sensed bandwidths as summarized in table 4.5.

Table 4.5 Comparison of difference configurations

Ref.	Frequency Range (MHz)	Bandwidth (MHz)	Time Resolution (s)	Frequency Resolution (kHz)	Type
[22]	80-5850	60	828	150	Narrowband
[23]	300-4900	20	360	300	Narrowband
[24]	450-2700	Variable	0.42	15/100/200	Narrowband
[28]	806-2750	Variable	5-10	15/120/250	Narrowband
[25]	700-3000	2300	0.128	300	Wideband
[26]	770-5250	1500	1	200	Wideband
[27]	75-3000	500	12.5-15	10	Wideband

Particularly, all the campaigns were performed using low time resolution due to which transitions in the occupancy state of the signal is lower than the configured time resolution cannot be captured. This can lead to the under estimation of spectrum utilization. The common conclusions of the aforementioned campaigns are that spectrum is highly underutilized and it is influenced strongly by the spatial dimension.

The aim of this work is to investigate the spectrum utilization in Durham city, UK in both outdoor and indoor environments. In comparison to previous measurements [22-28], a custom designed wideband chirp channel sounder receiver is used to measure the received power in two bands: 1) 250 MHz to 1 GHz, 2) 2.2 GHz to 2.95 GHz. Moreover, measurements are performed at very high time resolution, which enables the receiver to capture the signal at frame or packet level due to which more realistic understanding of the spectrum utilization and transitions in occupancy states can be obtained.

4.2.2 Experimental Setup

The details of the experimental setup for both bands are given in the following two sub sections.

4.2.2.1 Band 1 (250 MHz to 1 GHz)

This band is allocated to various commonly used radio technologies like TETRA, TV, UHF radio frequency identification (RFID) and GSM 900. The receiver is configured to 750 MHz swept bandwidth centred at 625 MHz with time resolution of 3.2768 ms and raw data are processed using a high order Gaussian window to obtain a frequency resolution of 200 kHz. The chosen time and frequency resolutions provide a good trade-off to detect signals from various radio technologies. Particularly, it enables the detection of GSM 900 signal at the frame level[3] in each channel. The measurement is performed in an outdoor scenario, where a log-periodic antenna pointing towards the city centre was placed on top of the roof of the School of Engineering and Computing Sciences, Durham University, UK building as shown in figure 4.12. The selected antenna position provides high received power for most of the radio technologies during initial assessment, which is useful to avoid the hidden node problem due to propagation effects. The 24 hours long term measurement is performed from 09:30 pm (3rd July, 2014) to 09:30 pm (4th July, 2014). A total of 718560 sweeps were recorded over the duration of 24 hours which are sampled at 20 MHz and 499 sweeps were recorded continuously per minute.

[3] A GSM 900 frame duration is equivalent to 4.615 ms.

(a)

(b)

Figure 4.12 Setup for band 1: (a) log periodic antenna, (b) antenna view pointing towards city centre

4.2.2.2 Band 2 (2.2GHz to 2.95 GHz)

This band has two widely used services: a) 2.4 GHz WLAN, b) LTE 2600. The receiver is configured to 750 MHz swept bandwidth centred at 2.575 GHz with a time resolution of 204.8 µs. During the initial assessment, it is found that at the moment, the LTE 2600 service is not available in Durham city, UK. Thus the choice of the time resolution ensured packet level detection of the 2.4 GHz WLAN signal, which is on the order of a few 100 µsec [11]. The raw data are processed using a high order Gaussian window to obtain 1 MHz frequency resolution. The measurement is performed in an indoor environment on the 2nd floor of the School of Engineering and Computing Sciences, Durham University from 01:30 pm (15th July, 2014) to 01:30 pm (16th July, 2014). The received power is measured using a discone antenna, which was placed 1.5 m above the ground level as shown in figure 4.13. A total of 3598560 sweeps were recorded over the duration of 24 hours which are sampled at 80 MHz

and 2499 sweeps were recorded continuously per minute. Table 4.6 summarizes the parameters used to perform the measurements in both bands.

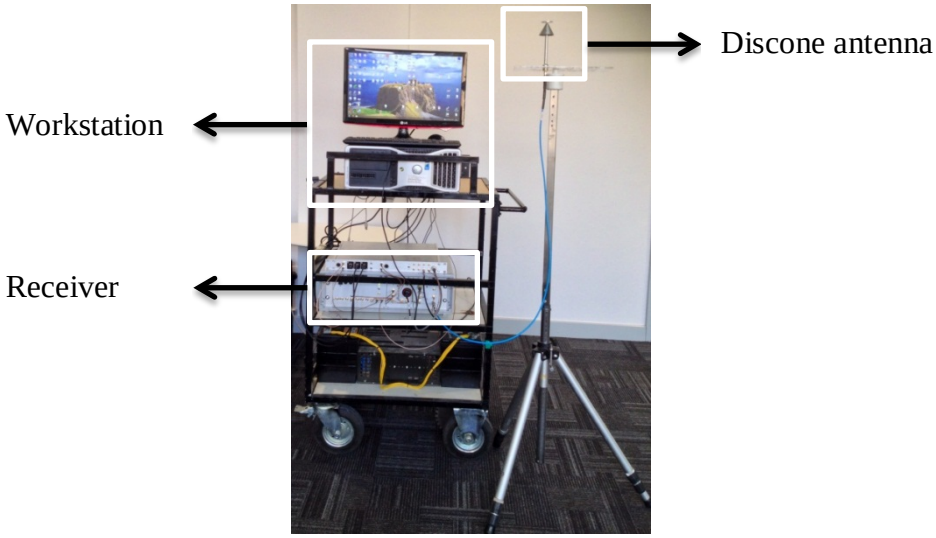

Figure 4.13 Setup for band 2

Table 4.6 Summary of Parameters

Parameter	Band 1	Band 2
Center Frequency (MHz)	625	2575
Sensed Bandwidth (MHz)	750	750
Time Resolution (μs)	3276.8	204.8
Frequency Resolution (kHz)	200	1000
Number of Sweeps	718560	3598560

4.2.3 Data Analysis Methodology

The raw data are calibrated for all gains and losses (receiver, cables and antenna), to get the received power by performing offline processing in MATLAB software package. In order to find the decision threshold, for energy detection algorithm, the thermal noise floor of the receiver is measured by performing a sensitivity test (as given in section 3.3.3). For this, the receiver is configured in both bands individually and data are recorded and processed according to the parameters as given in table 4.6. The noise floor of ~-109 dBm and ~-101 dBm were measured in band 1 and 2 respectively. So, the decision thresholds have been set to 10 dB above the respective noise floor.

4.2.4 Analysis

Figure 4.14 shows the maximum and average received power variations recorded over 24 hours period in band 1. Sub band 1, 250-470 MHz, is mainly assigned to military, aeronautical, and public safety radio technologies in the UK. The highest power levels are detected around 450-465 MHz, which is used for aeronautical services. The sub band 2, 470-880 MHz, is mainly dominated by broadcasting TV transmissions and high power levels are detected for TV channels 33, 49, 50, 54, 55, 58 and 59 while channels 62 and 63 power levels were detected relatively low at the measurement location. Moreover, these TV channels collectively consume around 72 MHz of spectrum in this sub band. The frequencies above 880 MHz are mainly used by UHF RFID and GSM 900 services. Figure 4.15 shows the duty cycle (DC), fraction of time a frequency bin is detected over the measurements duration, variations per minute over the measurement duration in band 1. Two kinds of trends over time can be noticed in the time-frequency map. Firstly, the frequency bin where the received power is always higher than the decision threshold, which is mostly the case for broadcasting signals, has continuous appearance e.g. TV channel 33. Secondly, discontinuous appearance represents the situations where the signal is not present either due to the propagation effects e.g. TV channel 58 or the signal is not transmitted by the transmitter e.g. GSM 900 downlink signal. Figure 4.16 shows the DC over 24 hours for different radio technologies and it is found that band 1 has an average DC, average over all frequency bins, of 0.0985. In order to investigate the time variations in the average DC over 24 hours, the value of average DC is computed per minute. Figure 4.17 shows the time variations in the spectrum utilization, percentage of average DC, in all sub-bands and band 1. Two types of observations can be made:

- A constant value of spectrum utilization indicates the situation where the received power levels are always above the decision threshold e.g. sub-band 2. Moreover, a drop in the received power level is observed in sub-band 2 after 04:30 am due to unknown reasons, which proportionally also affects the DC values as shown in figure 4.15. This causes a sudden drop in spectrum utilization as shown in figure 4.17.
- A variable value of spectrum utilization indicates the situation when the DC value is changed due to unavailability of the signal due to propagation effects or transmitter ON/OFF behaviour e.g. sub-bands 1 and 3. Sub-band 3 is mainly

dominated by GSM 900 uplink (890-915 MHz) and GSM 900 downlink (935-960 MHz) signals and it can be observed that spectrum utilization tends to drop in non-office hours till 05:30 am and have substantial increase in the spectrum utilization during office hours and later on in the evening.

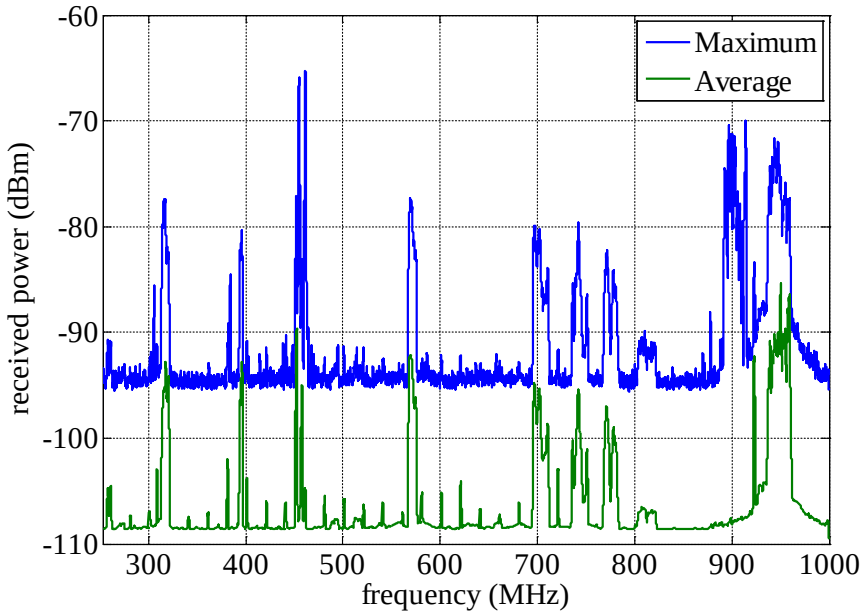

Figure 4.14 Received power level variations in band 1

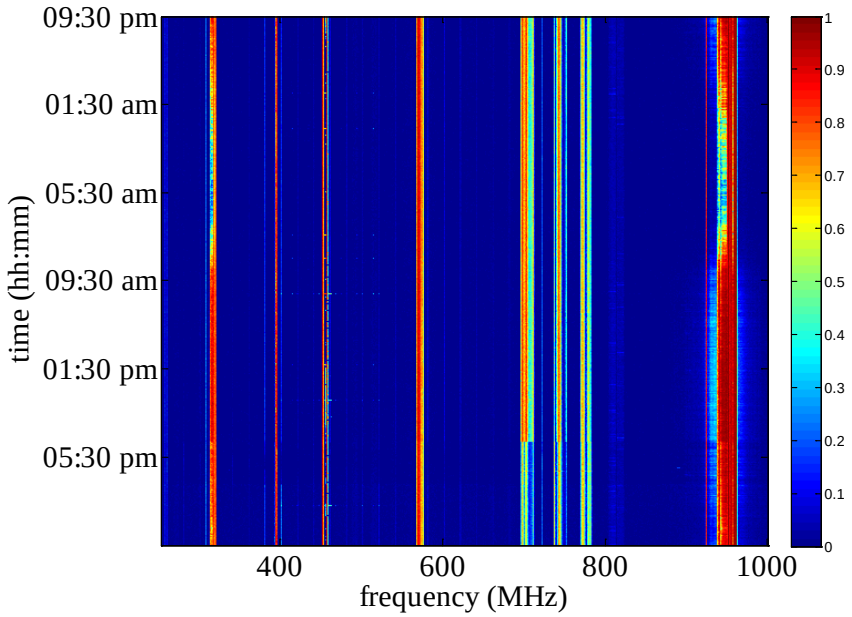

Figure 4.15 Time-frequency map of DC per minute in band 1

Figure 4.18 shows the received power level variations recorded over 24 hours in an indoor environment for band 2. The frequencies from 2.4 GHz to 2.5 GHz, sub-

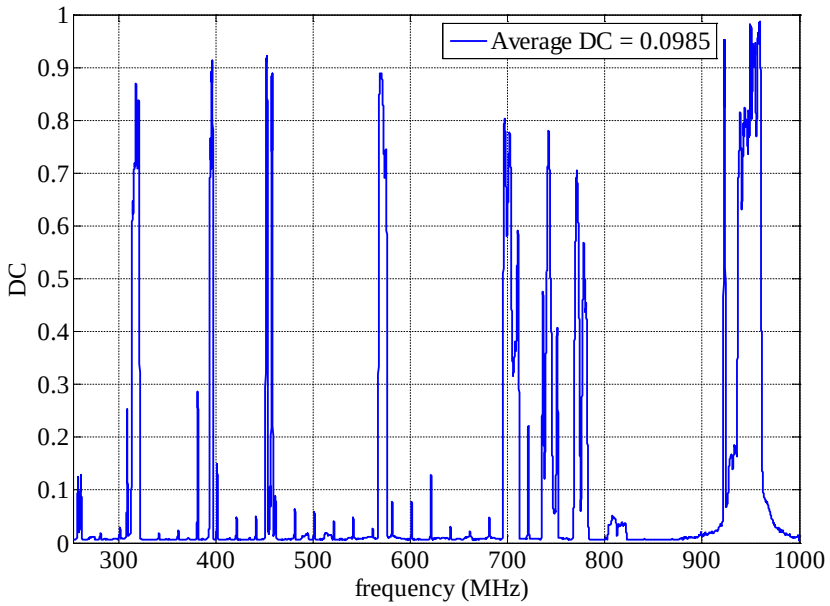

Figure 4.16 24 hours DC in band 1

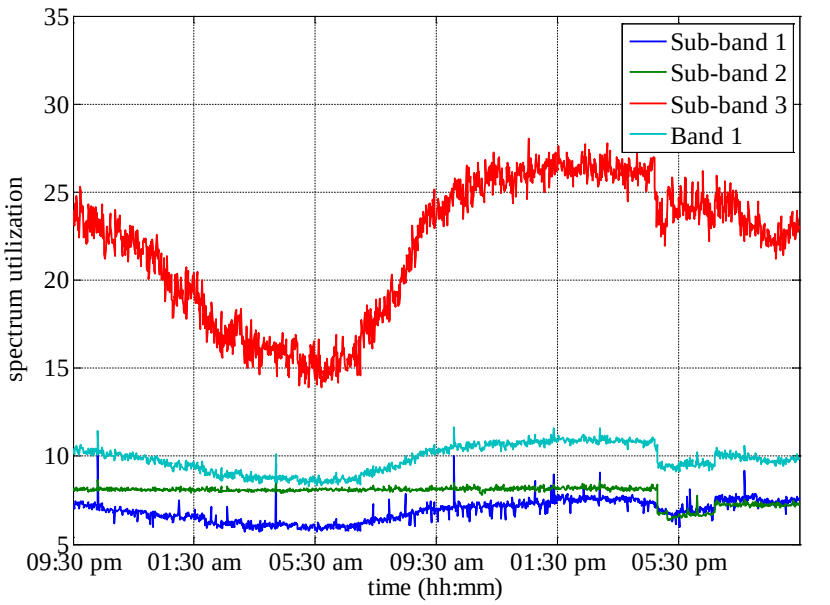

Figure 4.17 Time variations in spectrum utilization over 24 hours in band 1

band 5, are widely used by short range services like 2.4 GHz WLAN, Bluetooth and Zigbee. The 2.4 GHz WLAN signal is detected mainly during the measurement which is generated from Durham University wireless network access points, which provides the wireless internet services for staff and students. In the frequency ranges 2.2-2.4 GHz (sub-band 4) and 2.5-2.95 GHz (sub-band 6), no significant activity is recorded, which makes them a suitable choice for CR applications. Figure 4.19 shows the time frequency occupancy map of DC per minute by applying -91 dBm decision

threshold. The discontinuous occupancy pattern can be observed in the 2.4 GHz ISM band (part of sub-band 5), which indicates the ON/OFF behaviour of the WLAN traffic generated by the WLAN transmitters (e.g. access points, mobile phones, laptop). This ON/OFF behaviour of transmission in the GSM 900 and 2.4 GHz WLAN is very important to understand and can be exploited to create the spectrum opportunities for CR users, where they can access the frequency bin/channel/band in the time domain [29].

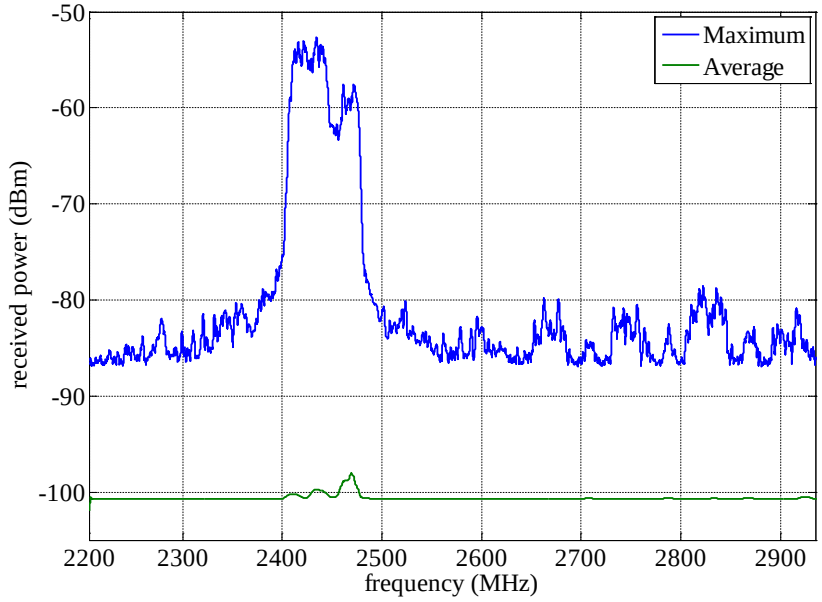

Figure 4.18 Received power level variations in band 2

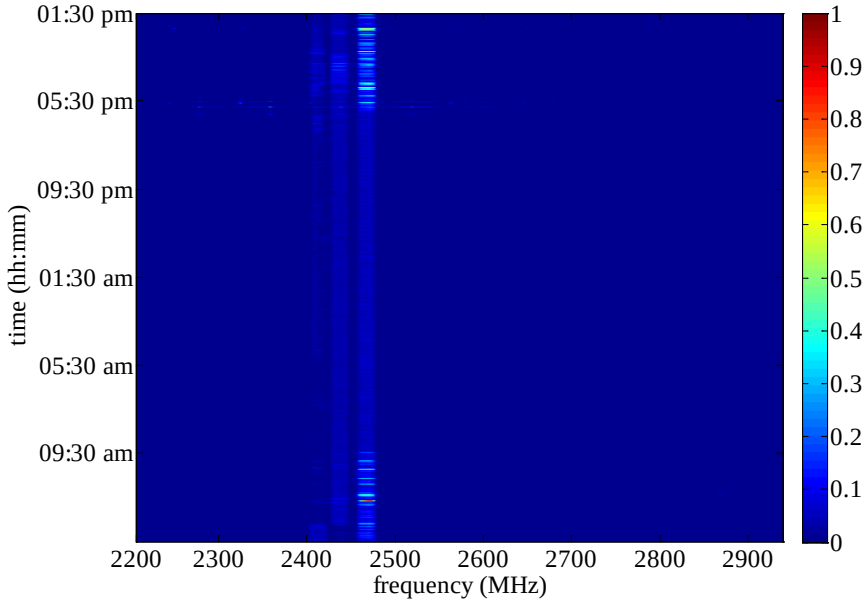

Figure 4.19 Time-frequency occupancy map of DC per minute in band 2

Figure 4.20 shows the DC of band 2 where around 0.0089 of average DC is observed, which is around 11 times lower than band 1. Figure 4.21 shows the time variations in spectrum utilization per minute in band 2 and where the main activity is recorded in sub-band 5. Unlike the cyclic behaviour in spectrum utilization in sub-band 3, the variations in sub-band 5 is more impulsive in nature from 09:30 am to 6:30 pm, having a highest recorded value of 31.22 %.

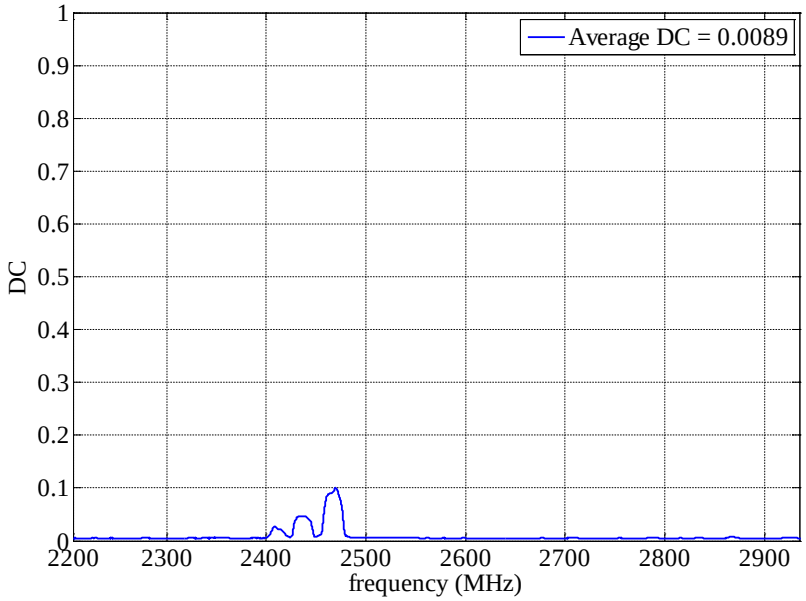

Figure 4.20 24 hours DC in band 2

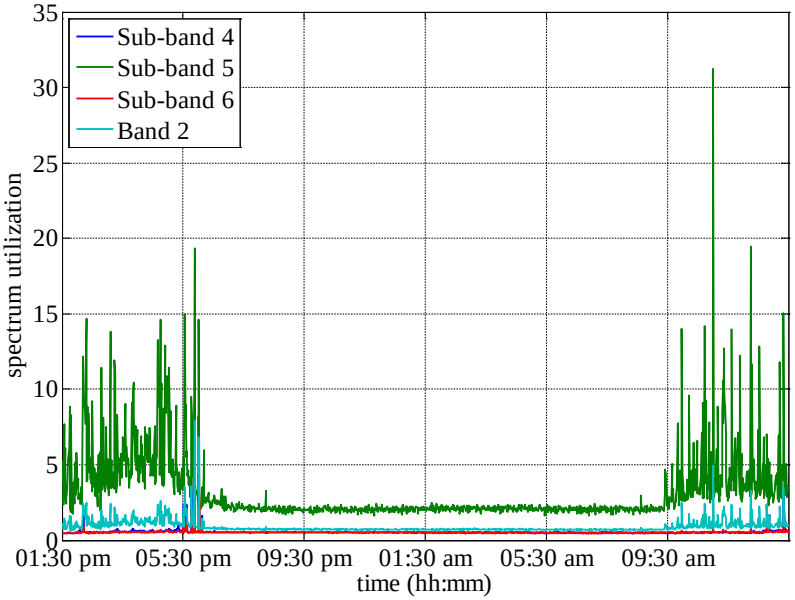

Figure 4.21 Time variations in spectrum utilization over 24 hours in band 2

Table 4.7 provides a comparison of spectrum utilization over 24 hours among different sub bands. Sub band 3 is highly utilized due to the presence of GSM 900, particularly due to the downlink signal. While sub bands 1 and 2 are relatively less utilized having spectrum utilization less than 8%. Band 2 is of more interest for CR applications because sub bands 4 and 6 have less than 1% spectrum utilization which is about 625 MHz of unoccupied bandwidth while sub band 5 have spectrum utilization of 3.15%. The overall spectrum utilization in both bands is 8.08%, which indicates that the spectrum is highly underutilized at the measurement location in Durham city, UK and CR applications can benefit from it by accessing it opportunistically in time and frequency.

Table 4.7 Comparison of spectrum utilization over 24 hours among different frequency ranges

<table>
<tr><th>Sub-band</th><th>Frequency Range (MHz)</th><th colspan="3">Spectrum Utilization</th></tr>
<tr><td>1</td><td>250 – 470</td><td>6.88</td><td rowspan="3">9.85</td><td rowspan="6">8.08</td></tr>
<tr><td>2</td><td>470 – 880</td><td>7.90</td></tr>
<tr><td>3</td><td>880 – 1000</td><td>21.91</td></tr>
<tr><td>4</td><td>2200 – 2400</td><td>0.55</td><td rowspan="3">0.89</td></tr>
<tr><td>5</td><td>2400 – 2500</td><td>3.15</td></tr>
<tr><td>6</td><td>2500 – 2950</td><td>0.52</td></tr>
</table>

Empirical CDF of DC provides essential information and can be used to predict the behaviour of local users of a network, which will enable the CR users to access the spectrum holes [30]. Figure 4.22-4.23 shows the empirical distributions of different frequency ranges in band 1 and 2 respectively, while associated statistical parameters of the distribution are listed in table 4.8. A common observation is that most of the empirical CDFs relating to respective frequency ranges where the activity of local users of a network is low, the CDF tends to concentrate more towards the zero DC value, which makes them potential candidates for CRN.

4.2.5 Summary

The 24 hour of measurements taken in Durham city, UK show that the radio spectrum is highly underutilized and its utilization can be increased by accessing it opportunistically. The spectrum utilization in services like GSM 900 and 2.4 GHz WLAN is relatively high in office hours compared to non-office hours. Moreover, due to the ON/OFF behaviour of the transmitter in these radio technologies, spectrum holes can be accessed in the time domain. On the other hand, a database of partially occupied (sub-band 1 and 2) or fully unoccupied (sub-band 4 and 6) frequency bins

can be made and shared to CR users so that by reutilizing the spectrum utilization can be improved.

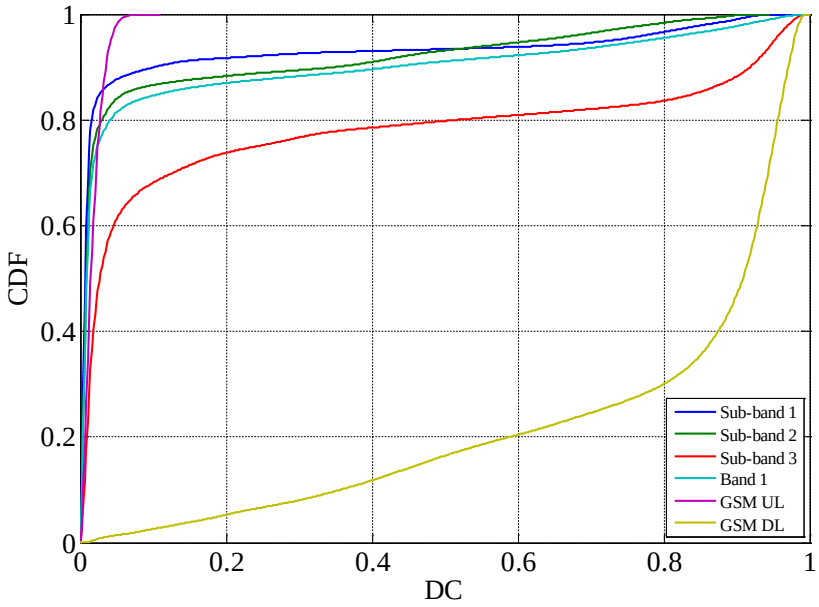

Figure 4.22 Empirical distribution of DC for different frequency ranges in band 1

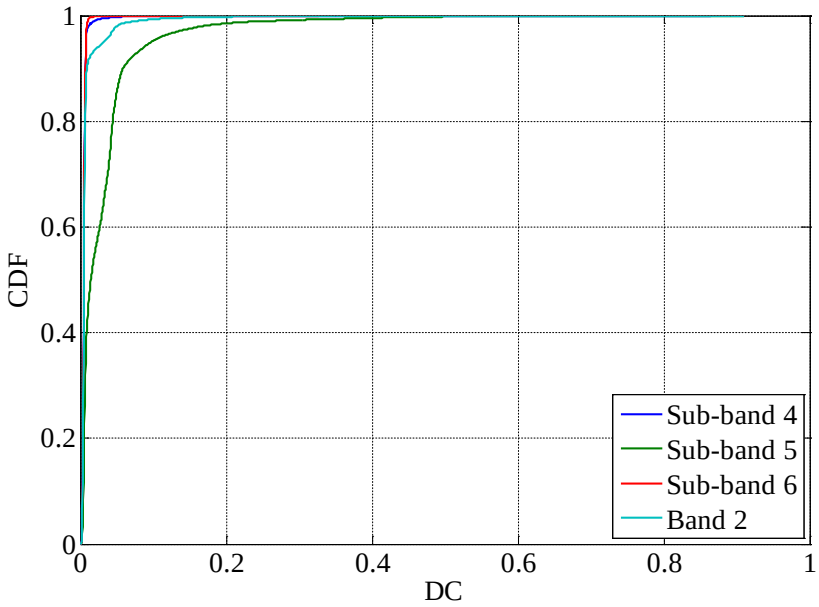

Figure 4.23 Empirical distribution of DC for different frequency ranges in band 2

Table 4.8 Statistical parameters of CDF for different frequency ranges

	Parameter				
Band	Minimum	Mean	Median	Standard deviation	Maximum
Sub-band 1	0	0.4940	0.4940	0.2872	0.9900
Sub-band 2	0	0.4719	0.4719	0.2745	0.9459
Sub-band 3	0	0.4990	0.4990	0.2901	1
GSM UL	0	0.0541	0.0541	0.0332	0.1102
GSM DL	0	0.4990	0.4990	0.2901	1
Band 1	0	0.4990	0.4990	0.2901	1
Sub-band 4	0	0.2268	0.1789	0.2027	0.8651
Sub-band 5	0	0.4423	0.4376	0.2598	0.9104
Sub-band 6	0	0.1559	0.1531	0.0924	0.3265
Band 2	0	0.4439	0.4396	0.2605	0.9104

4.3 Short Term Spectrum Occupancy Measurement

4.3.1 Background

In the previous section, the spectrum occupancy measurements were performed over 24 hours to understand the long term variations in the spectrum utilization, where data were analysed with the resolution of one minute. As a limited number of sweeps were recorded per minute, the receiver was mostly kept in the idle state (~40-50 seconds per minute) and was unable to record all the occupancy variations.

In this section, spectrum occupancy results from short term measurements in 2.4-2.5 GHz band will be presented where data were collected continuously for 20 minutes. The measurements were performed in an indoor environment where first the received power is measured using omnidirectional antennas and then using directional antennas, to characterize the spectrum occupancy in the angular dimension. A total of 120 data files are taken in 20 minutes where each file contains continuous recording of 2 seconds. Here, it can also be noticed that the digitizer requires ~10 seconds to perform both digitization and data transfer (from digitizer local memory to PC) functions. The raw data collected in section 4.1 is used to evaluate the short term spectrum occupancy in 2.4-2.5 GHz band.

4.3.2 Data Analysis Methodology

The raw data are calibrated from all gains and losses (receiver, cables and antenna), to get the received power by performing offline processing in MATLAB and to get 400 kHz resolution bandwidth. In order to determine the presence of a

signal, an energy detection algorithm is used where a decision threshold of -97 dBm is chosen, which is set to 10 dB above the noise floor.

4.3.3 Analysis

Analysis is presented in two parts based on the type of antenna used for measurement.

4.3.3.1 Omnidirectional Measurements

Figure 4.24 shows the maximum and average received power level variations in the sensed bandwidth over the duration of 20 minutes. The 2.4 GHz WLAN signal is detected, which is generated by Durham University wireless network and particularly significant activities are recorded on channel "1" (2.401-2.423 GHz) and channel "12" (2.456-2.478 GHz). Besides 2.4 GHz WLAN signals, a CW transmission is also detected at 2.47 GHz from an unknown source. Figure 4.25 shows the time-frequency map of DC for every 2 seconds, where it can be noticed that channel "12" has a higher network traffic (DC) compared to channel "1". Figure 4.26 shows the DC over the measurements duration i.e. 20 minutes, where apart from a CW transmission, the DC values of all detected WLAN channels are less than 0.2. The average DC is found to be 0.046, which indicates that the sensed bandwidth have low usage in both time and frequency. However, it is beneficial from the point of view of CR users as they can access the spectrum holes in the time domain when channels "1" or "12" are in the idle state (as explained in section 4.1) or can use partially occupied frequency bins (between channel "1" and "12") in both the time and frequency dimensions or fully unoccupied frequency bins i.e. from 2.478 GHz to 2.5 GHz. Figure 4.27 shows the time variations in the spectrum utilization which is computed every 2 seconds, where channel "12" has highest spectrum utilization most of the time compared to channel "1" over the measurement duration.

4.3.3.2 Directional Measurements

The directional measurements were performed using three antennas (A1, A2, A3) with time resolution of 819.2 µsec per antenna or angular dimension. Figure 4.28 shows the maximum and average received power level variations recorded in all directions. For channel "1" and "12" highest received power levels were recorded on antennas A3 and A1 or A2 respectively. Moreover, the intermediate frequency bins between channels "1" and "12" were observed significantly strong on antenna A3 in comparison to the other antennas. Figures 4.29 shows the time frequency map of DC

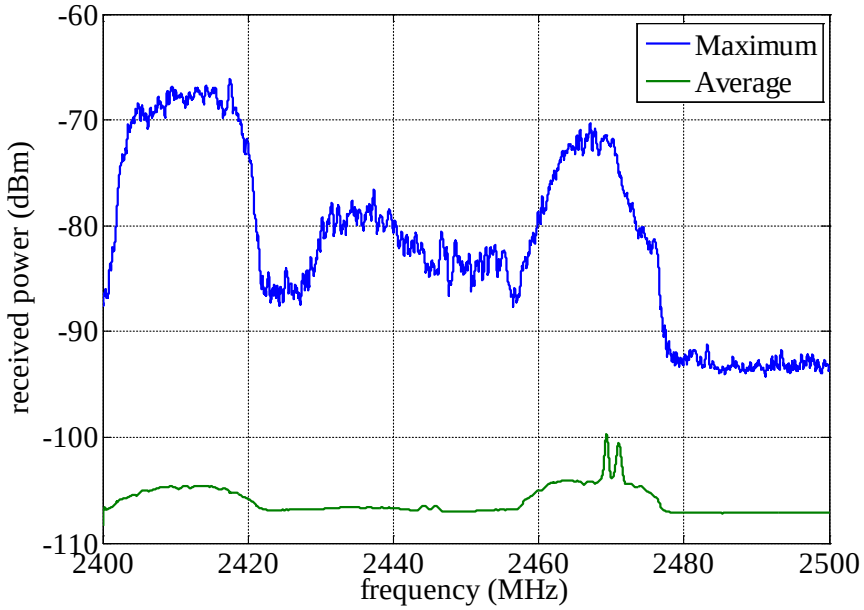

Figure 4.24 Received power level variations in 2.4-2.5 GHz band

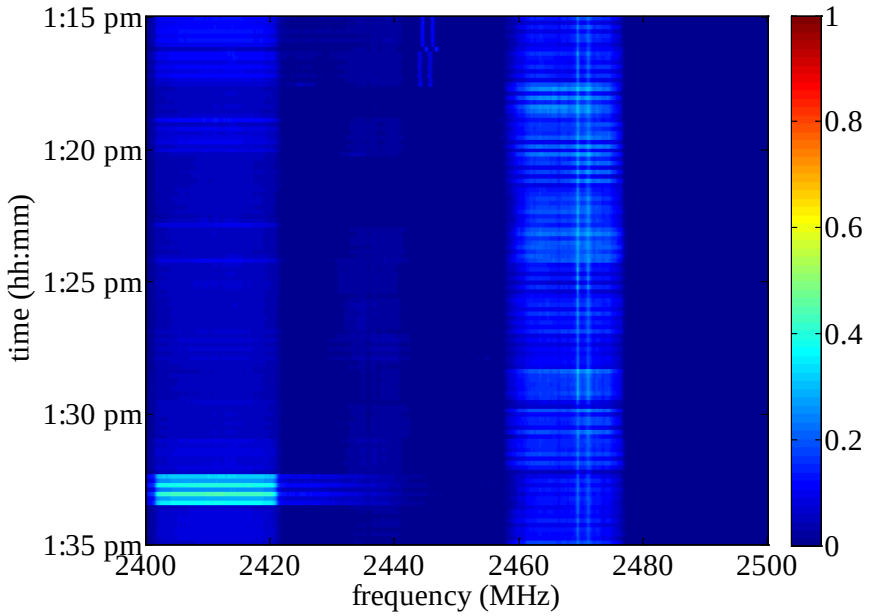

Figure 4.25 Time-frequency occupancy map of DC per 2 seconds in 2.4-2.5 GHz band

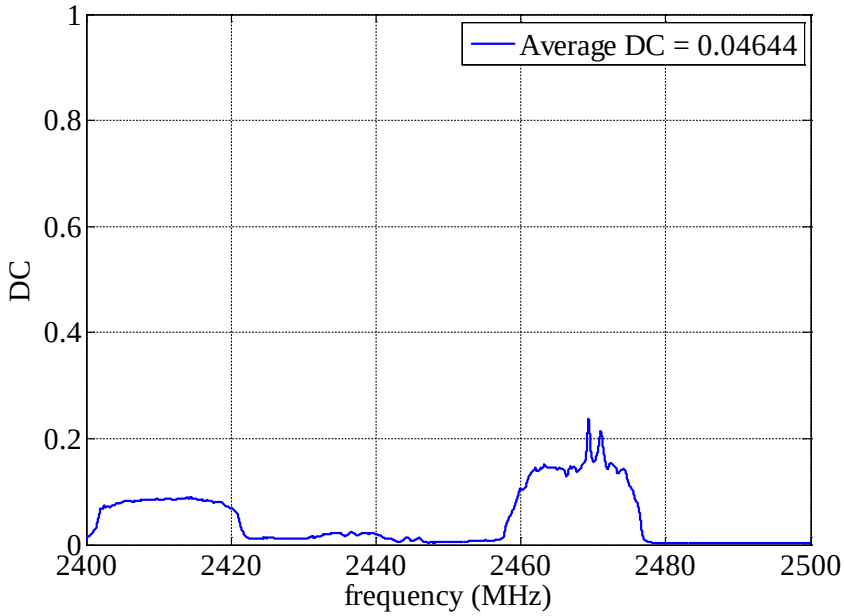

Figure 4.26 20 minutes DC in 2.4-2.5 GHz band

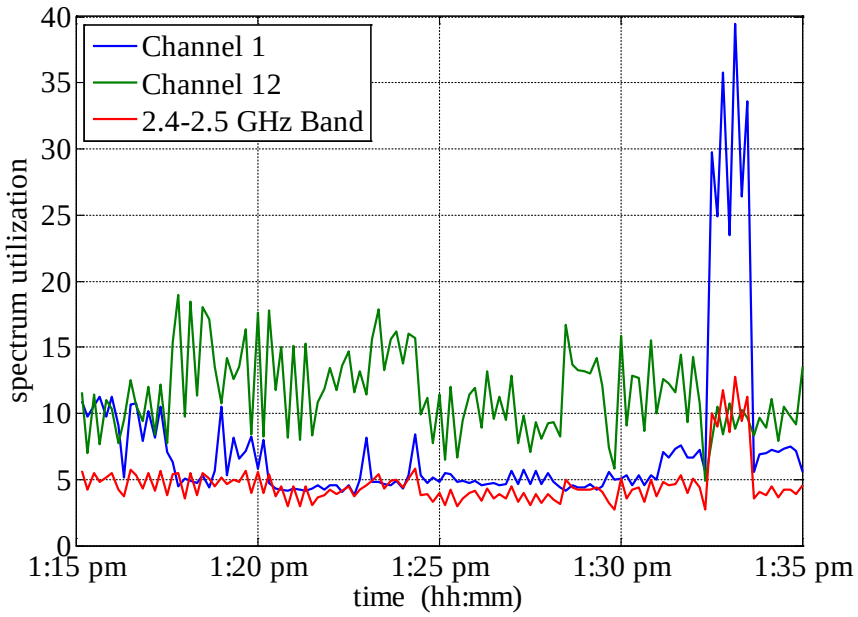

Figure 4.27 Time variations in spectrum utilization over 20 minutes for different frequency ranges in 2.4-2.5 GHz band

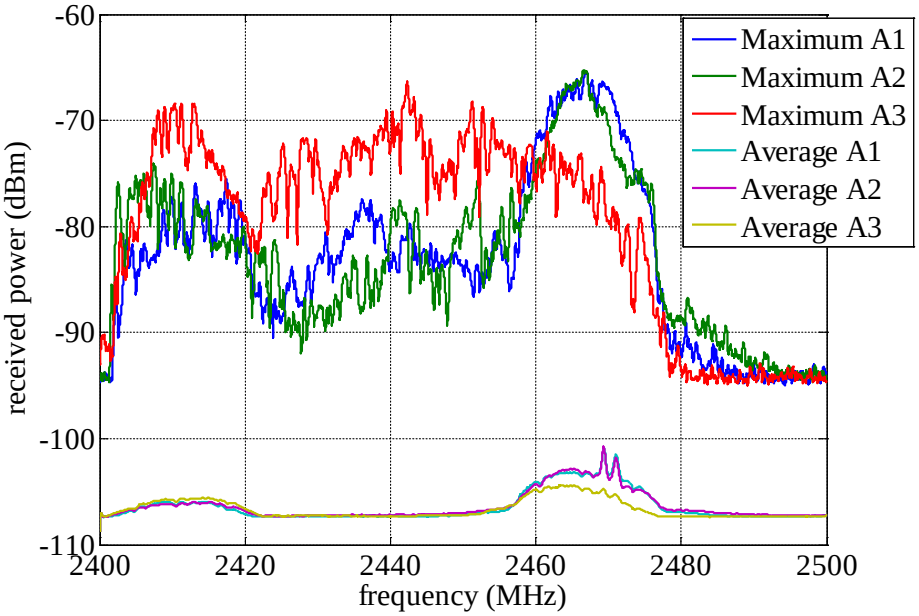

Figure 4.28 Received power level variations in 2.4-2.5 GHz in three angular diminsions

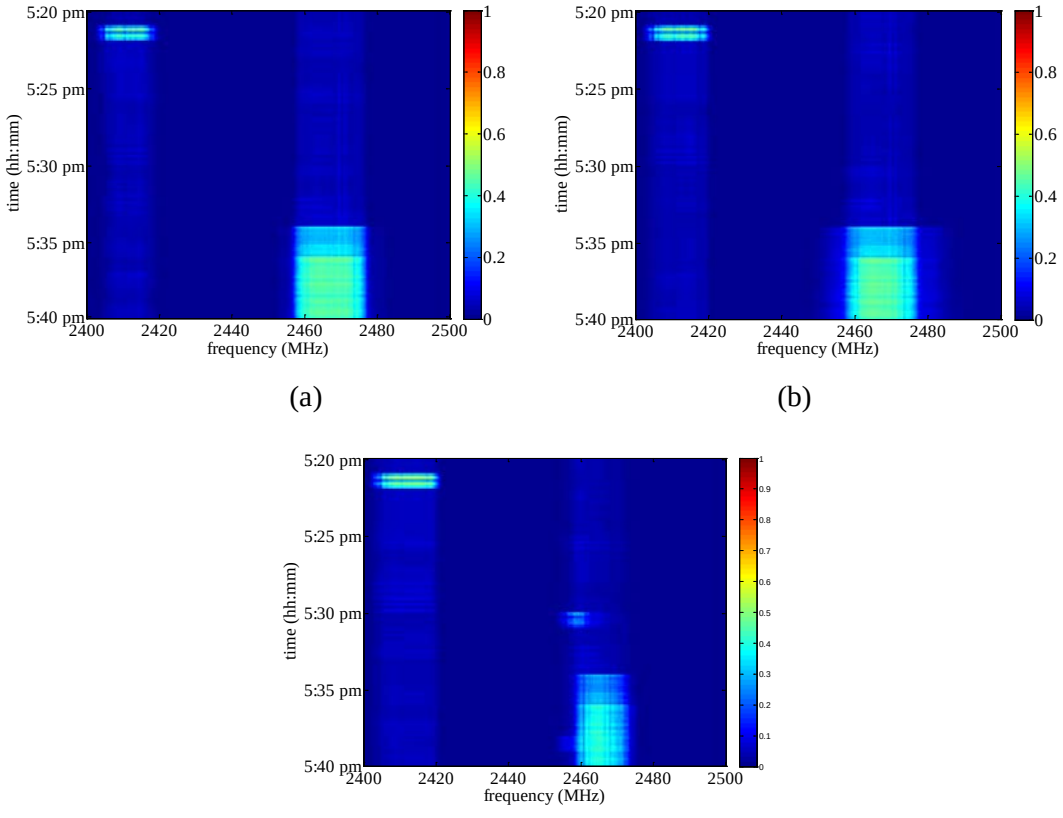

(a) (b)

(c)

Figure 4.29 Time-frequency occupancy map of DC per 2 seconds in three angular dimensions in 2.4-2.5 GHz band: a) A1, b) A2, c) A3

DC computed every 2 seconds of measurement data, where it can be observed that at the measurement location, most of the network activity is present in channel “1” and

"12". Figure 4.30 shows the DC over 20 minutes of measurement duration where the highest average DC is observed at antenna A2. Figure 4.31-4.32 shows the time evaluation of spectrum utilization in channel "1" and channel "12" in all directions, where the highest spectrum utilization can be observed on antenna A3 and antennas

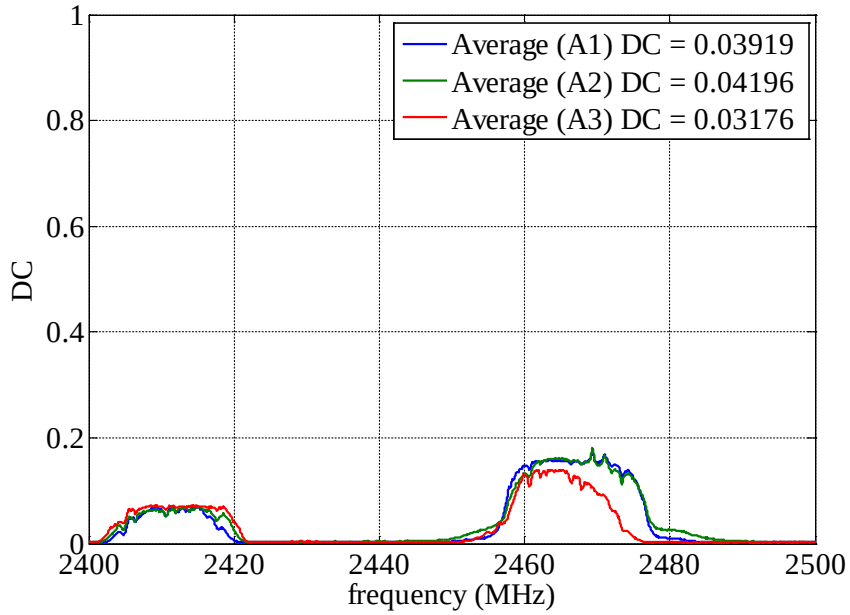

Figure 4.30 20 minutes DC in 2.4-2.5 GHz band in three angular dimensions

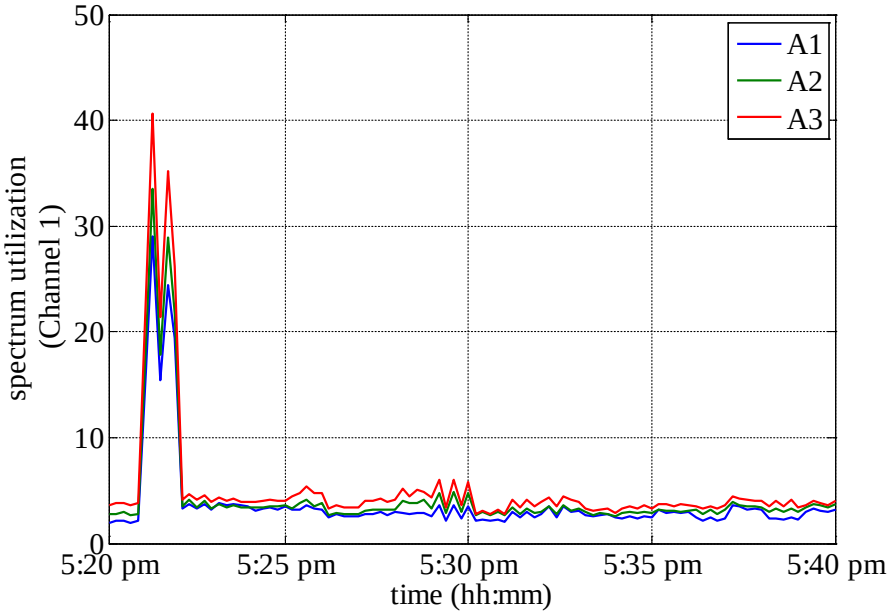

Figure 4.31 Time variations in spectrum utilization over 20 minutes in Channel "1"

A1-A2 for the respective channel. Figure 4.33 shows the spectrum utilization of the overall sensed bandwidth which is varying in the range ~1-11% and the impact of the angular dimension can also be observed.

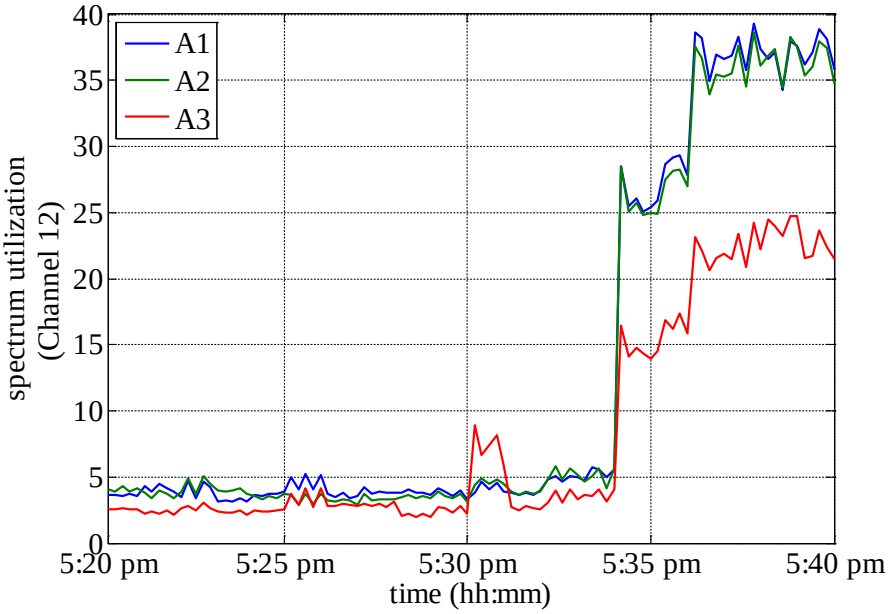

Figure 4.32 Time variations in spectrum utilization over 20 minutes in Channel "12"

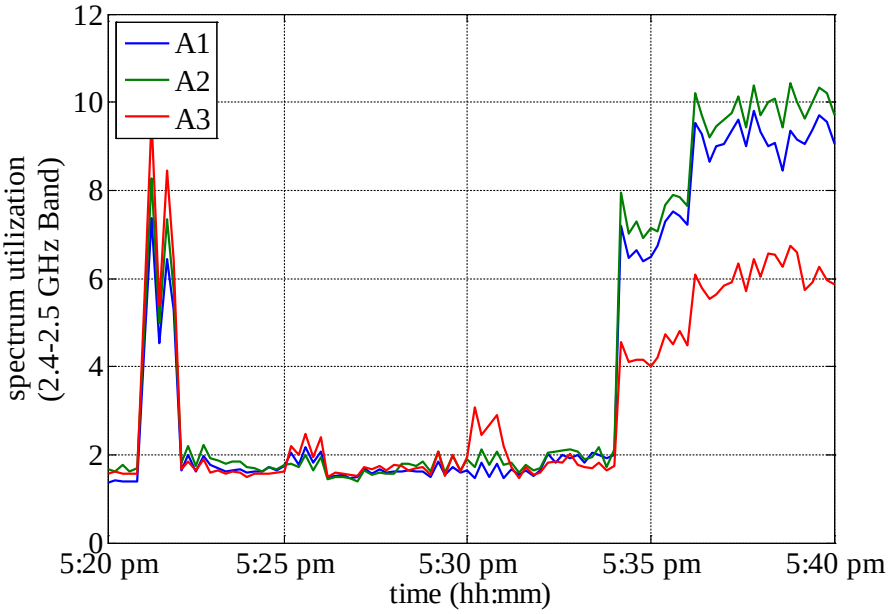

Figure 4.33 Time variations in spectrum utilization over 20 minutes in 2.4-2.5 GHz band

Table 4.9 summarizes the spectrum utilization for both antenna types. For the omnidirectional antenna, the overall spectrum utilization is found less than 5% with the highest spectrum utilization recorded for channel "12". In case of the directional measurements, the highest overall spectrum utilization is observed on antenna A2. Channel "12" has the highest spectrum utilization in all directions

compared to channel “1”. Moreover, the lowest spectrum utilization for channel “1” and channel “12” is recorded over antennas A1 and A3 respectively.

Table 4.9 Comparison of spectrum utilization over 20 minutes among different frequency ranges

			Spectrum Utilization		
			Channel “1”	Channel “12”	2.4-2.5 GHz
Antenna Type	Omni-directional	-	7.4013	11.5071	4.6449
	Directional	A1	3.7515	12.9776	3.9191
		A2	4.3158	12.6841	4.1967
		A3	5.1859	8.2525	3.1760

The empirical CDF of DC values is also an important parameter to understand and can be used to predict the behaviour of local users of a network [30]. Figure 4.36 shows the empirical CDF of DC values computed using omnidirectional measurements where it can be observed that channel “12” has higher DC than the other channels at 80 % of CDF values. Figure 4.37-4.39 shows the empirical CDFs computed for the respective frequency range using directional antennas. Table 4.10 summarizes the statistical parameters of the empirical CDFs computed for both omnidirectional and directional antenna measurements.

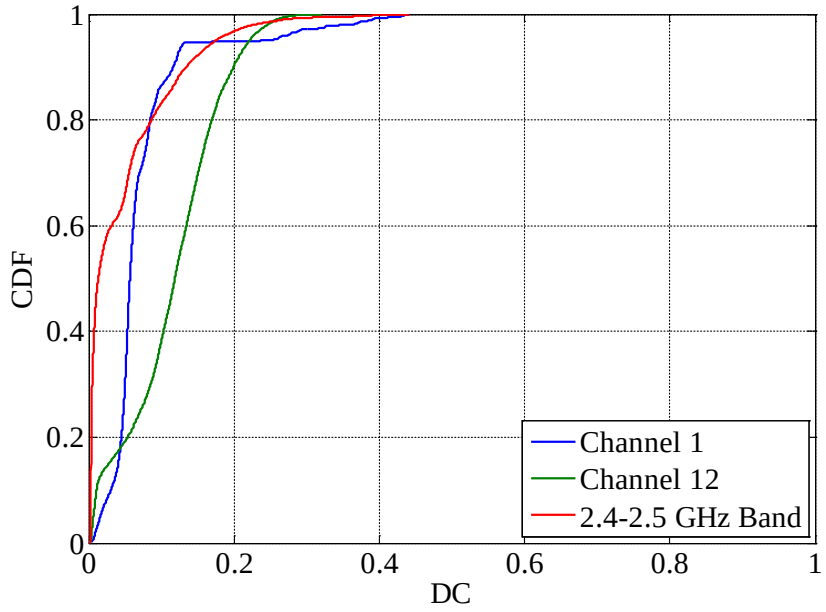

Figure 4.34 Empirical distribution of DC for different frequency ranges in 2.4-2.5 GHz band

4.3.4 Summary

The short term spectrum occupancy measurement is performed using omnidirectional and directional antennas. The spectrum occupancy is analysed using

parameters like DC, average DC and their empirical distribution are presented along with their statistical parameters.

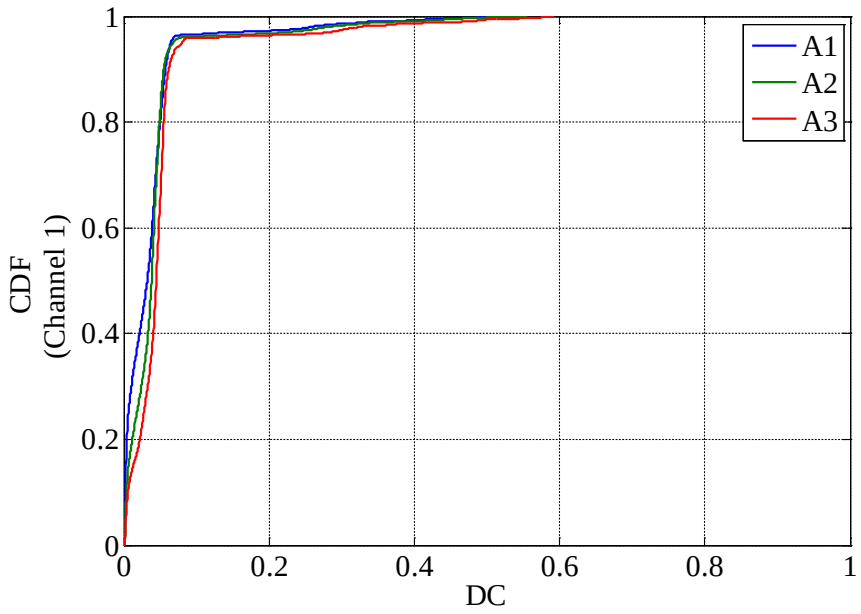

Figure 4.35 Empirical distribution of DC for different frequency ranges in channel "1"

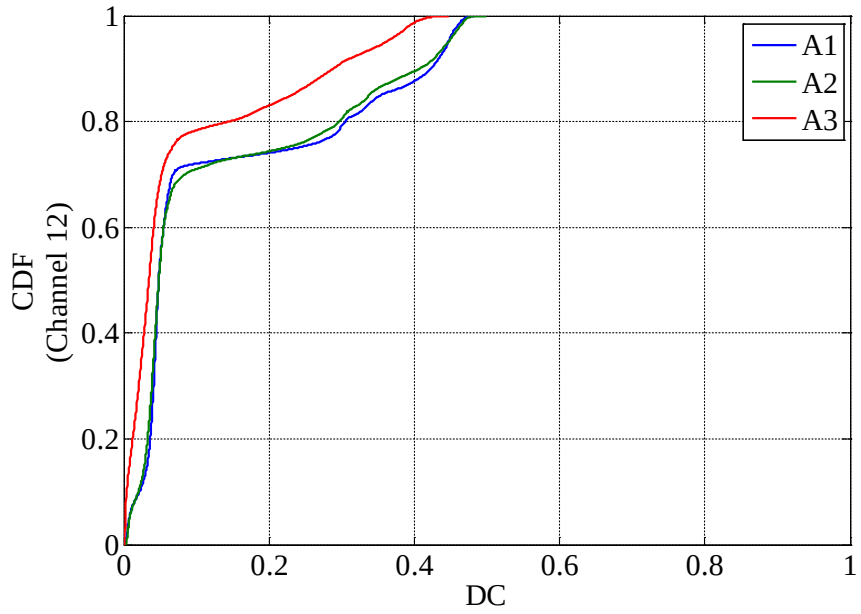

Figure 4.36 Empirical distribution of DC for different frequency ranges in channel "12"

Channel "12" was found to have the highest spectrum utilization in both omnidirectional and directional antenna measurements compared to channel "1". Overall, the 2.4-2.5 GHz is an important band for CR applications, where it can

access partially occupied frequency bins i.e. WLAN channels, in the time domain and fully unoccupied frequency bins in the frequency domain or any of their combination.

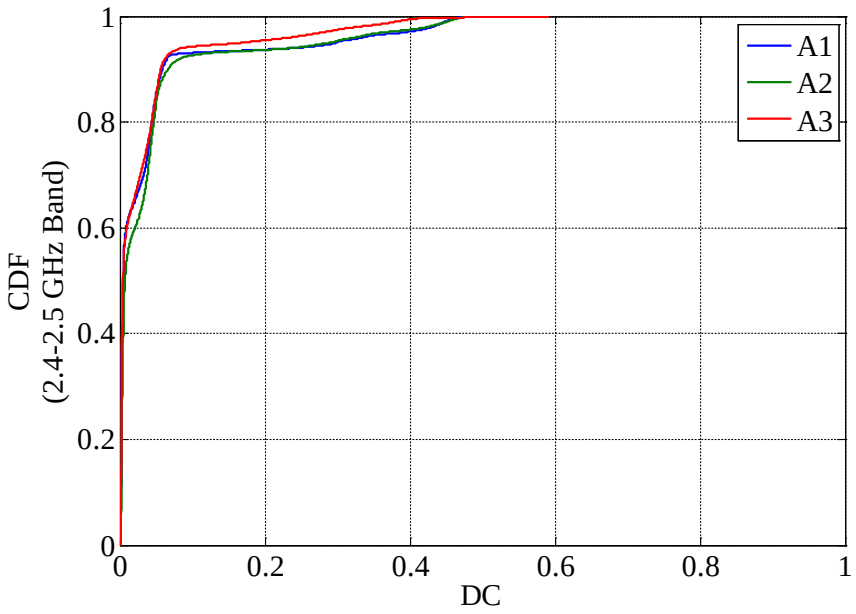

Figure 4.37 Empirical distribution of DC for different frequency ranges in 2.4-2.5 GHz band

Table 4.10 Statistical parameters of CDF for different frequency ranges

	Parameter				
Band	Minimum	Mean	Median	Standard Deviation	Maximum
Channel “1”	0.0023	0.2173	0.2215	0.1288	0.4408
Channel “12”	0.0014	0.157	0.1569	0.0900	0.3209
2.4-2.5 GHz	0.0009	0.2157	0.2138	0.1257	0.4408
Channel “1”(A1)	0	0.2352	0.2244	0.1621	0.5308
Channel “1”(A2)	0	0.2498	0.2425	0.1688	0.5549
Channel “1”(A3)	0	0.2951	0.2940	0.1715	0.5923
Channel “12”(A1)	0.0004	0.2410	0.2410	0.1390	0.4820
Channel “12”(A2)	0.0017	0.2458	0.2457	0.1411	0.4987
Channel “12”(A3)	0	0.2236	0.2236	0.1295	0.4481
2.4-2.5 GHz(A1)	0	0.2535	0.2529	0.1472	0.5308
2.4-2.5 GHz(A2)	0	0.2627	0.2618	0.1527	0.5549
2.4-2.5 GHz(A3)	0	0.2958	0.2957	0.1713	0.5923

4.4 Cooperative Spectrum Occupancy Measurement

4.4.1 Background

One of the key challenges in the deployment of CRN is to avoid the hidden node problem. Multiple CR users can cooperative by sharing their local occupancy decision to each other (decentralized cooperation) or to a central fusion station

(centralized cooperation), in order to reliably detect the spectrum hole so that the hidden node problem can be minimized [31].

Particularly in the 2.4 GHz ISM band, an experiment was conducted to study how much cooperation can benefit a CR user from other users in the network [32]. To quantify the amount of benefit, a parameter is formulated which measured the amount of distinct occupancy events i.e. which are only detected by a CR user however cannot be detected by other users in CRN. The experiment was composed of two sensing nodes to represents two CR users: 1) fixed position for reference, 2) mobile, which is moved on a predefined route so that the effect of the spatial dimension on the amount of distinct occupancy events can be measured. In this work, we have conducted a similar measurement campaign where three sensing nodes i.e. two fixed (Node 1 & 2) and a mobile (Node 3), which is moved on a predefine route, are used to find distinct occupancy events in an indoor environment and quantify the amount of cooperation available for an individual CR user or to all users in a CRN.

4.4.2 Experimental Setup

The experiment is conducted using three chirp channel sounder receivers referred to as Node 1, Node 2 and Node 3 in an indoor environment. Nodes 1 and 2 were placed at fixed locations while Node 3 is assembled on a trolley (as shown in figure 4.13) for mobility purposes. The experiment was conducted on the 2nd floor of School of Engineering and Computing Sciences at Durham University, UK on 13th August, 2014 from 09:32 pm to 10:33 pm.

Each node was equipped with a discone antenna and placed at 1.5 m above the ground level. Node 1 was placed inside the office 287 and Node 2 was placed near office 234 in a corridor while Node 3 is moved on a pre-defined route as shown in figure 4.38. Node 3 is moved from office 215 towards office 285 and then from office 217 to office 215 with approximately a step size of 4.5-5 m in the respective corridor. The step size between end and start of corridors is approximately less than 1 m. A total of 26 measurement locations were traversed and monitored.

Each node was configured to sense 100 MHz swept bandwidth from 2.4 to 2.5 GHz with a sweep duration of 204.8 µsec and baseband data were sampled at 80 MHz. Moreover, 500 sweeps were recorded at every location for each node. Table

4.11 lists the key parameters of the conducted measurements campaign and it also makes a comparison with the experiment conducted in [32].

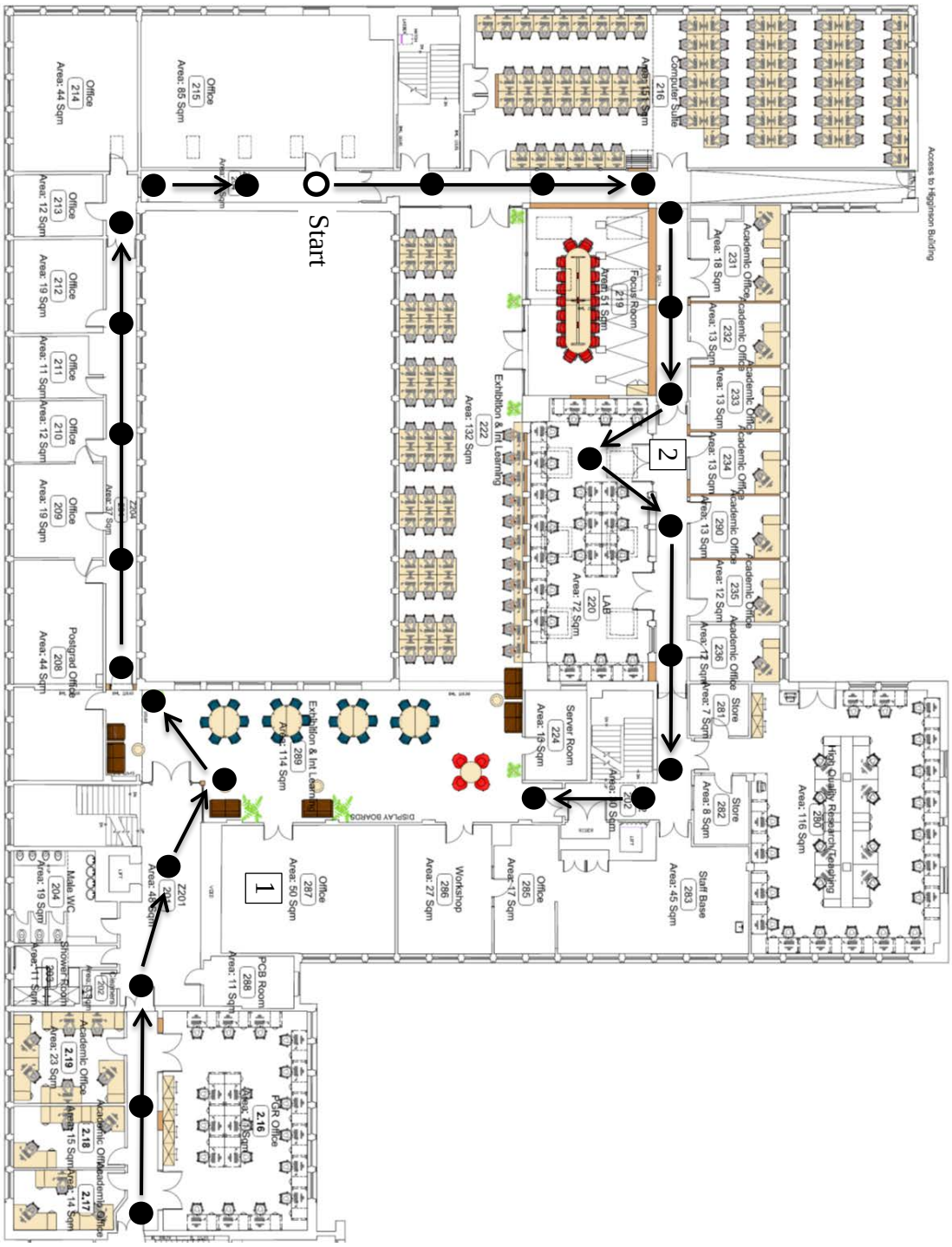

Figure 4.38 Layout of measurement campaign

Table 4.11 Comparison of parameters

Experiment	[32]	This Work
Antenna	Discone	Discone
Number of Nodes	2	3
Sensing Node	SA	Chirp Channel Sounder Receiver
Time Resolution	250 ms	204.8 µs
Number of Sweeps	200	500
Step size of Grid	12.5-15 m	5 m

4.4.3 Data Analysis Methodology

The raw data are calibrated from all gains and losses (receiver, cables and antenna), to get the received power by performing offline processing in MATLAB and to get 400 kHz resolution bandwidth. In order to determine the presence of a signal, an energy detection algorithm is used where a decision threshold of -97 dBm is chosen, which is set 10 dB above the noise floor.

The amount of distinct occupancy events which a node can provide to others for network cooperation is calculated using the following four parameters.

4.4.3.1 Parameter 1 [4]*:*

$$P^{l}{}_{i\to j} = \frac{1}{N_f}\sum_{f=1}^{N_f} \frac{\sum_{n=1}^{N_s} \beta^{l}{}_{i}(t,f) \,\&\, !\beta^{l}{}_{j}(t,f)}{\sum_{n=1}^{N_s} \beta^{l}{}_{i}(t,f) \mid \beta^{l}{}_{j}(t,f)} \qquad \text{Equation 4.1}$$

where i, j, k represents the indices of nodes, N_f defines the number of frequency points, N_s defines the number of sweeps recorded per measurement location, $\beta^{l}{}_{i}(t,f)$ and $\beta^{l}{}_{j}(t,f)$defines the binary time-frequency map of i^{th} and j^{th} nodes, which is computed using an energy detection technique at measurement location l, where $l = 1,2,..,26$. The symbol & denotes logical AND operator, ! denotes logical NOT operator, | denotes logical OR operator and $P^{l}{}_{i\to j}$ defines the amount of probability that the i^{th} node has detected distinct occupancy events in comparison to the j^{th} node in the binary time-frequency map at measurement location l. The higher value of parameter $P^{l}{}_{i\to j}$ shows that cooperation between the i^{th} and j^{th} nodes is beneficial as the i^{th} node can provide distinct occupancy event information to j^{th} nodes for cooperation in order to reduce the hidden node problem.

[4] This parameter is used in [32] while current work modifies this parameter to three new parameters.

4.4.3.2 Parameter 2:

$$P^{l}{}_{i\to jk} = \frac{1}{N_f}\sum_{f=1}^{N_f} \frac{\sum_{n=1}^{N_s} \beta^{l}{}_{i}(t,f) \,\&\, !\beta^{l}{}_{j}(t,f) \,\&\, !\beta^{l}{}_{k}(t,f)}{\sum_{n=1}^{N_s} \beta^{l}{}_{i}(t,f) \mid \beta^{l}{}_{j}(t,f) \mid \beta^{l}{}_{k}(t,f)} \qquad \text{Equation 4.2}$$

The parameter $P^{l}{}_{i\to jk}$ denotes the amount of distinct occupancy events which the i^{th} node can provide collectively to both j^{th} and k^{th} at measurement location l. This parameter is very interesting to understand as it will provide the overall contribution of the i^{th} node for other members of CRN in the support of network cooperation. The higher value of the parameter means that it can help other members of the network to reduce the hidden node problem at their respective locations.

Two important issues associated with cooperative spectrum sensing are optimum node position to avoid the hidden node problem and node selection criteria to increase network cooperation among users. Parameter 2 can be beneficial to solve the aforementioned problems by selecting positions or nodes which yield higher values of parameter 2.

4.4.3.3 Parameter 3:

$$P^{l}{}_{ij\to k\,(AND)} = \frac{1}{N_f}\sum_{f=1}^{N_f} \frac{\sum_{n=1}^{N_s} \beta^{l}{}_{i}(t,f) \,\&\, \beta^{l}{}_{j}(t,f) \,\&\, !\beta^{l}{}_{k}(t,f)}{\sum_{n=1}^{N_s} \beta^{l}{}_{i}(t,f) \mid \beta^{l}{}_{j}(t,f) \mid \beta^{l}{}_{k}(t,f)} \qquad \text{Equation 4.3}$$

Parameters 1 and 2 are essential to study the contribution of an individual node in CRN to reduce the hidden node problem. However, binary occupancy decisions of two or more nodes can be combined to find the cumulative amount of distinct occupancy events for network cooperation. Parameter 3, $P^{l}{}_{ij\to k\,(AND)}$, represents the probability of distinct occupancy events for network cooperation which are obtained by combining binary occupancy decisions of the i^{th} node and j^{th} node, using AND hard combining techniques[5], for k^{th} node.

4.4.3.4 Parameter 4:

$$P^{l}{}_{ij\to k(OR)} = \frac{1}{N_f}\sum_{f=1}^{N_f} \frac{\sum_{n=1}^{N_s} \beta_i(t,f) \mid \beta_j(t,f) \,\&\, !\beta_k(t,f)}{\sum_{n=1}^{N_s} \beta_i(t,f) \mid \beta_j(t,f) \mid \beta_k(t,f)} \qquad \text{Equation 4.4}$$

[5] Under AND hard combining technique, a signal is considered present if it is detected at both nodes.

Parameter 4, $P^{l}{}_{ij\rightarrow k(OR)}$, denoted the amount of distinct occupancy events for network cooperation which the i^{th} node and j^{th} node can provide to the k^{th} node using OR hard combining technique[6].

4.4.4 Analysis

Figure 4.39 shows the spectrum utilization for each node, whereas Nodes 1 and 2 are fixed, so their spectrum utilization is independent of location however representing the time variations in the respective spectrum utilization. Node 1 has mostly higher spectrum utilization values compared to Node 2 and Node 3. In order to find that cooperation is possible among nodes, the spectrum utilization of mutual occupancy events (detected by all nodes) and distinct occupancy events (detected by only one of the nodes) at a given time-frequency map index is also computed. The mutual occupancy events, which are not beneficial for network cooperation, are found to be less than 2 %. In comparison, distinct occupancy events have higher utilization i.e. between 19-34 %, which means that network cooperation is possible and beneficial. Here, it is also important to note that, network cooperation can be useful if spectrum utilization of distinct occupancy events is higher than mutual occupancy events.

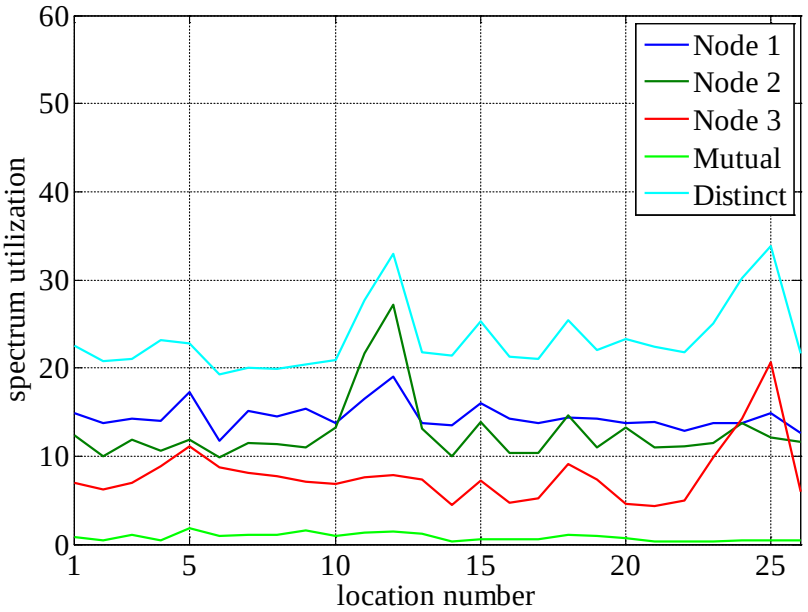

Figure 4.39 Spectrum utilization for each node along with spectrum utilization for mutual and distinct occupancy events

[6] Under OR hard combining technique, a signal is considered present if it is detected at any one of the nodes.

In order to find which node is more suitable for network cooperation, parameters 1 and 2 are calculated for each node. Figure 4.40 shows the amount of distinct occupancy events which Node 1 can provide to Node 2, Node 3 and collectively to Nodes 2 and 3. First observation is that higher probability values are observed for Node 3 due to a change in location in comparison to the fixed position of Node 2. Moreover, it can also be observed that when Nodes 1 and 3 have mutual events the probability values tend to drop while the increase in values represents those locations where distinct events have been observed and are more useful for cooperation. Parameter 2 has smaller values as it looks for distinct occupancy events which are only present in Node 1 and also not being detected by Nodes 2 and 3. Figure 4.41 shows the contribution of Node 2 which other nodes can benefit from in the network. It can be observed that Node 3 can get more benefits due to variations

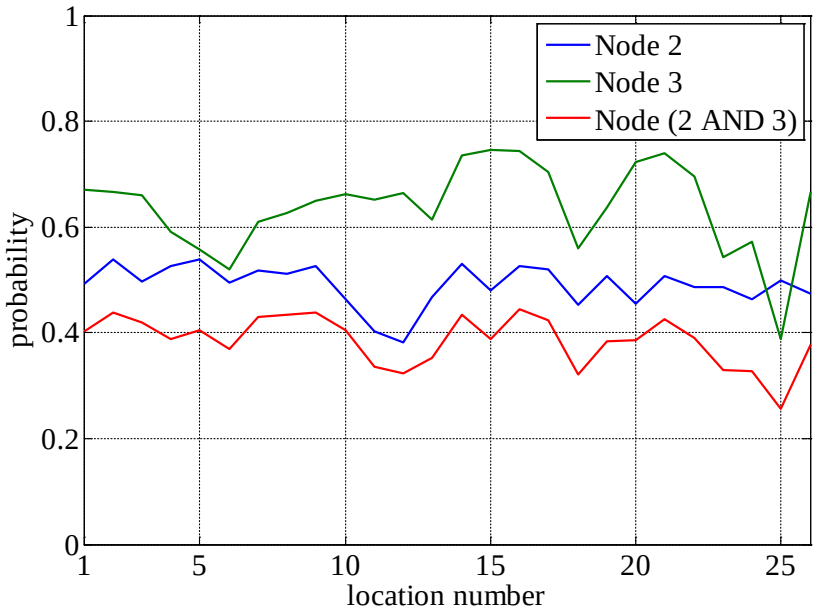

Figure 4.40 Probability of distinct occupancy events from Node 1 to others

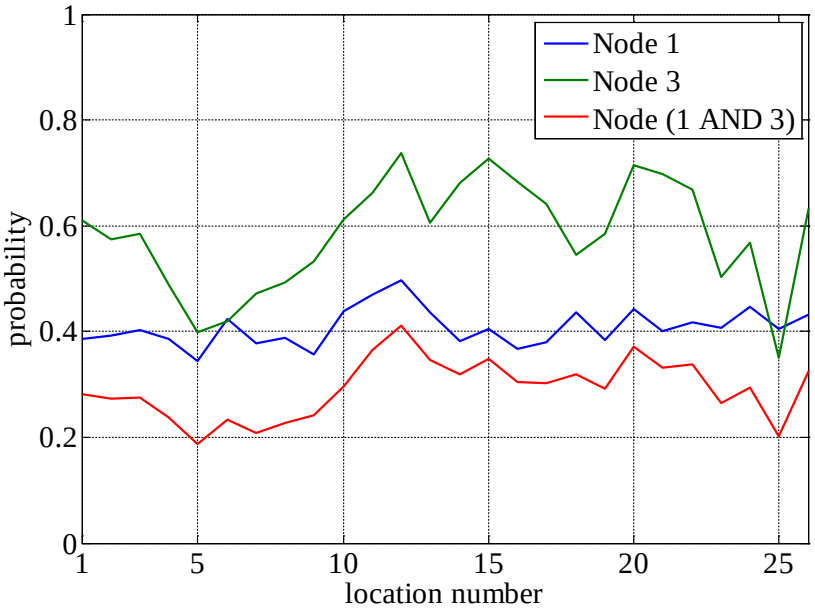

Figure 4.41 Probability of distinct occupancy events from Node 2 to others

in location which produces more distinct events and have high probability compared to the fixed position of Node 1. Figure 4.42 shows the contribution of Node 3 to fixed location nodes i.e. Node 1 and Node 2. Compared to Node 1 and Node 2 contributions, Node 3 has lower values of probabilities due to having lower spectrum utilization.

The occupancy decisions of nodes are combined with respect to corresponding time and frequency indices, to analyse the changes in the amount of distinct occupancy events. The occupancy decisions of two nodes are combined using OR or AND techniques and then compared with occupancy decisions of other node to compute distinct occupancy events. Figure 4.43-4.45 shows the amount of distinct events using hard combining techniques where the OR combining technique yields the highest values. As the OR technique allows all occupancy events during the combing process it has more chances to find a distinct occupancy event in comparison to the AND technique which is based on mutual distinct occupancy events among the nodes.

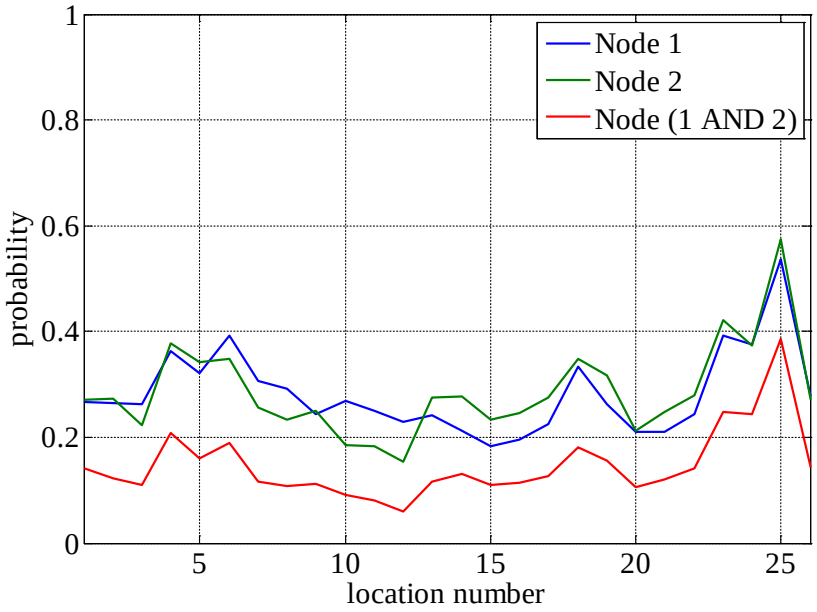

Figure 4.42 Probability of distinct occupancy events from Node 3 to others

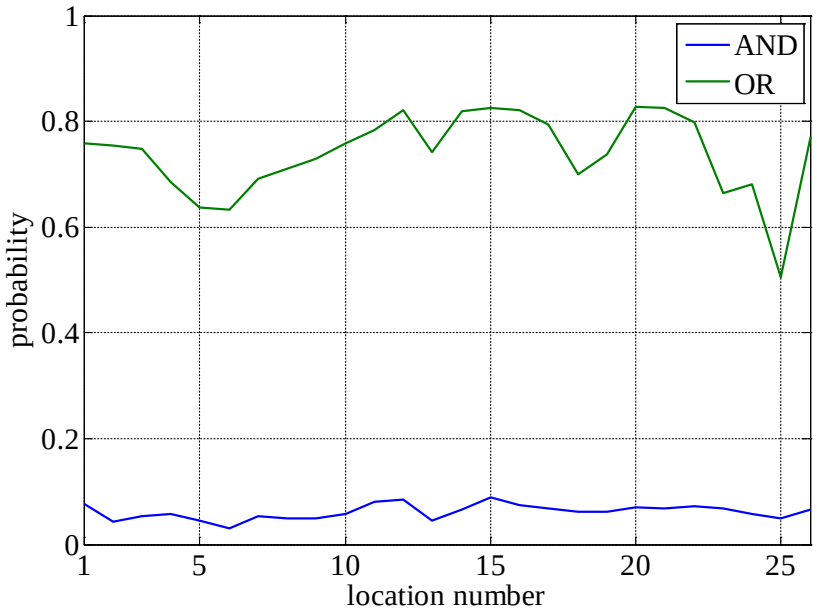

Figure 4.43 Probability of distinct occupancy events by combining occupancy events of Nodes 1 and 2 for Node 3

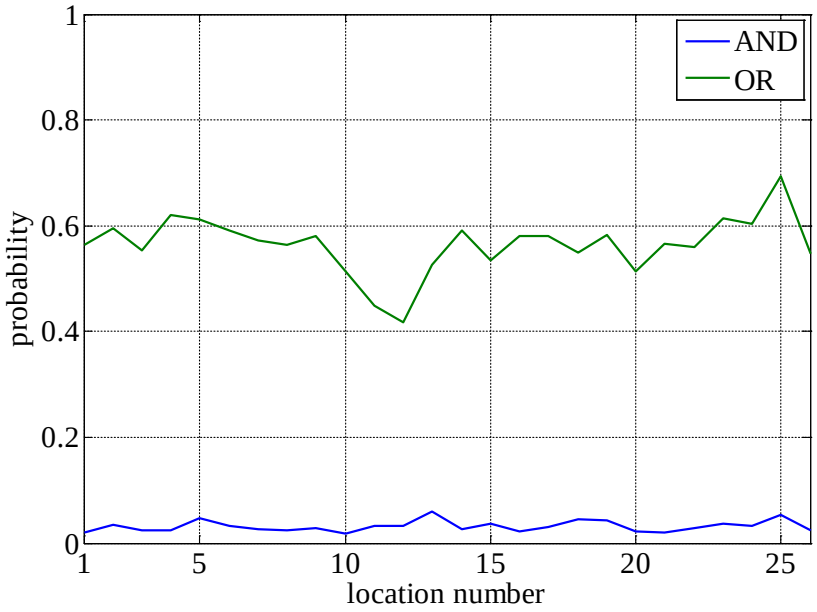

Figure 4.44 Probability of distinct occupancy events by combining occupancy events of Nodes 1 and 3 for Node 2

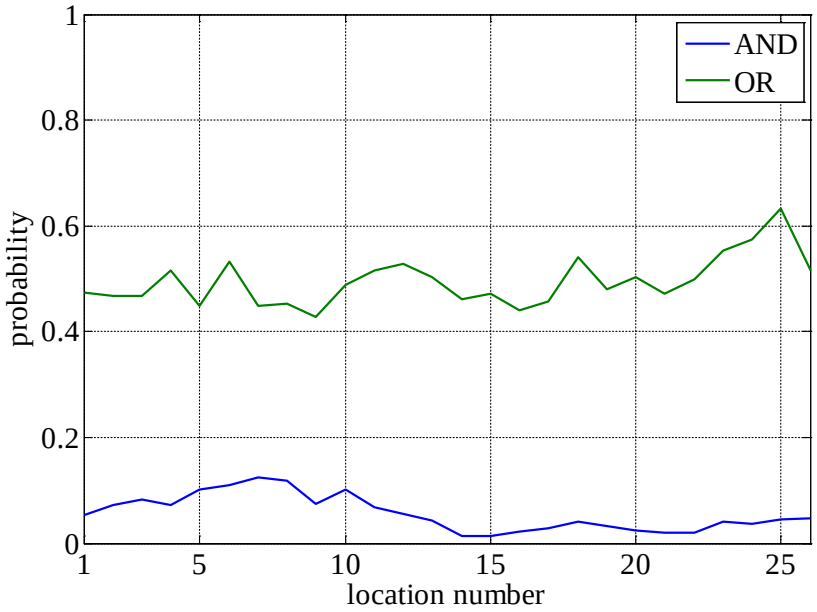

Figure 4.45 Probability of distinct occupancy events by combining occupancy events of Nodes 2 and 3 for Node 1

4.4.5 Summary

Distributed occupancy measurements have been performed using three nodes where two nodes were placed at fixed locations and a third node is moved on a predefined route in an indoor environment. The spectrum utilization of distinct occupancy events have been found in the range of 19-34 %, which indicates that the nodes can cooperate to reduce the hidden node problem.

The amount of cooperation given by a node or nodes is computed for an individual node, where it has been found that the space dimension affects the amount of distinct events significantly. Moreover, the local binary decision for each node has been combined to enhance network cooperation using hard combining techniques, where the OR technique outperforms the AND technique.

4.5 Summary

Long term measurements were conducted over 24 hours in both indoor and outdoor environments using a chirp channel sounder receiver. These measurements are performed by sensing 750 MHz sensing bandwidth in the respective frequency range with high time-frequency resolutions to investigate spectrum utilization at a frame or packet level in Durham City, UK. The radio spectrum in Durham City, UK is highly underutilized and exhibits significant potential for spectrum reutilization. To improve spectrum utilization, a CR user can play a vital role by accessing spectrum opportunities in both time and frequency at a given measurement location.

Short term measurements were conducted for 20 minutes in an indoor environment with the intention to investigate methods to access 2.4 GHz WLAN spectrum holes in the time domain. The measurements were conducted between 2.4-2.5 GHz with a sensing bandwidth of 100 MHz and WLAN packets were detected based on the received power. It is found that for continuous time a semi-Markov model, the idle time window can also be modelled using gamma, lognormal and Weibull distributions.

Cooperative spectrum occupancy measurements are conducted using three sensing nodes where two nodes were placed at fixed locations and a third node was moved in the corridors to study the impact of the spatial dimension on spectrum utilization and the amount of distinct occupancy events for cooperation. The distinct occupancy events are essential for CR users cooperation to reliably detect the spectrum holes to avoid the hidden node problem and also limit the interference to local users of the network. The amount of distinct occupancy events is found to be higher if the local occupancy decisions of nodes is combined using the OR hard combining technique in comparison to the AND hard combining technique or the individual contribution of a node for CRN cooperation.

4.6 References

[1] S. Haykin, "Cognitive radio: brain-empowered wireless communications," *Selected Areas in Communications, IEEE Journal on,* vol. 23, pp. 201-220, 2005.

[2] R. Tandra, S. M. Mishra, and A. Sahai, "What is a Spectrum Hole and What Does it Take to Recognize One?," *Proceedings of the IEEE,* vol. 97, pp. 824-848, 2009.

[3] D. Finn, J. Tallon, L. A. DaSilva, P. Van Wesemael, S. Pollin, W. Liu, *et al.*, "Experimental Assessment of Tradeoffs among Spectrum Sensing Platforms," presented at the Wintech 2011, Las Vegas, Nevada, 2011.

[4] T. Yucek and H. Arslan, "A survey of spectrum sensing algorithms for cognitive radio applications," *Communications Surveys & Tutorials, IEEE,* vol. 11, pp. 116-130, 2009.

[5] L. De Vito, "Methods and technologies for wideband spectrum sensing," *Measurement,* vol. 46, pp. 3153-3165, 2013.

[6] S. Hongjian, A. Nallanathan, W. Cheng-Xiang, and C. Yunfei, "Wideband spectrum sensing for cognitive radio networks: a survey," *Wireless Communications, IEEE,* vol. 20, pp. 74-81, 2013.

[7] V. Blaschke, T. Renk, and F. K. Jondral, "A Cognitive Radio Receiver Supporting Wide-Band Sensing," in *Communications Workshops, 2008. ICC Workshops '08. IEEE International Conference on*, 2008, pp. 499-503.

[8] S. Salous, "Chirp sounder measurements for broadband wireless networks and cognitive radio," in *Communication Systems Networks and Digital Signal Processing (CSNDSP), 2010 7th International Symposium on*, 2010, pp. 846-851.

[9] D. Denkovski, M. Pavloski, V. Atanasovski, and L. Gavrilovska, "Parameter settings for 2.4 GHz ISM spectrum measurements," in *Applied Sciences in Biomedical and Communication Technologies (ISABEL), 2010 3rd International Symposium on*, 2010, pp. 1-5.

[10] D. Cabric, S. M. Mishra, and R. W. Brodersen, "Implementation issues in spectrum sensing for cognitive radios," in *Signals, Systems and Computers, 2004. Conference Record of the Thirty-Eighth Asilomar Conference on*, 2004, pp. 772-776 Vol.1.

[11] H. Yuxing, W. Jiangtao, D. Cabric, and J. D. Villasenor, "Probabilistic Estimation of the Number of Frequency-Hopping Transmitters," *Wireless Communications, IEEE Transactions on*, vol. 10, pp. 3232-3240, 2011.

[12] X. Wenyuan, "Channel Surfing: Defending Wireless Sensor Networks from Interference," in *Information Processing in Sensor Networks, 2007. IPSN 2007. 6th International Symposium on*, 2007, pp. 499-508.

[13] S. Geirhofer, T. Lang, and B. M. Sadler, "A Measurement-Based Model for Dynamic Spectrum Access in WLAN Channels," in *Military Communications Conference, 2006. MILCOM 2006. IEEE*, 2006, pp. 1-7.

[14] M. Lopez-Benitez and F. Casadevall, "Time-Dimension Models of Spectrum Usage for the Analysis, Design, and Simulation of Cognitive Radio Networks," *Vehicular Technology, IEEE Transactions on*, vol. 62, pp. 2091-2104, 2013.

[15] M. Wellens, J. Riihijärvi, and P. Mähönen, "Empirical time and frequency domain models of spectrum use," *Physical Communication*, vol. 2, pp. 10-32, 3, 2009.

[16] S. Geirhofer, T. Lang, and B. M. Sadler, "Cognitive Radios for Dynamic Spectrum Access - Dynamic Spectrum Access in the Time Domain: Modeling and Exploiting White Space," *Communications Magazine, IEEE*, vol. 45, pp. 66-72, 2007.

[17] L. Stabellini, "Quantifying and Modeling Spectrum Opportunities in a Real Wireless Environment," in *Wireless Communications and Networking Conference (WCNC), 2010 IEEE*, 2010, pp. 1-6.

[18] Z. Wang and S. Salous, "Spectrum Occupancy Statistics and Time Series Models for Cognitive Radio," *Journal of Signal Processing Systems*, vol. 62, pp. 145-155, 2011/02/01 2011.

[19] M. Matinmikko, M. Mustonen, M. Hoyhtya, *et al.*, "Distributed and directional spectrum occupancy measurements in the 2.4 GHz ISM band," in *Wireless Communication Systems (ISWCS), 2010 7th International Symposium on*, 2010, pp. 676-980.

[20] M. Matinmikko, M. Mustonen, M. Hoyhtya, *et al.*, "Cooperative spectrum occupancy measurements in the 2.4 GHz ISM band," in *Applied Sciences in Biomedical and Communication Technologies (ISABEL), 2010 3rd International Symposium on*, 2010, pp. 1-5.

[21] kenbotong. *TDJ-0825DSA*. Available: http://kenbotong.com/

[22] M. H. Islam, C. L. Koh, O. Ser Wah, Q. Xianming, Y. Y. Lai, W. Cavin, *et al.*, "Spectrum Survey in Singapore: Occupancy Measurements and Analyses," in *Cognitive Radio Oriented Wireless Networks and Communications, 2008. CrownCom 2008. 3rd International Conference on*, 2008, pp. 1-7.

[23] T. Harrold, R. Cepeda, and M. Beach, "Long-term measurements of spectrum occupancy characteristics," in *New Frontiers in Dynamic Spectrum Access Networks (DySPAN), 2011 IEEE Symposium on*, 2011, pp. 83-89.

[24] J. Xue, Z. Feng, and P. Zhang, "Spectrum Occupancy Measurements and Analysis in Beijing," *IERI Procedia*, vol. 4, pp. 295-302, 2013.

[25] K. A. Qaraqe, H. Celebi, M. S. Alouini, A. El-Saigh, L. Abuhantash, M. M. Al-Mulla, *et al.*, "Measurement Analysis of Wideband Spectrum Utilization in Indoor Outdoor Environments," presented at the International Conference on Communications Technologies (ICCT 2010), 2010.

[26] M. Wellens, J. Wu, and P. Mahonen, "Evaluation of Spectrum Occupancy in Indoor and Outdoor Scenario in the Context of Cognitive Radio," in *Cognitive Radio Oriented Wireless Networks and Communications, 2007. CrownCom 2007. 2nd International Conference on*, 2007, pp. 420-427.

[27] M. Lopez-Benitez, A. Umbert, and F. Casadevall, "Evaluation of Spectrum Occupancy in Spain for Cognitive Radio Applications," in *Vehicular Technology Conference, 2009. VTC Spring 2009. IEEE 69th*, 2009, pp. 1-5.

[28] R. I. C. Chiang, G. B. Rowe, and K. W. Sowerby, "A Quantitative Analysis of Spectral Occupancy Measurements for Cognitive Radio," in *Vehicular Technology Conference, 2007. VTC2007-Spring. IEEE 65th*, 2007, pp. 3016-3020.

[29] A. A. Cheema and S. Salous, "High resolution temporal occupancy measurements to characterize idle time window in ISM band," in *General Assembly and Scientific Symposium (URSI GASS), 2014 XXXIth URSI*, 2014, pp. 1-4.

[30] M. Wellens and P. Mahonen, "Lessons learned from an extensive spectrum occupancy measurement campaign and a stochastic duty cycle model," in *Testbeds and Research Infrastructures for the Development of Networks &*

Communities and Workshops, 2009. TridentCom 2009. 5th International Conference on, 2009, pp. 1-9.

[31] I. F. Akyildiz, B. F. Lo, and R. Balakrishnan, "Cooperative spectrum sensing in cognitive radio networks: A survey," *Phys. Commun.*, vol. 4, pp. 40-62, 2011.

[32] M. Wellens, J. Riihijarvi, M. Gordziel, and P. Mahonen, "Evaluation of Cooperative Spectrum Sensing Based on Large Scale Measurements," in *New Frontiers in Dynamic Spectrum Access Networks, 2008. DySPAN 2008. 3rd IEEE Symposium on*, 2008, pp. 1-12.

5 Conclusions and Future work

5.1 Conclusions

The primary objective of this thesis was to develop a homogeneous test-bed for the distributed channel measurements mainly passive. Moreover, high bandwidth, time-frequency resolutions, sensitivity and IDR were expected and set as design goals. The developed test-bed was validated experimentally to meet the design goals and have abilities to perform the wideband and high time-frequency resolution measurements in two frequency bands.

The demand of radio spectrum is growing rapidly and it is becoming a difficult task to accommodate the emerging radio technologies in the current frequency allocation scheme. In addition, radio spectrum in the current frequency allocation scheme is heavily underutilized in time, frequency and space. To address the aforementioned problems, a CR can play a vital role as it is capable of finding spectrum holes in the current frequency allocation scheme and can reassign it to the emerging radio technologies to overcome the radio spectrum demand and also to improve the spectrum utilization.

For CR, reliable detection of the spectrum holes is important to characterize the radio spectrum utilization and also to define the opportunistic spectrum access methods, with the constraint to limit the interference to local users of the network. Different wideband measurement techniques are explained in chapter 2 for the detection of the spectrum holes. In comparison to the homodyne and heterodyne techniques, the proposed linear FMCW based wideband measurement technique has high time resolution and requires low sampling rate. The design parameters for reliable detection of the spectrum holes using the proposed measurement technique are summarized in chapter 2.

The implementation detail of the proposed system in both hardware and software aspects are given in chapter 3. The details of each custom designed and commercial component of the associated unit and their interconnection details are provided. Calibration of the measuring system gains (RF attenuator, SC circuit) is performed to get the correct received power and performance (sensitivity, IDR) is

experimentally computed for a CW signal. To explore the spectrum holes in space, a total of six receivers are developed. Their calibration and performance are analysed in chapter 3.

Both omnidirectional and directional measurements were performed in the 2.4 GHz ISM band to capture the 2.4 GHz WLAN signal based on the received power in chapter 4. The occupancy data were analysed to find the statistics of the idle time window in channels and establish the method to access the spectrum holes in 2.4 GHz WLAN signal in the time domain. The empirical distributions of idle time window were computed and it is found that the distributions like lognormal, gamma and Weibull can also be used to model the statistic of the idle time window.

Long term high time and frequency resolution spectrum occupancy measurements were performed for 24 hours in both indoor and outdoor environments in Durham city, UK to quantify the spectrum utilization. The results show that the radio spectrum is highly underutilized and exhibits a significant opportunity to reutilize in time and frequency for the CR users.

Short term high time and frequency resolution measurements are performed in the 2.4 GHz ISM band for 20 minutes using the omnidirectional and directional antennas. The occupancy data are analysed to find the spectrum utilization. The results show that the 2.4 GHz WLAN channels are highly underutilized and CR users can access the channels in both time and frequency.

Distributed occupancy measurements were performed to investigate how much cooperation sensing node or nodes can provide to others in real environments. An indoor measurement was conducted to capture the 2.4 GHz WLAN signal to find and compute the amount of the distinct occupancy events, which a node or nodes can share with others in a CRN for reliable detection of the spectrum holes.

5.2 Future Work

Although developed test-bed is validated experimentally to its full capacity however following recommendations can provide possible enhancements in both hardware and radio spectrum utilization modelling:

- The offline processing time can be eliminated by performing real time computation of the occupancy state by computing results in a real time embedded system e.g. FPGA.
- Active measurements using the linear chirp signal in CRN is a very challenging task as the transmitted signal to excite the radio channel can provide interference to the local users of the network and also to the CR users. However, it can be performed by first performing passive measurement to find the spectrum holes in frequency dimension and then use these for active measurements.
- Both long term and short term occupancy data are analysed in a limited capacity. The occupancy data can be further used to build better models, which can predict the occupancy state over a wideband in the time and frequency dimensions.
- Due to time constraint, in first phase of hardware development three receivers were completed and used to conduct cooperative spectrum occupancy measurements. The full capability of test-bed can be used to perform long term cooperative spectrum occupancy measurements and data can be analysed to see the effect of space dimension on the spectrum utilization and availability of the spectrum holes.

Appendix A C++ Code to Program Parameters of DDS

The implementation details of codes, which are used to program parameters of the DDS are given in this appendix. Prior of execution of these codes, the software drivers of DDS must be installed on the host PC. They are two types of DDS used in this project which are differentiated base on the frequency of "Refout" signal: 1) 1.0498 MHz, 2) 33.59375 MHz

The user can program DDS in one of the following options by inputting:

- Start, step and start frequencies.
- Centre frequency, bandwidth and sweep duration.
- Start and stop frequencies for fixed duration (819.2 µsec) signal (for testing purpose).
- CW frequency (to generate single frequency tone) mode
- Mode of operations i.e. free run or trigger

A.1 Code for Type 1 DDS

```
using   namespace     MOL;
using   namespace     MOL::DSM2;
using   namespace     System::Threading;

#include <stdio.h>
#include <conio.h>
#include <cstdlib>
#include <math.h>

int main( )
{

// file pointer for text file
        FILE *pFile  ;
// opening text file in write mode
        pFile = fopen("C:\\Euvis\\ClkDivFactor.txt", "w")   ;

        if ( pFile == NULL )
        {
                printf("The file Can't be open \n") ;
```

```
        }



while ( 1 )
{
// DSM 202 object instantiation
        DSM_Group_API      dsm202_group;
        DSMX2              dsm202;
//local variables declaration and initialization
        int opt ;
        int opt1 ;
        unsigned __int64 start, stop, step, Center, BW ;
        unsigned int width, TrigDivNum, GAP ;
        float duration, durationSweep, frequencyUpdates, OneFrequencyUpdateTime,
        tempStep, tempStep1;

        GAP = 0 ;       // GAP points between sweeps (testing purpose)
        stop  = 0;      // stop frequency
        step  = 0;      // step frequency
        start = 0 ;     // start frequency
        Center = 0;     // centre frequnecy
        BW = 0;         // bandwidth

        duration = 0;
        durationSweep=0;
        frequencyUpdates=0;
        OneFrequencyUpdateTime = 0;
        tempStep = 0 ;
        tempStep1 = 0 ;

        //setting sampling clock frequency
        dsm202.Clock_Frequency = 2150e6;

// confirming the detection of DSM 202 module via USB port
        if( dsm202_group.number == 0 )
        {
                printf( "DSM 202 Module is not detected !!\n" );
                printf("press any key to exit ...");
                getch() ;
                return 1;
        }

// getting the module series number
```

```
        int       SeriesNumber = dsm202_group.get_sn(0);
        printf( "Found Device with ID : %d\n\n", SeriesNumber );


 // initialization of DSM202 module
        dsm202.ini( SeriesNumber );
// confirming the detected module id number is belongs to DSM202 family
        if( dsm202.module_id_number != (unsigned)MODULE_ID::DSM202 )
        {
                printf( "Got ID number: %d\n", dsm202.module_id_number );
                printf( "No DSM Module Exists!!\n" );
                return 1;
        }

// programming of parameters
        dsm202.abort  = true;                   // stops all output waveforms

// User's options
printf("Enter Frequency in range of 250MHz to 1000MHz \n"
"1. Enter Start, Step and Stop frequencies of FMCW signal in Hz \n"
"2. Enter Center, BW frequencies in Hz and duration of FMCW signal in sec   \n"
"3. Enter Start and Stop frequencies of FMCW signal in Hz   \n"
"4. Enter CW frequency in Hz   \n"
"5. Exit \n"
"Enter option : " );

        scanf("%d", &opt1);
        switch(opt1)
        {
        case 1 :

        printf("Start(Hz) : ");
        scanf("%u", &start);
        printf("Step(Hz)  : ");
        scanf("%u", &step);
        printf("Stop(Hz)  : ");
        scanf("%u", &stop);

        dsm202.abort          = true;
        dsm202.chirp1         = 1.9977*start; // defines chirp start frequency address
        dsm202.chirp2         = 1.9977*stop; // defines chirp stop frequency address
        dsm202.chirp3         = 1.9977*step ;// defines chirp step frequency address

        //setting up marker signal
```

```
 dsm202.marker_start  = dsm202.datalength /2 ;
// defines marker width
dsm202.marker_width = dsm202.datalength ;

duration =  ( 32 / dsm202.Clock_Frequency ) * ( dsm202.datalength + 8 +
GAP ) ;
TrigDivNum =  ceil(1.0498e6 * duration)  ;
break ;

case 2 :
printf("Center Frequency(Hz)    : ");
scanf("%u", &Center);
printf("Bandwidth(Hz)          : ");
scanf("%u", &BW);
printf("Sweep Duration(Sec)     : ");
scanf("%f", &durationSweep);

OneFrequencyUpdateTime = 32 / dsm202.Clock_Frequency;
frequencyUpdates = -8 + durationSweep / OneFrequencyUpdateTime  ;

dsm202.abort   = true;
dsm202.chirp1 = 1.9977*(Center - BW/2 );  // defines chirp start frequency
                                          //address
dsm202.chirp2 = 1.9977*(Center + BW/2 );  // defines chirp stop frequency
                                          // address
dsm202.chirp3 = BW ;
dsm202.chirp3 = 1.9977*( dsm202.chirp3 / frequencyUpdates ); // defines
                                          // chirp step frequency address
//setting up marker signal
dsm202.marker_start   = dsm202.datalength /2 ;
// defines marker width
dsm202.marker_width = dsm202.datalength ;

duration =  ( 32 / dsm202.Clock_Frequency ) * ( dsm202.datalength + 8 +
GAP ) ;
TrigDivNum =  ceil(1.0498e6 * duration)  ;
break ;

case 3 :
printf("Start(Hz) : ");
scanf("%u", &start);
printf("Stop(Hz)  : ");
scanf("%u", &stop);
```

```
dsm202.abort            = true;
dsm202.chirp1           = 1.9977*start; // defines chirp start frequency address
dsm202.chirp2           = 1.9977*stop; // defines chirp stop frequency address

tempStep1 =  ((dsm202.Clock_Frequency/32) * 0.000818733860 - 9 - GAP );
step =  ( ( stop - start ) / tempStep1 )  ;

dsm202.chirp3           = 1.9977*step ; // defines chirp step frequency address

//setting up marker signal
dsm202.marker_start   = dsm202.datalength /2 ;
// defines marker width
dsm202.marker_width = dsm202.datalength ;

duration =   ( 32 / dsm202.Clock_Frequency ) * ( dsm202.datalength + 8 +
GAP ) ;
TrigDivNum =  ceil(1.0498e6 * duration)  ;
break ;

case 4 :
printf("CW(Hz) : ");
scanf("%u", &start);

dsm202.abort            = true;
dsm202.chirp1           = 1.9977*start; // defines chirp start frequency address
dsm202.chirp2           = 1.9977*start; // defines chirp stop frequency address
dsm202.chirp3           = 0 ;     // defines chirp step frequency address

TrigDivNum =  860;
break ;

case 5 :
exit(0);
break ;

}
```

// saving the clock dividing factor into text file, which will be read by software written in NI LabVIEW .

```
if (TrigDivNum == 0)
{
        TrigDivNum = 1 ;
}
```

```
        fprintf(pFile, "%d \n", TrigDivNum ) ;
        fclose(pFile); //closing the text file

printf(  "1. FMCW Waveform in free Run Mode\n"
        "2. FMCW Waveform in Trigger Mode \n"
        "3. Exit \n"
        "Enter option : " );

        scanf("%d", &opt);
        switch(opt)
        {

        case 1 :
        dsm202.triangle_chirp               = false;
        dsm202.marker_filter_count1         = 0;
        dsm202.free_run                     = true;
        break ;

        case 2:

        dsm202.triangle_chirp               = false;
        dsm202.marker_filter_count1         = 0;
        dsm202.arm                          = true;
        break ;

        case 3:
        exit(0);
        break ;

        default:
        printf(" Please select options between 1-3 ... \n") ;
        break ;

        }

printf("press any key to configure again ... \n ");
getch() ;

system("cls")  ; // to clear screen for next configuration
}

return 0;
}
```

A.2 Code for Type 2 DDS

```
using   namespace      MOL;
using   namespace      MOL::DSM2;
using   namespace      System::Threading;

#include <stdio.h>
#include <conio.h>
#include <cstdlib>
#include <math.h>

int main( )
{

// file pointer for text file
        FILE *pFile  ;
// opening text file in write mode
        pFile = fopen("C:\\Euvis\\ClkDivFactor.txt", "w")   ;

        if ( pFile == NULL )
        {
                printf("The file Can't be open \n") ;
        }



while ( 1 )
{
// DSM 202 Object instantiation
        DSM_Group_API      dsm202_group;
        DSMX2              dsm202;
//local variables declaration and initialization
        int opt ;
        int opt1 ;
        unsigned __int64 start, stop, step, Center, BW ;
        unsigned int width, TrigDivNum, GAP ;
        float duration, durationSweep, frequencyUpdates, OneFrequencyUpdateTime,
        tempStep, tempStep1;

        GAP = 0 ;       // GAP points between sweeps (testing purpose)
        stop  = 0;      // stop frequency
        step  = 0;      // step frequency
        start = 0 ;     // start frequency
        Center = 0;     // center frequnecy
```

```
        BW = 0;         // bandwidth

        duration = 0;
        durationSweep=0;
        frequencyUpdates=0;
        OneFrequencyUpdateTime = 0;
        tempStep = 0 ;
        tempStep1 = 0 ;

        //setting sampling clock frequency
        dsm202.Clock_Frequency = 2150e6;

// confirming the detection of DSM 202 module via USB port
        if( dsm202_group.number == 0 )
        {
                printf( "DSM 202 Module is not detected !!\n" );
                printf("press any key to exit ...");
                getch() ;
                return 1;
        }

// getting the module series number
        int     SeriesNumber = dsm202_group.get_sn(0);
        printf( "Found Device with ID : %d\n\n", SeriesNumber );


 // initialization of DSM202 module
        dsm202.ini( SeriesNumber );
// confirming the detected module id number is belongs to DSM202 family
        if( dsm202.module_id_number != (unsigned)MODULE_ID::DSM202 )
        {
                printf( "Got ID number: %d\n", dsm202.module_id_number );
                printf( "No DSM Module Exists!!\n" );
                return 1;
        }

// programming of parameters
        dsm202.abort  = true;                   // stops all output waveforms

// User's options
printf("Enter Frequency in range of 250MHz to 1000MHz \n"
"1. Enter Start, Step and Stop frequencies of FMCW signal in Hz \n"
"2. Enter Center, BW frequencies in Hz and duration of FMCW signal in sec   \n"
"3. Enter Start and Stop frequencies of FMCW signal in Hz   \n"
```

```
"4. Enter CW frequency in Hz   \n"
"5. Exit \n"
"Enter option : " );

        scanf("%d", &opt1);
        switch(opt1)
        {
        case 1 :

        printf("Start(Hz) : ");
        scanf("%u", &start);
        printf("Step(Hz)  : ");
        scanf("%u", &step);
        printf("Stop(Hz)  : ");
        scanf("%u", &stop);

        dsm202.abort            = true;
        dsm202.chirp1           = 1.9977*start; // defines chirp start frequency address
        dsm202.chirp2           = 1.9977*stop; // defines chirp stop frequency address
        dsm202.chirp3           = 1.9977*step ;// defines chirp step frequency address

        //setting up marker signal
         dsm202.marker_start  = dsm202.datalength /2 ;
        // defines marker width
        dsm202.marker_width = dsm202.datalength ;

        duration =   ( 32 / dsm202.Clock_Frequency ) * ( dsm202.datalength + 8 +
        GAP ) ;
        TrigDivNum =  ceil(33.59375e6 * duration)  ;
        break ;

        case 2 :
        printf("Center Frequency(Hz)    : ");
        scanf("%u", &Center);
        printf("Bandwidth(Hz)          : ");
        scanf("%u", &BW);
        printf("Sweep Duration(Sec)     : ");
        scanf("%f", &durationSweep);

        OneFrequencyUpdateTime = 32 / dsm202.Clock_Frequency;
        frequencyUpdates = -8 + durationSweep / OneFrequencyUpdateTime  ;

        dsm202.abort   = true;
        dsm202.chirp1 = 1.9977*(Center - BW/2 );  // defines chirp start frequency
```

```
                                                    //address
dsm202.chirp2 = 1.9977*(Center + BW/2 );  // defines chirp stop frequency
                                                    // address
dsm202.chirp3 = BW ;
dsm202.chirp3 = 1.9977*( dsm202.chirp3 / frequencyUpdates ); // defines
                                                    // chirp step frequency address
//setting up marker signal
dsm202.marker_start   = dsm202.datalength /2 ;
// defines marker width
dsm202.marker_width = dsm202.datalength ;

duration =   ( 32 / dsm202.Clock_Frequency ) * ( dsm202.datalength + 8 +
GAP ) ;
TrigDivNum =  ceil(33.59375e6 * duration)  ;
break ;

case 3 :
printf("Start(Hz) : ");
scanf("%u", &start);
printf("Stop(Hz)  : ");
scanf("%u", &stop);

dsm202.abort          = true;
dsm202.chirp1         = 1.9977*start; // defines chirp start frequency address
dsm202.chirp2         = 1.9977*stop; // defines chirp stop frequency address

tempStep1 =  ((dsm202.Clock_Frequency/32) * 0.000818733860 - 9 - GAP );
step =  ( ( stop - start ) / tempStep1 )  ;

dsm202.chirp3         = 1.9977*step ; // defines chirp step frequency address

//setting up marker signal
dsm202.marker_start   = dsm202.datalength /2 ;
// defines marker width
dsm202.marker_width = dsm202.datalength ;

duration =   ( 32 / dsm202.Clock_Frequency ) * ( dsm202.datalength + 8 +
GAP ) ;
TrigDivNum =  ceil(33.59375e6 * duration)  ;
break ;

case 4 :
printf("CW(Hz) : ");
scanf("%u", &start);
```

```
dsm202.abort            = true;
dsm202.chirp1           = 1.9977*start; // defines chirp start frequency address
dsm202.chirp2           = 1.9977*start; // defines chirp stop frequency address
dsm202.chirp3           = 0 ;     // defines chirp step frequency address

TrigDivNum =  860;
break ;

case 5 :
exit(0);
break ;

}
```

// saving the clock dividing factor into text file, which will be read by software written in NI LabVIEW .

```
if (TrigDivNum == 0)
{
        TrigDivNum = 1 ;
}
fprintf(pFile, "%d \n", TrigDivNum ) ;
fclose(pFile); //closing the text file

printf(  "1. FMCW Waveform in free Run Mode\n"
"2. FMCW Waveform in Trigger Mode \n"
"3. Exit \n"
"Enter option : " );

scanf("%d", &opt);
switch(opt)
{

case 1 :
dsm202.triangle_chirp               = false;
dsm202.marker_filter_count1         = 0;
dsm202.free_run                     = true;
break ;

case 2:

dsm202.triangle_chirp               = false;
dsm202.marker_filter_count1         = 0;
```

```
        dsm202.arm                          = true;
        break ;

        case 3:
        exit(0);
        break ;

        default:
        printf(" Please select options between 1-3 ... \n") ;
        break ;

        }

printf("press any key to configure again ... \n ");
getch() ;

system("cls")  ; // to clear screen for next configuration
}

return 0;
}
```

Appendix B Level Converter PCB

B.1 Schematic

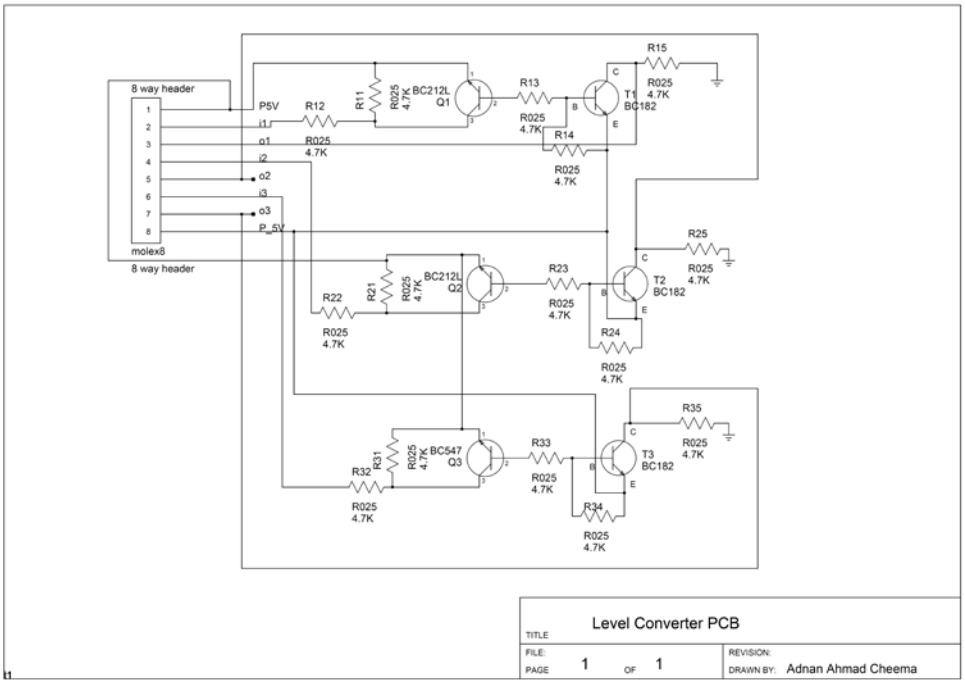

B.2 Top

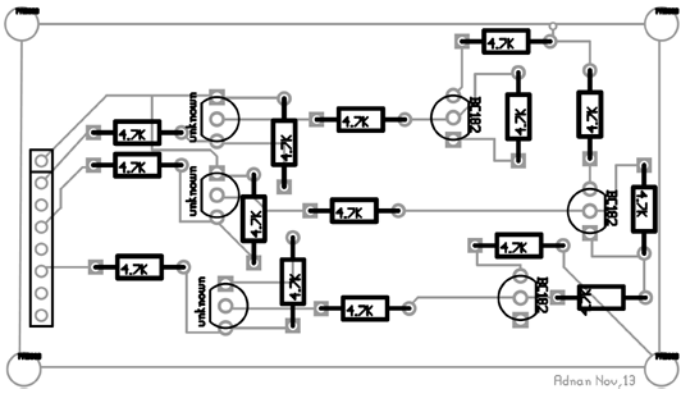

B.3 Bottom

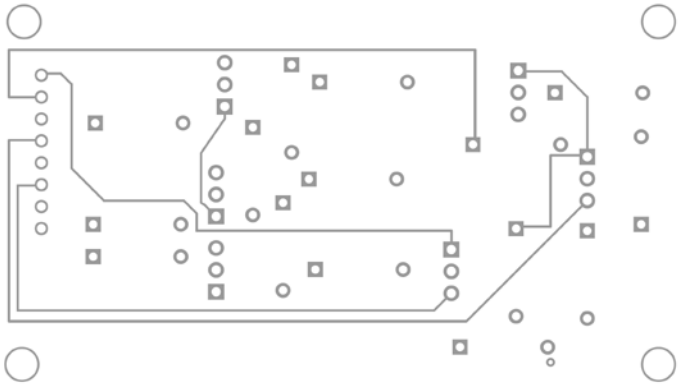

Appendix C FPGA PCB

C.1 Schematic

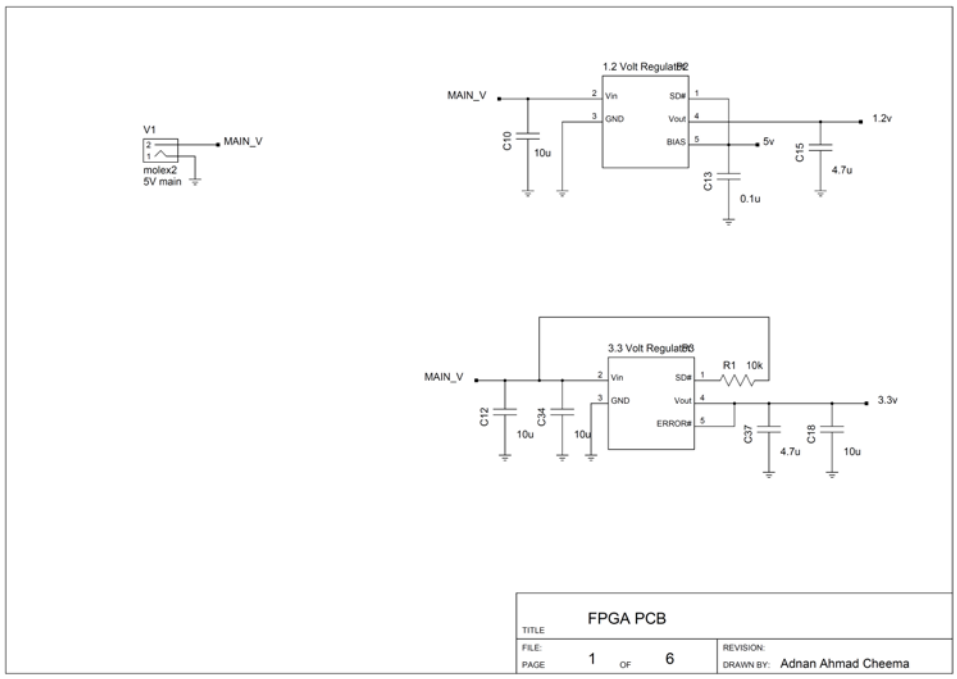

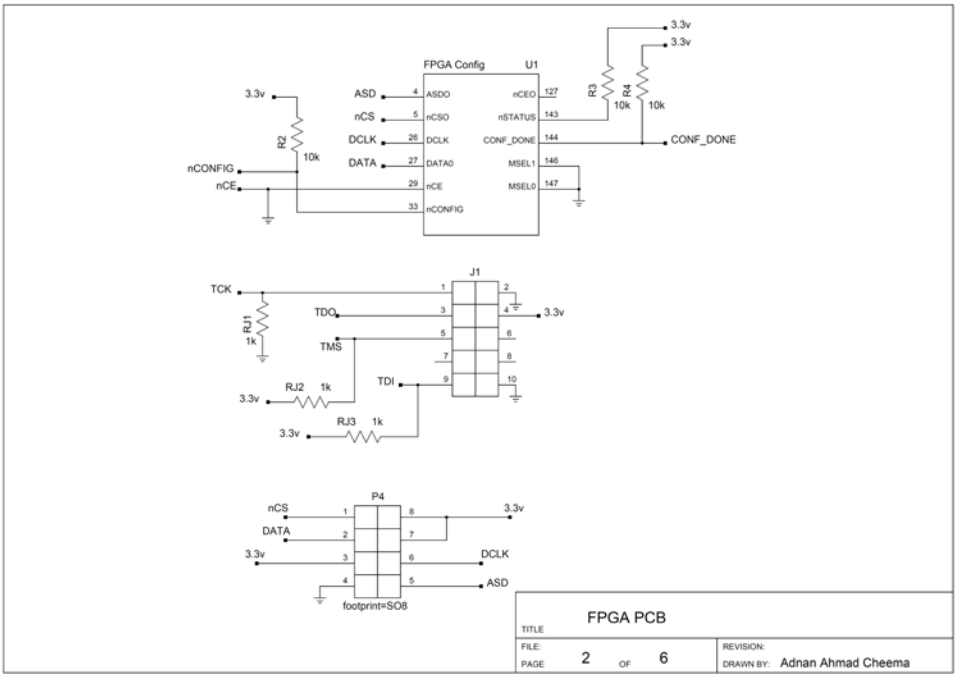

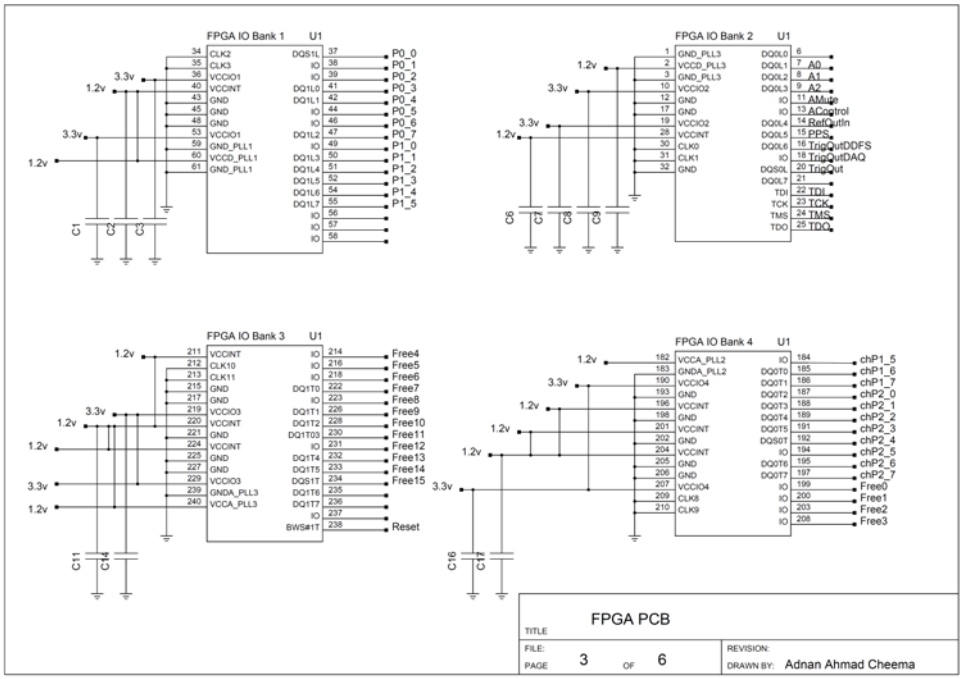
FPGA IO Bank 1 U1
FPGA IO Bank 2 U1
FPGA IO Bank 3 U1
FPGA IO Bank 4 U1
P0_0
P0_1
P0_2
P0_3
P0_4
P0_5
P0_6
P0_7
P1_0
P1_1
P1_2
P1_3
P1_4
P1_5
A0
A1
A2
AMute
ACntrol
RefOutIn
PPS
TrigOutDDFS
TrigOutDAQ
TrigOut
TDI
TCK
TMS
TDO
Free4
Free5
Free6
Free7
Free8
Free9
Free10
Free11
Free12
Free13
Free14
Free15
Reset
chP1_5
chP1_6
chP1_7
chP2_0
chP2_1
chP2_2
chP2_3
chP2_4
chP2_5
chP2_6
chP2_7
Free0
Free1
Free2
Free3
FPGA PCB
TITLE
FILE:
PAGE 3 OF 6
REVISION:
DRAWN BY: Adnan Ahmad Cheema

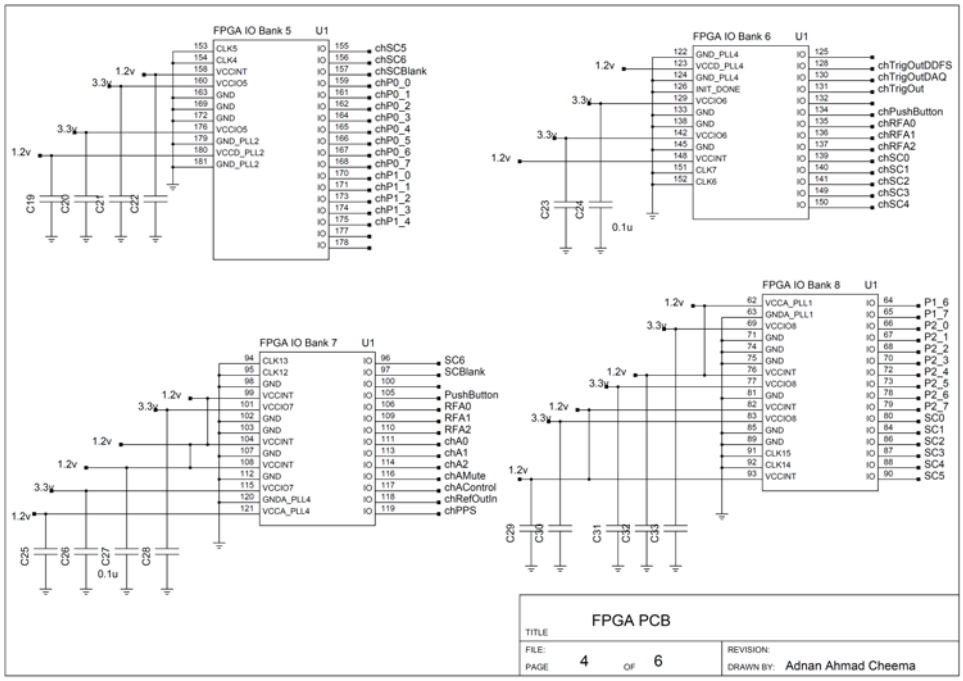
FPGA IO Bank 5 U1
FPGA IO Bank 6 U1
FPGA IO Bank 7 U1
FPGA IO Bank 8 U1
chSC5
chSC6
chSCBlank
chP0_0
chP0_1
chP0_2
chP0_3
chP0_4
chP0_5
chP0_6
chP0_7
chP1_0
chP1_1
chP1_2
chP1_3
chP1_4
chTrigOutDDFS
chTrigOutDAQ
chTrigOut
chPushButton
chRFA0
chRFA1
chRFA2
chSC0
chSC1
chSC2
chSC3
chSC4
SC6
SCBlank
PushButton
RFA0
RFA1
RFA2
chA0
chA1
chA2
chAMute
chAControl
chRefOutIn
chPPS
P1_6
P1_7
P2_0
P2_1
P2_2
P2_3
P2_4
P2_5
P2_6
P2_7
SC0
SC1
SC2
SC3
SC4
SC5
0.1u
FPGA PCB
TITLE
FILE:
PAGE 4 OF 6
REVISION:
DRAWN BY: Adnan Ahmad Cheema

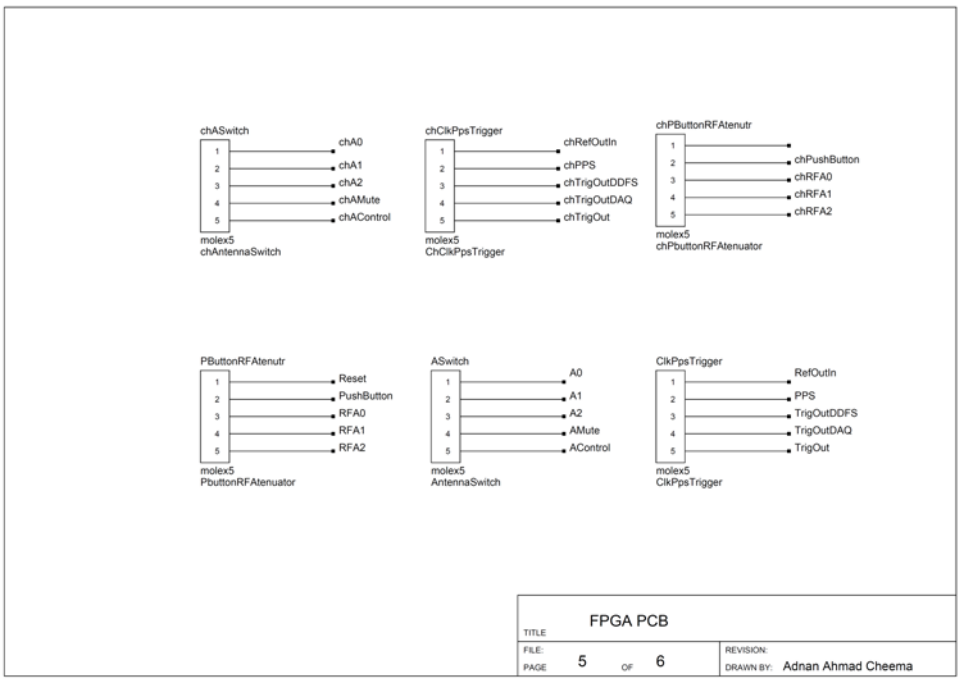
chASwitch
chA0
chA1
chA2
chAMute
chAControl
molex5
chAntennaSwitch
chClkPpsTrigger
chRefOutIn
chPPS
chTrigOutDDFS
chTrigOutDAQ
chTrigOut
molex5
ChClkPpsTrigger
chPButtonRFAtenutr
chPushButton
chRFA0
chRFA1
chRFA2
molex5
chPbuttonRFAtenuator
PButtonRFAtenutr
Reset
PushButton
RFA0
RFA1
RFA2
molex5
PbuttonRFAtenuator
ASwitch
A0
A1
A2
AMute
AControl
molex5
AntennaSwitch
ClkPpsTrigger
RefOutIn
PPS
TrigOutDDFS
TrigOutDAQ
TrigOut
molex5
ClkPpsTrigger
TITLE
FPGA PCB
FILE:
PAGE 5 OF 6
REVISION:
DRAWN BY: Adnan Ahmad Cheema

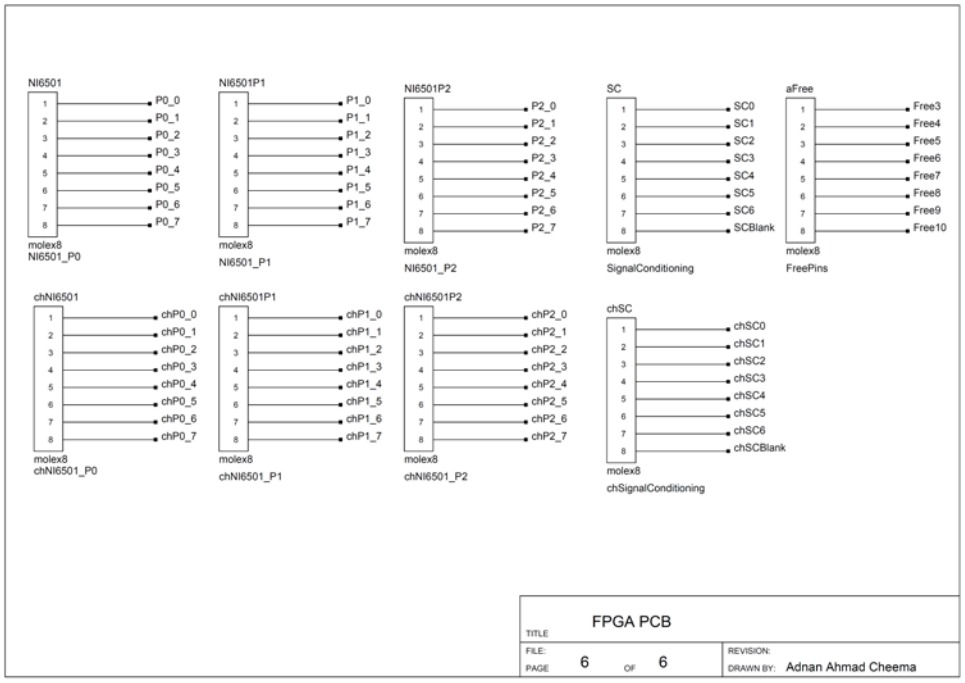
NI6501
P0_0
P0_1
P0_2
P0_3
P0_4
P0_5
P0_6
P0_7
molex8
NI6501_P0
NI6501P1
P1_0
P1_1
P1_2
P1_3
P1_4
P1_5
P1_6
P1_7
molex8
NI6501_P1
NI6501P2
P2_0
P2_1
P2_2
P2_3
P2_4
P2_5
P2_6
P2_7
molex8
NI6501_P2
SC
SC0
SC1
SC2
SC3
SC4
SC5
SC6
SCBlank
molex8
SignalConditioning
aFree
Free3
Free4
Free5
Free6
Free7
Free8
Free9
Free10
molex8
FreePins
chNI6501
chP0_0
chP0_1
chP0_2
chP0_3
chP0_4
chP0_5
chP0_6
chP0_7
molex8
chNI6501_P0
chNI6501P1
chP1_0
chP1_1
chP1_2
chP1_3
chP1_4
chP1_5
chP1_6
chP1_7
molex8
chNI6501_P1
chNI6501P2
chP2_0
chP2_1
chP2_2
chP2_3
chP2_4
chP2_5
chP2_6
chP2_7
molex8
chNI6501_P2
chSC
chSC0
chSC1
chSC2
chSC3
chSC4
chSC5
chSC6
chSCBlank
molex8
chSignalConditioning
TITLE
FPGA PCB
FILE:
PAGE 6 OF 6
REVISION:
DRAWN BY: Adnan Ahmad Cheema

C.2 Top

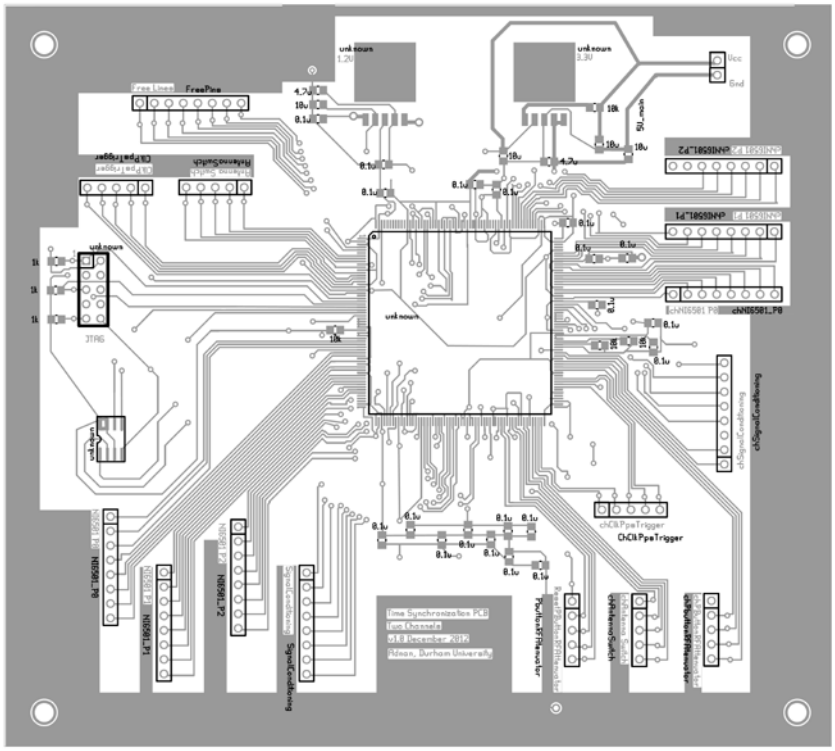

C.3 Bottom

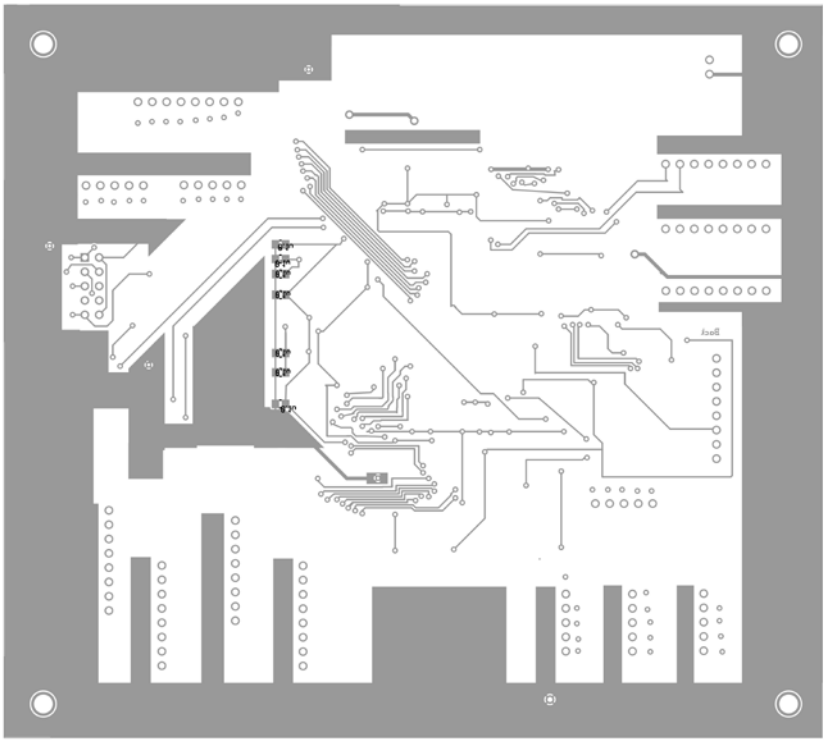

Appendix D Design of Command and Control Unit

D.1 Receiver

D.1.1 Interconnections

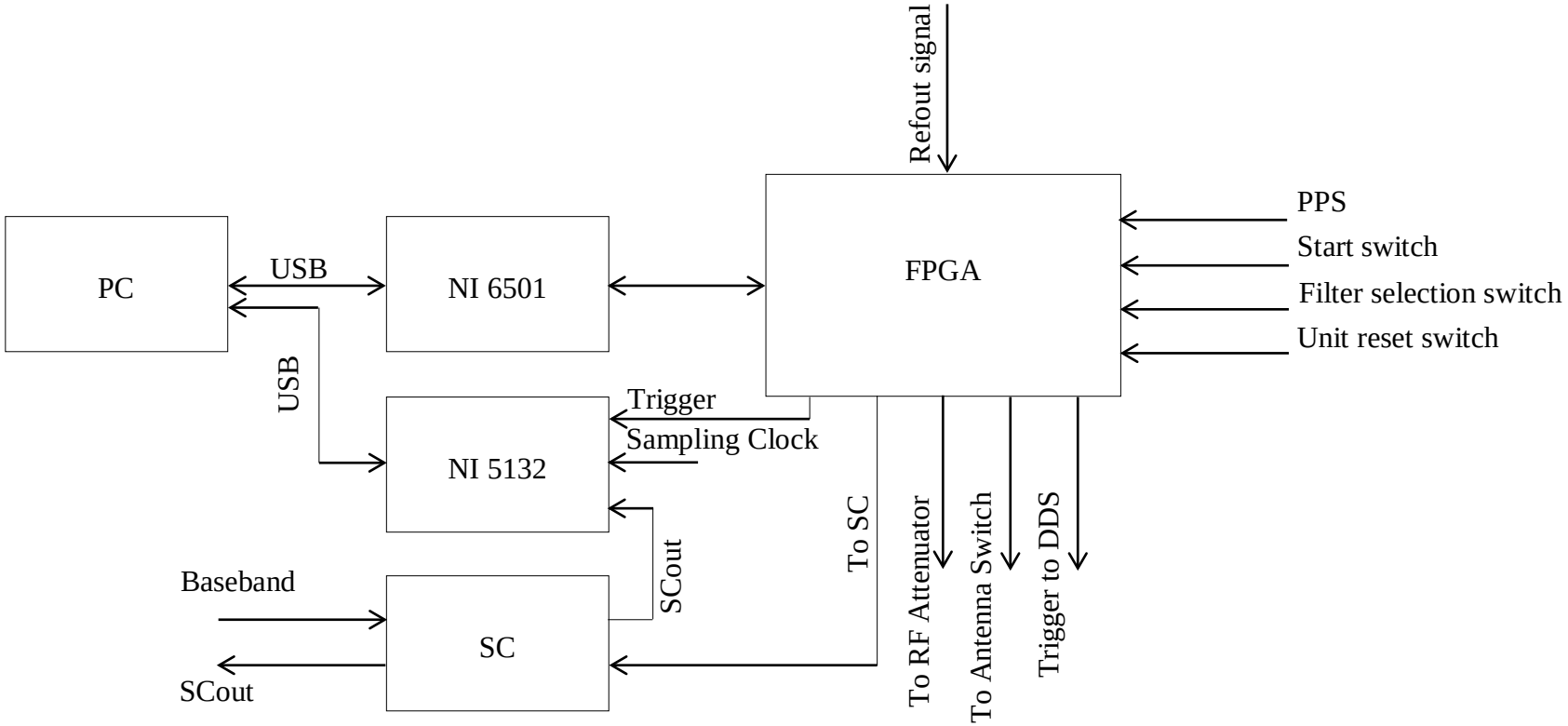

D.1.2 Pin Assignment

D.1.2.1 FPGA

Port legend	Pin Number	Signal	comments
Antenna Switch	1	Control	Enable/Disable antenna switch
	2	Mute	Enable/Disable individual RF port
	3	Data	Connected to antenna switch control lines
	4		
	5		
ClkPpsTrigger	1	Refout	Connected to LO unit
	2	PPS	
	3	Trigger	Trigger signal for LO unit
	4	Trigger	Trigger signal for NI 5132
	5	-	-
NI6501_P0	1-8	Data	Connected to P0 of NI 6501
NI6501_P1	1-8	Data	Connected to P1 of NI 6501
NI6501_P2	1-8	Data	Connected to P2 of NI 6501
SignalConditioning	1-7	Data	Connected to SC control lines
	8	-	-
ResetPbuttonRFAttenuator	1	Reset	Connected to Reset switch
	2	Start	Connected to Start switch
	3	Data	Connected to RF attenuator control lines
	4		
	5		

D.1.2.2 NI 5132

Port legend	Pin Number	Signal	comments
CH 0	1	Trigger	Connected to command and control unit
CH 1	2	Baseband	Connected to SCout port
PFI	3	Sampling clock	Connected to reference clock and distribution unit

D.1.2.3 NI 6501

Port legend	Pin Number	Signal	comments
P0	1-8	Data	Connected to FPGA PCB
P1	1-8	Data	Connected to FPGA PCB
P2	1-8	Data	Connected to FPGA PCB

D.1.3 Prototype layout

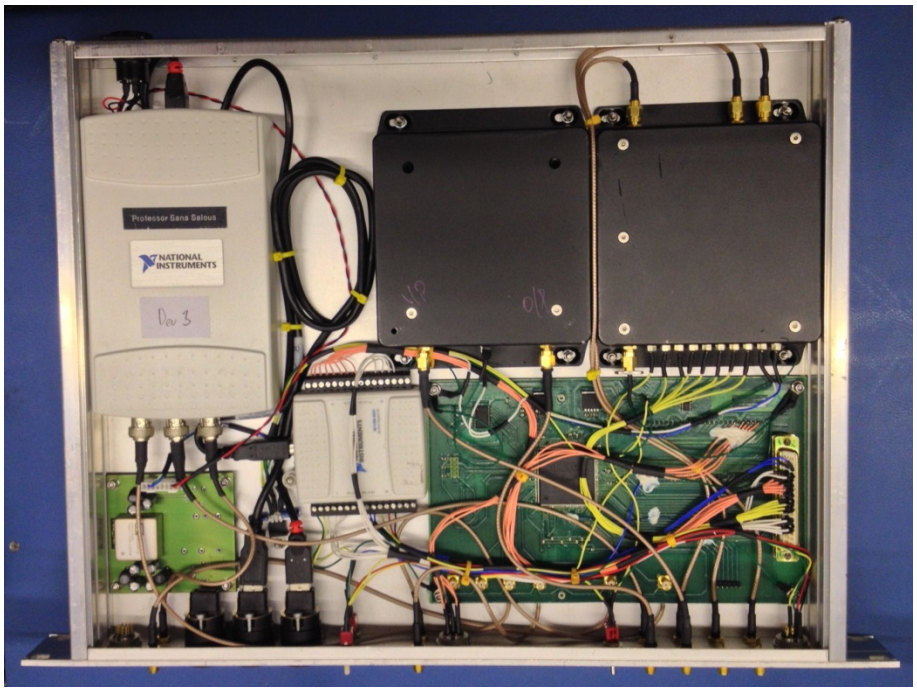

D.2. Prototype for Transmitter

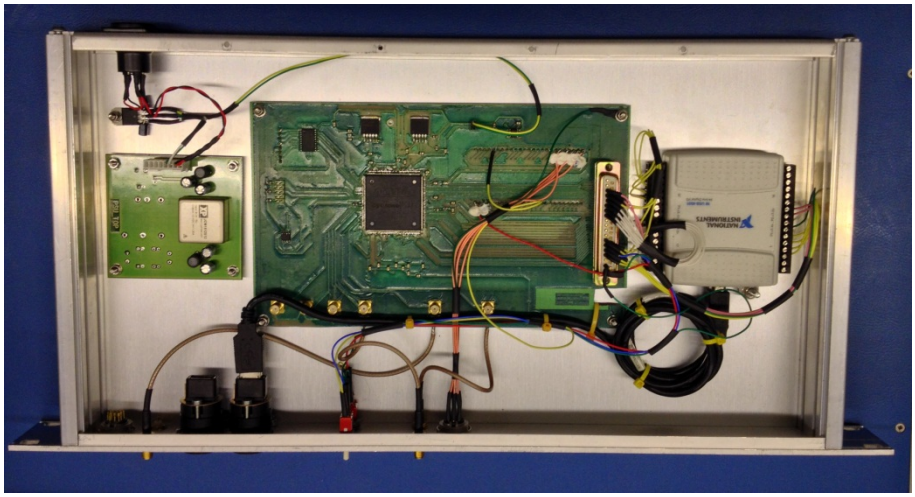

Appendix E Block Diagram of LabVIEW Application

E.1 Block Diagram of Initialization and Configuration Algorithm

E.1.1 NI 6501

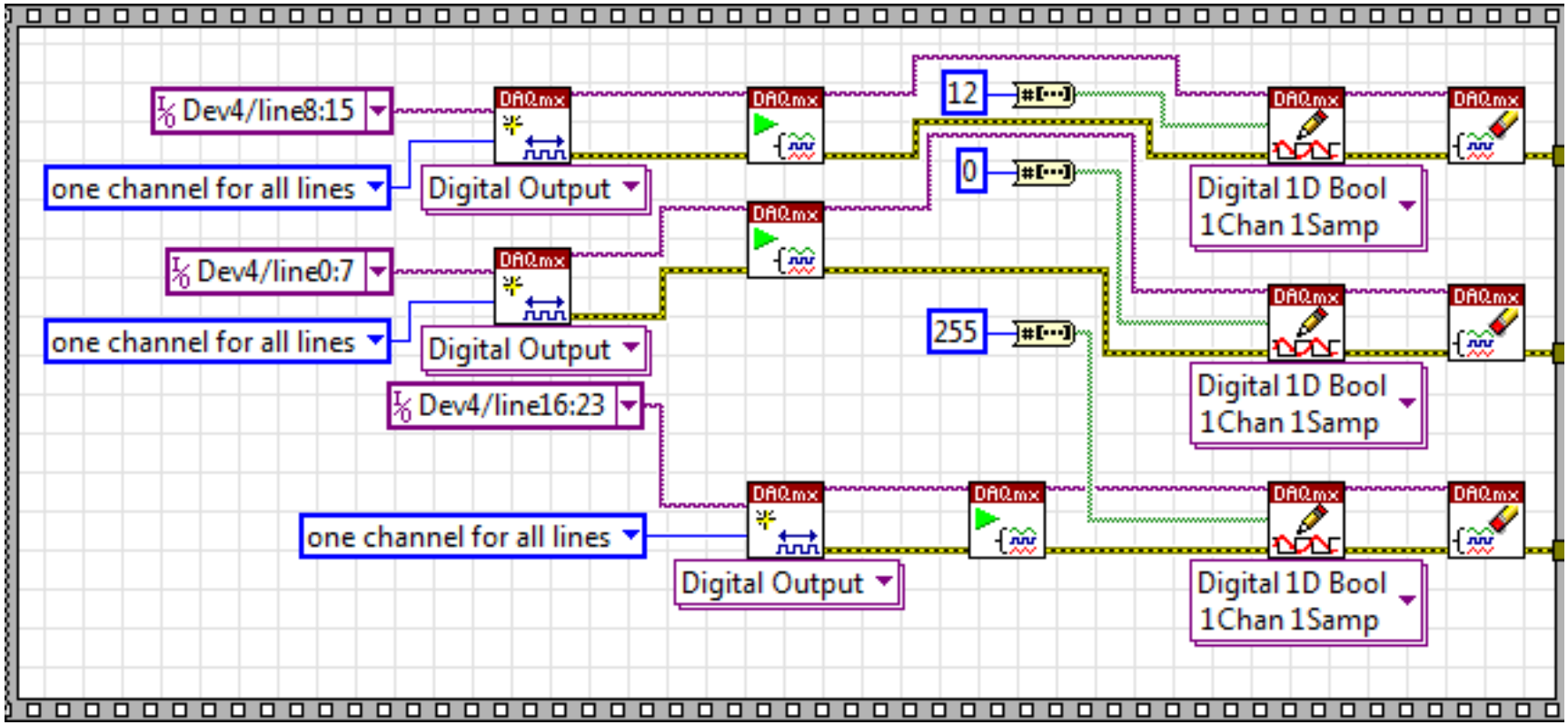

E.1.2 NI 5132

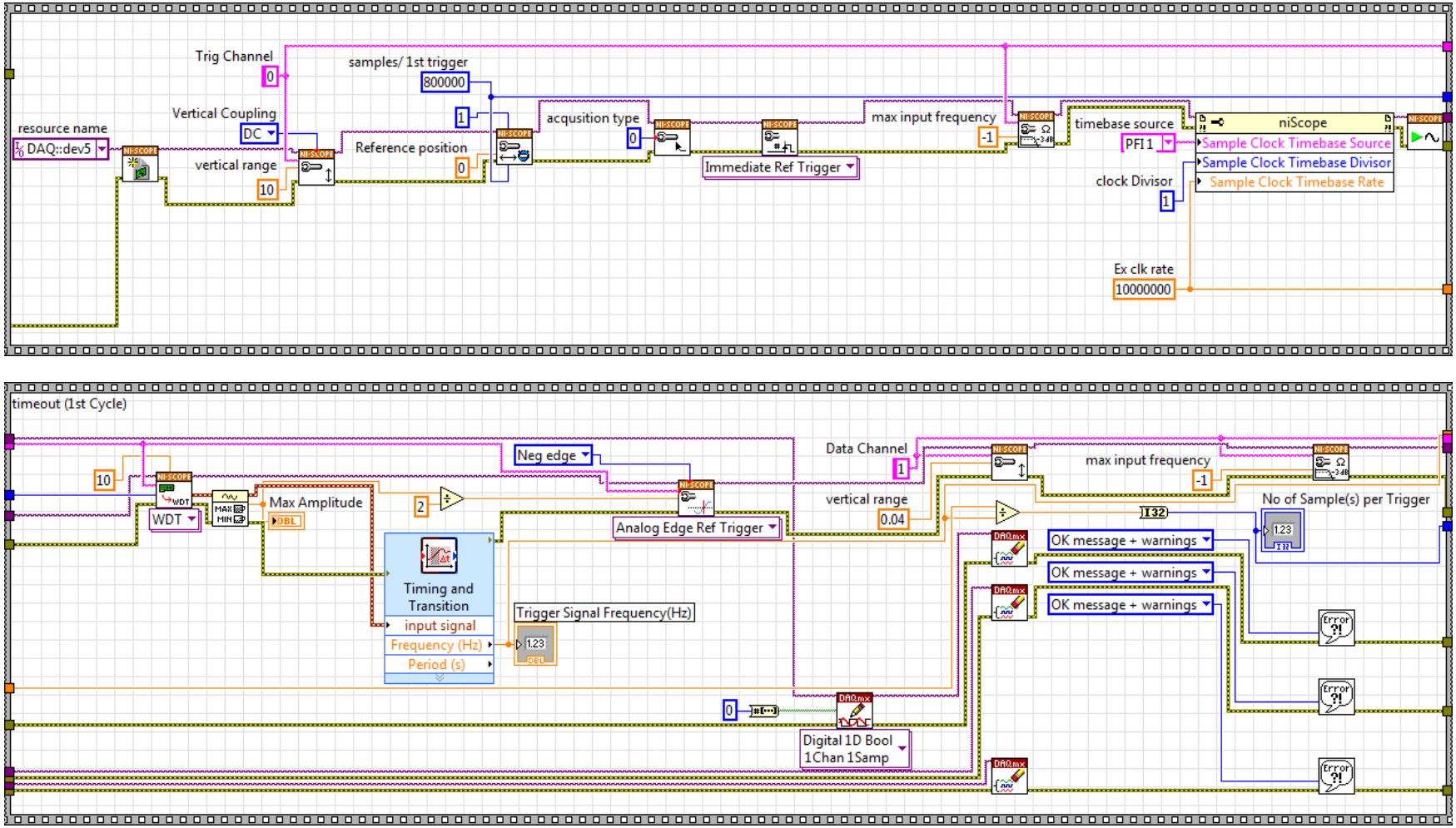
Trig Channel
0
samples/ 1st trigger
800000
Vertical Coupling
DC
resource name
DAQ::dev5
vertical range
10
Reference position
0
1
acqusition type
0
Immediate Ref Trigger
max input frequency
-1
timebase source
PFI 1
niScope
Sample Clock Timebase Source
Sample Clock Timebase Divisor
Sample Clock Timebase Rate
clock Divisor
1
Ex clk rate
10000000
timeout (1st Cycle)
10
WDT
Max Amplitude
2
Neg edge
Analog Edge Ref Trigger
Timing and Transition
input signal
Frequency (Hz)
Period (s)
Trigger Signal Frequency(Hz)
Data Channel
1
vertical range
0.04
max input frequency
-1
No of Sample(s) per Trigger
OK message + warnings
OK message + warnings
OK message + warnings
0
Digital 1D Bool
1Chan 1Samp

E.2 Block Diagram of Data Transfer and Trigger Generation Algorithm

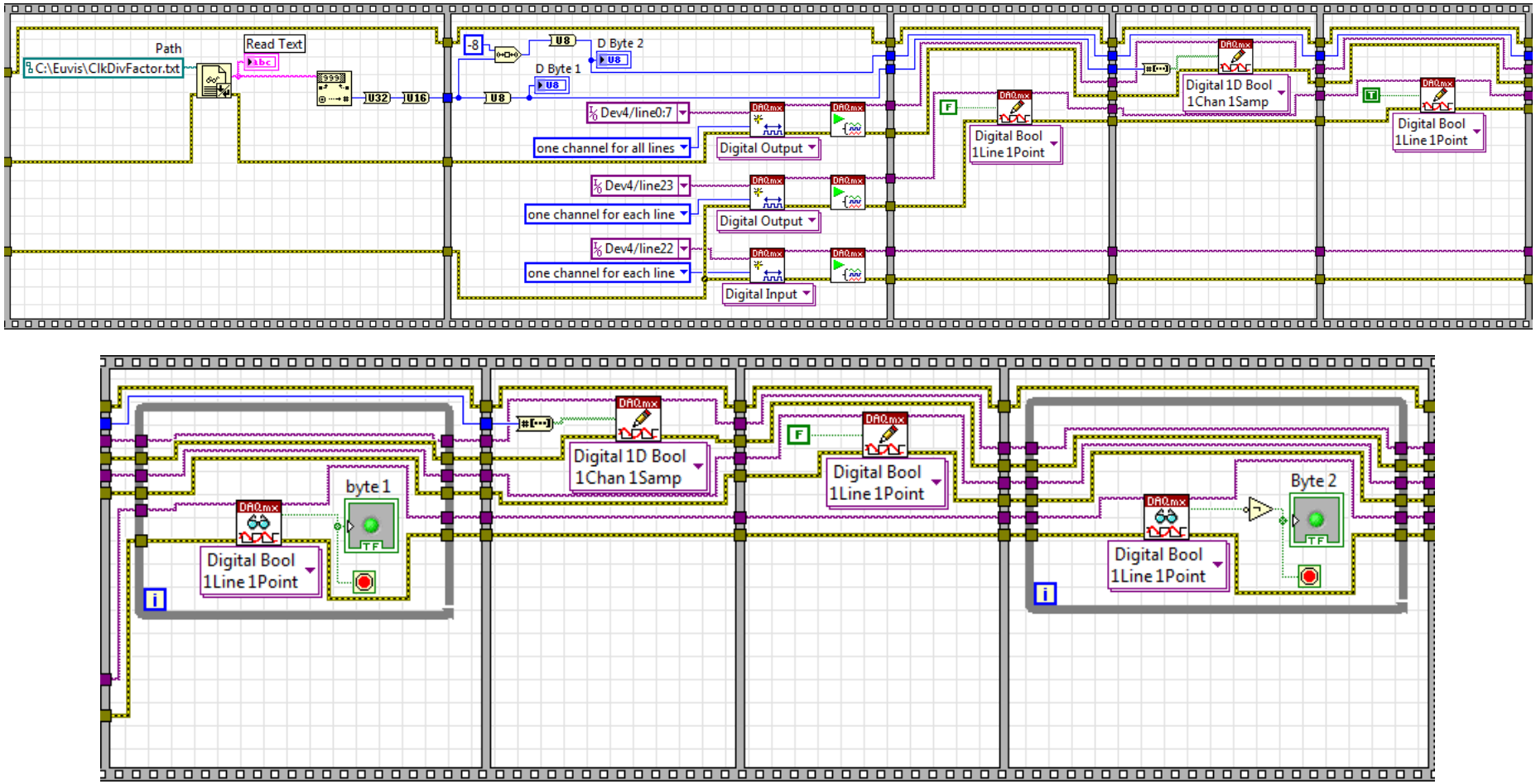

E.3 Block Diagram of Synchronization Algorithm

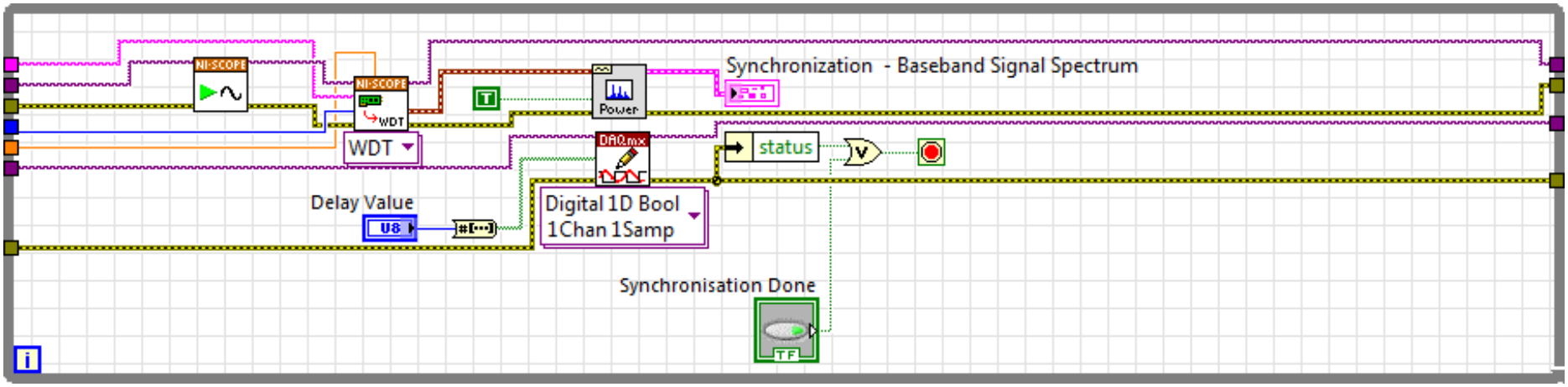

E.4 Block Diagram of Gains Calculation Algorithm

E.4.1 RF Attenuator

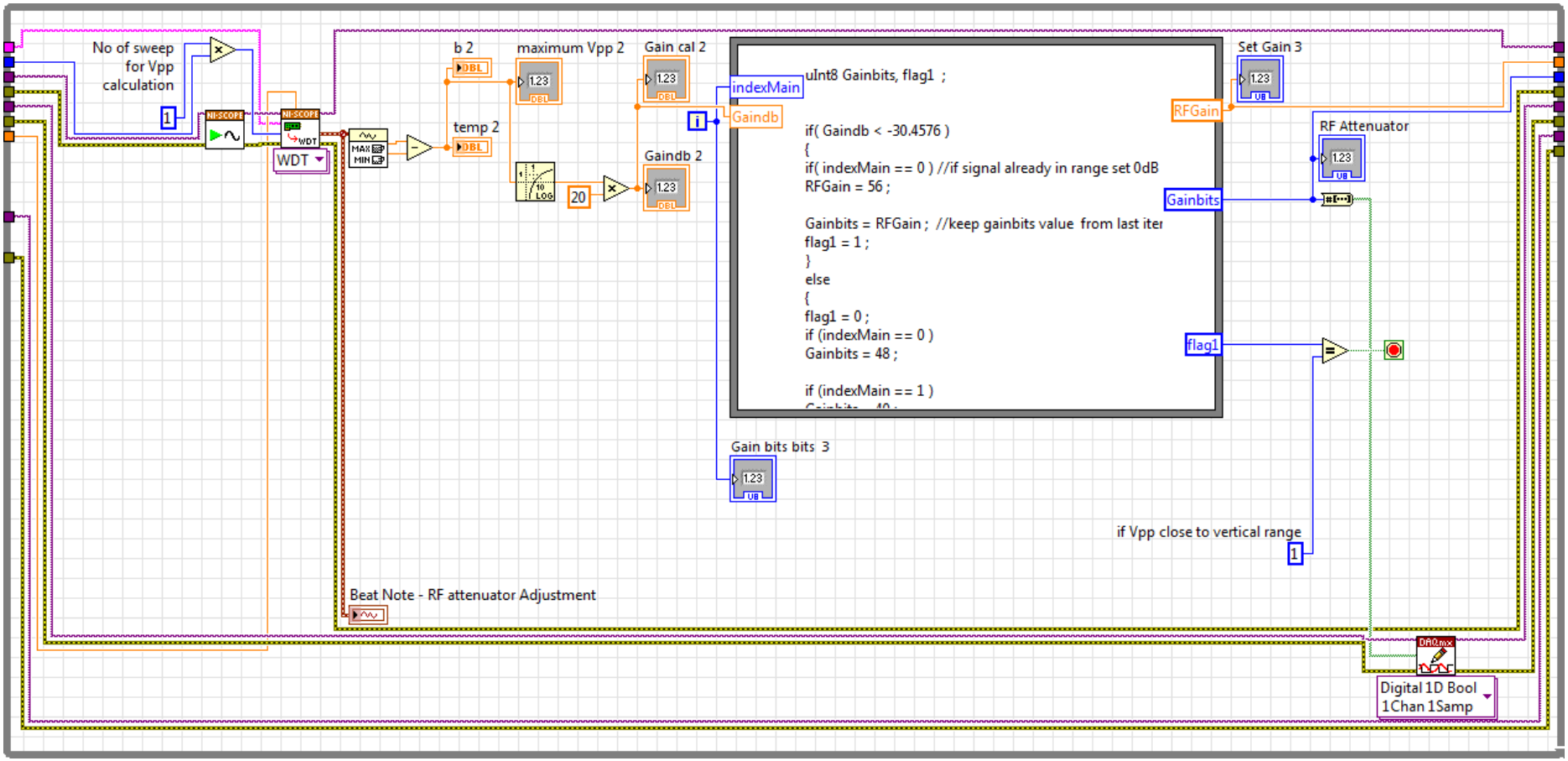

E.4.2 SC Circuit

E.4.2.1 SC Circuit Gain Calculator

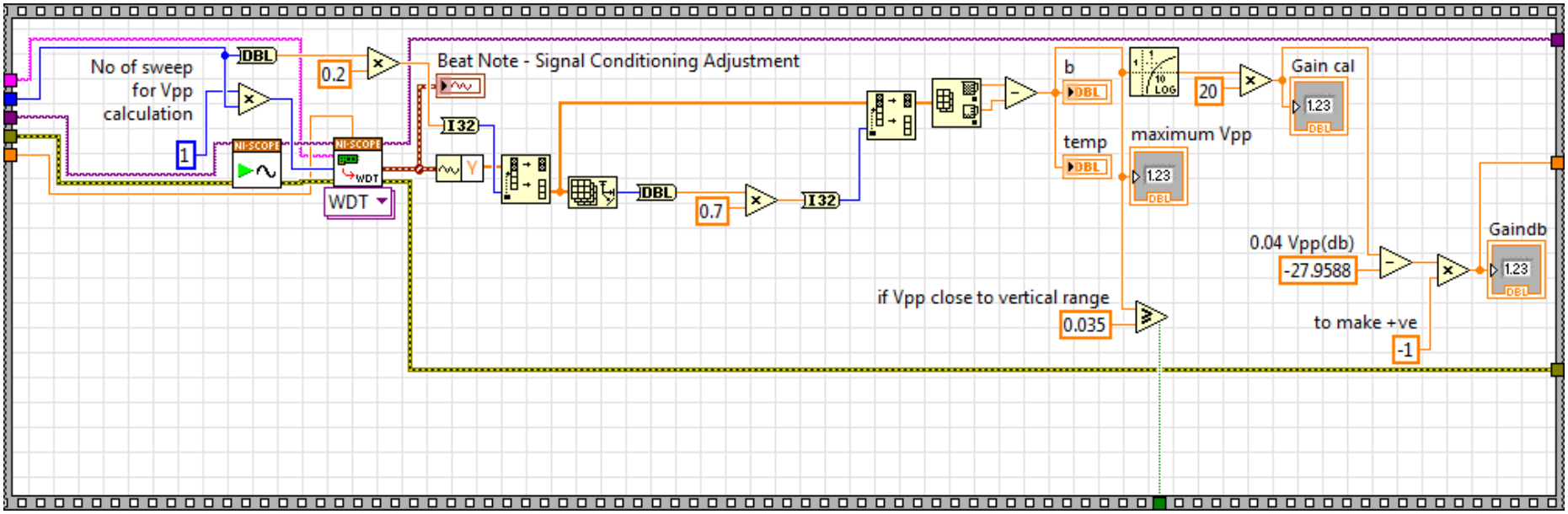

E.4.2.2 SC Circuit Gain Mapping and Transfer

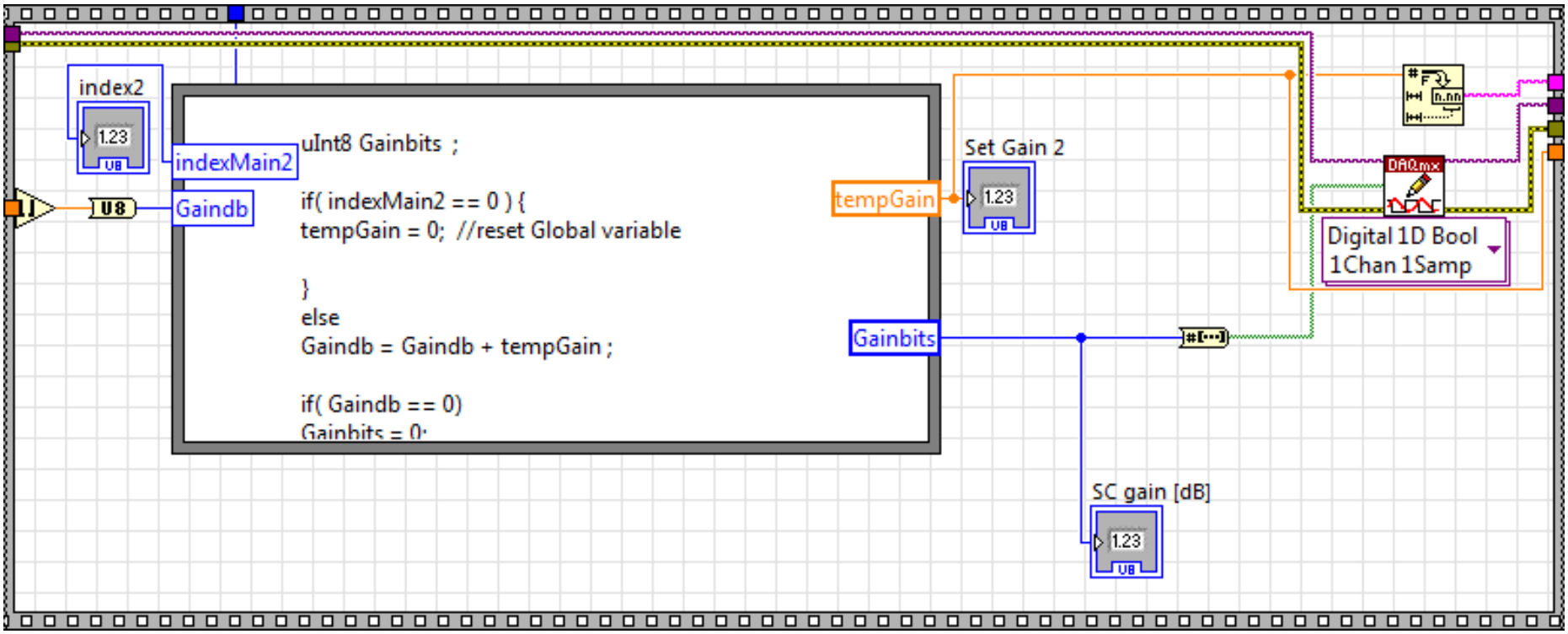

E.5 Block Diagram of Data Storage Algorithm

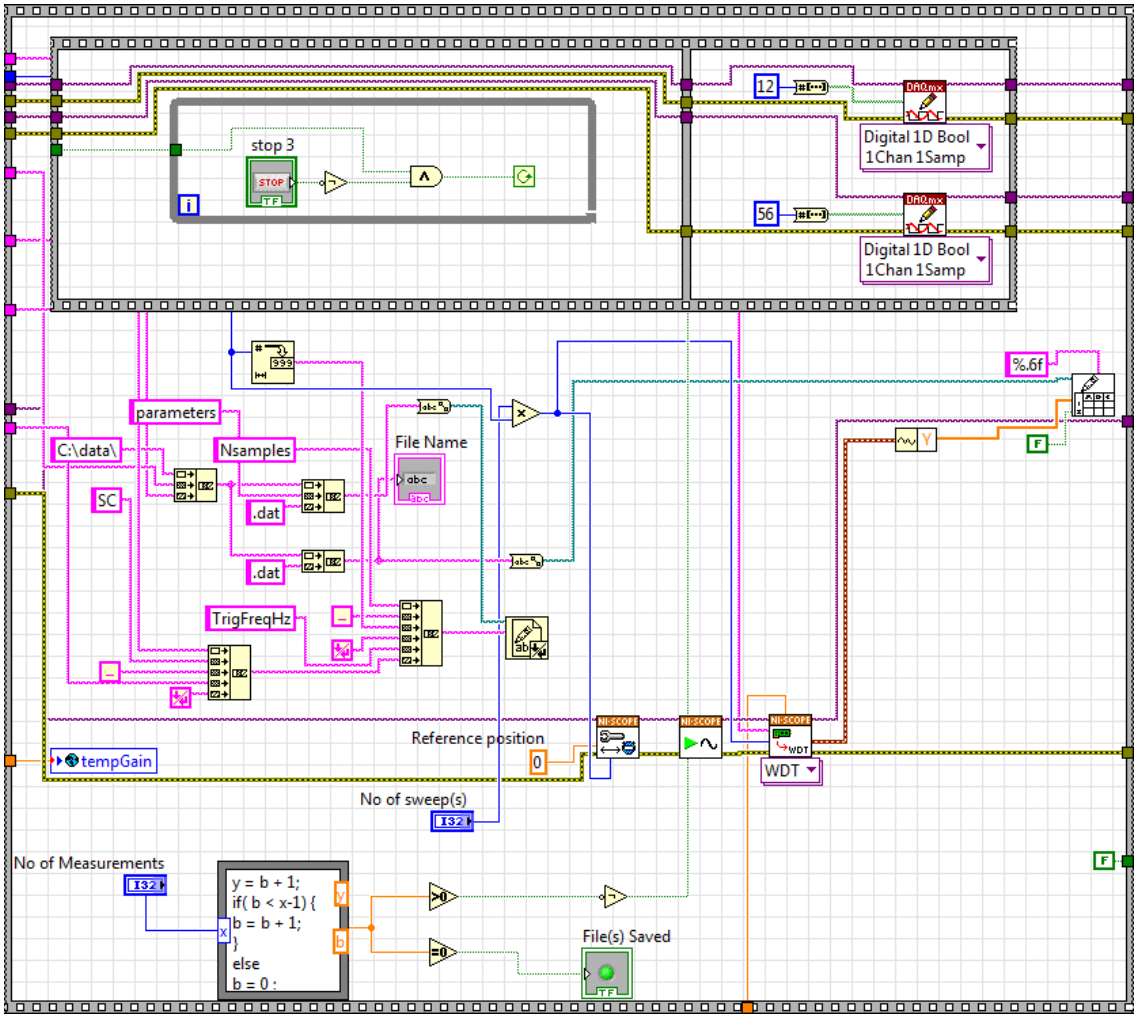

Appendix F Verilog HDL Code for FPGA

The implementation detail of Verilog HDL code for FPGA chip is given in this appendix. The code for receiver's command and control unit is responsible to create full duplex communication link between host PC and FPGA, generates trigger signals for DDS and digitizer and control signals for RF attenuator, SC bits and eight ways antenna switch. While, code for transmitter's command and control unit generates trigger signals for DDS and digitizer and eight ways antenna switch.

F.1 Code for Receiver's Command and Control unit

```
module TimeSyncAdnan(clk,Pbutton, ByteToWrite, ByteFlag, LabviewFlag,
RFAttenIn, triggerOut, temp, temp2, temp3, SC, RFAtten, AntennaSwitchBits,
control, Mute, temp4, RFAttenOut);

input clk, ByteFlag, Pbutton;
input [15:0] ByteToWrite ;
input [2:0]RFAttenIn ;

output triggerOut, LabviewFlag, temp, temp2, temp3, control, Mute, temp4;
output [6:0] SC ;
output [2:0] AntennaSwitchBits ;
output [2:0]RFAttenOut;

reg triggerOut ;
reg temp, temp2, temp3, temp4 ;
reg [6:0] SC ;
reg [2:0] AntennaSwitchBits ;
reg [2:0]RFAttenOut;
reg flag1;
reg flag2;
reg flag3;
reg flag2a;
reg flag3a;
reg flagPbutton ;
reg AntennaStart ; // default bits for antenna switch
reg LabviewFlag;
reg control, Mute ; // flags for antenna switch

integer dcountr, dcountr1, dcountr2 ;
integer delay, delaytemp, TrigDivNum,TrigDivNum1, TrigDivNum2, index ;

initial
```

```
begin

        triggerOut = 1'b0 ;

        TrigDivNum = 0 ;
        TrigDivNum1 = 0;
        TrigDivNum2 = 0;

        delay = 0;
        delaytemp = 0;

        temp = triggerOut ;
        temp2 = 1'b0;
        temp3 = 1'b0;
        temp4 = 1'b0;

        flag1 = 1'b0 ;
        flag2 = 0 ;
        flag3 = 1'b0;
        flag2a = 0 ;
        flag3a = 1'b0;

        flagPbutton = 1'b0;

        LabviewFlag = 1'b0 ;

        control = 1'b0;
        Mute    = 1'b0;
        AntennaSwitchBits = 3'b000 ;
        AntennaStart = 1'b0;
        RFAttenOut = 3'b111 ; // 0 dB RF attenuation

        dcountr  = 0 ;
        dcountr1 = 0 ;
        dcountr2 = 0;
end

always @(posedge Pbutton)
begin
        flagPbutton = 1'b1;
end
```

```
always @ (posedge clk)
begin
        if ( flagPbutton == 1'b1)
        begin

        // two bytes reception from Labveiw using NI 6501
                if( ByteFlag == 1'b1 && flag2 == 1'b0 )
                begin

                        for (index=0;index < 8 ; index = index+1 )
                        begin
                        TrigDivNum1  = TrigDivNum1 +ByteToWrite[index]*(
                        2**index ); //binary to decimal conversion
                        end

                //setting LabviewFlag = high i.e. byte 1 is received successfully
                LabviewFlag = 1'b1 ;
                flag2 = 1'b1 ;
                end

                if( LabviewFlag == 1'b1 && ByteFlag == 1'b0 && flag3 == 1'b0 )
                //i.e second byte is available to read
                begin
                //adding second byte to  TrigDivNum
                        for (index=0;index < 8 ; index = index+1 )
                        begin
                        TrigDivNum2  = TrigDivNum2 + ByteToWrite[index]*(
                        2**(index+8) ); //binary to decimal conversion
                        end

                //setting LabviewFlag = low i.e. byte 2 is received successfully
                LabviewFlag = 1'b0 ;
                flag1 = 1'b1 ; // both bytes has been received, now generate  control
                //signals

                flag3 = 1'b1 ;
                TrigDivNum = TrigDivNum1 + TrigDivNum2 ;
                end

                //clock(RefOut) division section for trigger generation
                if ( flag1 == 1'b1)
                begin
                dcountr = dcountr + 1 ;
```

```
dcountr1 = dcountr1 + 1 ;

        if ( dcountr == TrigDivNum/2)
        begin
        triggerOut = 1'b1;
        temp = triggerOut ;
        end

        if ( dcountr == TrigDivNum )
        begin
        triggerOut = 1'b0;
        temp = triggerOut ;
        dcountr = 0;
        end
end

// to generate time-delayed trigger signal
if( flag1 )
begin
// receiving 8 bits delay value using NI 6501
delaytemp =   128*ByteToWrite[7]  +64*ByteToWrite[6]+
              32*ByteToWrite[5]   +16*ByteToWrite[4]+
              8*ByteToWrite[3]    +4*ByteToWrite[2]+
              2*ByteToWrite[1]    +1*ByteToWrite[0];

        if(  delay != delaytemp  ) //any change in delay value ,
        begin
        delay = delaytemp;  //update new delay value
        dcountr1 = dcountr1- delay ;  //with delay
        end

        if( AntennaStart == 1'b0 )
        begin
        Mute = 1'b1;
        AntennaSwitchBits = 3'b000 ;
        end

        //delayTrigger signal
        if ( dcountr1 == TrigDivNum/2)
        begin
        temp2 = 1'b1;
        temp3 = 1'b1;
        temp4 = 1'b1;
```

```
                        // increment antenna switch when its enable
                        if( AntennaStart == 1'b1 )
                        begin
                        AntennaSwitchBits = AntennaSwitchBits + 3'b001 ;
                        end
                    end

                    if ( dcountr1 == TrigDivNum )
                    begin
                    temp2 = 1'b0;
                    temp3 = 1'b0;
                    temp4 = 1'b0;
                    dcountr1 = 0;
                    AntennaStart = 1'b1 ;
                    end

                    //setting 8bit signal conditioning control bits
                    SC[0] = ByteToWrite[8] ;
                    SC[1] = ByteToWrite[9] ;
                    SC[2] = ByteToWrite[10] ;
                    SC[3] = ByteToWrite[11] ;
                    SC[4] = ByteToWrite[12] ;
                    SC[5] = ByteToWrite[13] ;
                    SC[6] = ByteToWrite[14] ;

                    //setting 3 bit RF attenuator control bits
                    RFAttenOut[0] = RFAttenIn[0];
                    RFAttenOut[1] = RFAttenIn[1];
                    RFAttenOut[2] = RFAttenIn[2];
                    //end of RF atten
                end

        end // end of flagPbutton if
end // of clk always

endmodule
```

F.2 Code for Transmitter's Command and Control unit

```
module TimeSyncAdnan(clk,Pbutton, ByteToWrite, ByteFlag, LabviewFlag,
triggerOut, temp, temp2, temp3, RFAtten, AntennaSwitchBits, control, Mute,
temp4,);

input clk, ByteFlag, Pbutton;
input [15:0] ByteToWrite ;

output triggerOut, LabviewFlag, temp, temp2, temp3, control, Mute, temp4;
output [2:0] AntennaSwitchBits ;

reg triggerOut ;
reg temp, temp2, temp3, temp4 ;
reg [2:0] AntennaSwitchBits ;
reg flag1;
reg flag2;
reg flag3;
reg flag2a;
reg flag3a;
reg flagPbutton ;
reg AntennaStart ; // default bits for antenna switch
reg LabviewFlag;
reg control, Mute ; // flags for antenna switch

integer dcountr, dcountr1, dcountr2 ;
integer TrigDivNum,TrigDivNum1, TrigDivNum2, index ;

initial
begin

        triggerOut = 1'b0 ;

        TrigDivNum = 0 ;
        TrigDivNum1 = 0;
        TrigDivNum2 = 0;

        delay = 0;
        delaytemp = 0;

        temp = triggerOut ;
        temp2 = 1'b0;
        temp3 = 1'b0;
        temp4 = 1'b0;
```

```
        flag1 = 1'b0 ;
        flag2 = 0 ;
        flag3 = 1'b0;
        flag2a = 0 ;
        flag3a = 1'b0;

        flagPbutton = 1'b0;

        LabviewFlag = 1'b0 ;

        control = 1'b0;
        Mute    = 1'b0;
        AntennaSwitchBits = 3'b000 ;
        AntennaStart = 1'b0;

        dcountr  = 0 ;
end

always @(posedge Pbutton)
begin
        flagPbutton = 1'b1;
end

always @ (posedge clk)
begin
        if ( flagPbutton == 1'b1)
        begin

        // two bytes reception from Labveiw using NI 6501
                if( ByteFlag == 1'b1 && flag2 == 1'b0 )
                begin

                        for (index=0;index < 8 ; index = index+1 )
                        begin
                        TrigDivNum1  = TrigDivNum1 +ByteToWrite[index]*(
                        2**index ); //binary to decimal conversion
                        end

                //setting LabviewFlag = high i.e. byte 1 is received successfully
                LabviewFlag = 1'b1 ;
                flag2 = 1'b1 ;
                end
```

```
if( LabviewFlag == 1'b1 && ByteFlag == 1'b0 && flag3 == 1'b0 )
//i.e second byte is available to read
begin
//adding second byte to  TrigDivNum
        for (index=0;index < 8 ; index = index+1 )
        begin
        TrigDivNum2  = TrigDivNum2 + ByteToWrite[index]*(
        2**(index+8) ); //binary to decimal conversion
        end

//setting LabviewFlag = low i.e. byte 2 is received successfully
LabviewFlag = 1'b0 ;
flag1 = 1'b1 ; // both bytes has been received, now generate  control
//signals

flag3 = 1'b1 ;
TrigDivNum = TrigDivNum1 + TrigDivNum2 ;
end

//clock(RefOut) division section for trigger generation
if ( flag1 == 1'b1)
begin
dcountr = dcountr + 1 ;

        if ( dcountr == TrigDivNum/2)
        begin
        triggerOut = 1'b1;
        temp = triggerOut ;

        temp2 = 1'b1;
        temp3 = 1'b1;
        temp4 = 1'b1;

                // increment antenna switch when its enable
                if( AntennaStart == 1'b1 )
                begin
                AntennaSwitchBits = AntennaSwitchBits + 3'b001 ;
                end

        end

        if ( dcountr == TrigDivNum )
        begin
        triggerOut = 1'b0;
```

```
                    temp = triggerOut ;
                    dcountr = 0;

                    temp2 = 1'b0;
                    temp3 = 1'b0;
                    temp4 = 1'b0;
                    AntennaStart = 1'b1 ;

                    end
                end

                if( flag1 )
                begin

                    if( AntennaStart == 1'b0 )
                    begin
                    Mute = 1'b1;
                    AntennaSwitchBits = 3'b000 ;
                    end
                end

        end // end of flagPbutton if
end // of clk always

endmodule
```

Appendix G MATLAB Code to get Received Power

```
close all
clear all

% User Inputs
SCIndex        = 0; % Enter signal conditioning index
RFIndex        = 0; % Enter RF attenuator index
Duration       = 1; % ( microsec ) 1 = 204.8 , 2 = 409.6, 3 = 819.2, 4 = 1.6384
BW             = 1; %   1 = 100 MHz, 2 = 750 MHz
Fs              = 80e6 ; % sampling frequency

% Calibration function
[SCGain, RFattenuator, SegmentSize, Hd] = CalCR (SCIndex, RFIndex, Fs,
Duration, BW ) ;

IRGain= 31; %dB
losses  =4; %dB

%% Raw data loading
FileInitial = strcat('file','_', num2str(1));
Ext = '.rd16';
disp(FileInitial);
filename = [strcat(FileInitial,Ext )];
fid=fopen(filename);
rawdata = fread(fid,'uint16');
fclose(fid);
ch1data= rawdata(1:length(rawdata));

%Convert raw data values in volt
R=0.22;
if ch1data>=16695;
        ch1data = (R/2) + ((ch1data/65532)*R);
else
        ch1data = (-R/2) + ((ch1data/65532)*R);
end;


%% Data partitioning in sweeps
Nsweep = floor(size(ch1data, 1) / SegmentSize)-1 ;
ch1data = ch1data( 1: Nsweep*SegmentSize, 1) ;
```

```
%% Filtering operation per sweep
for index=1:size(ch1data2, 2)
        ch1FilterSweep(:, index) = filter(Hd, ch1data2(:, index) - …
        mean (ch1data2(:, index) ));  %subtracting mean value from each sweep
end

%%envelop detection
ch2=  hilbert(ch1FilterSweep);
ch3=abs(ch2);

PowerdBm =10*log10( ((ch3  ).^2*1000 ) / 50 ) ;
PowerdBmRecv =    PowerdBm - SCGain + RFattenuator - IRGain + losses  ;

%%Applying moving average filter
a1 = 1 ;
b1 = ones(1, 15)  ;
for index2 = 1 : size(PowerdBmRecv, 2)
        PowerdBmRecvMA(:, index2) =    filter (b1/length(b1), a1,
                                       PowerdBmRecv(:, index2 ) ) ;
end

%% log-average of all sweeps
AvgPowerdBmRecvMA =  mean( PowerdBmRecvMA');
```

```
function [SCGain, RFattenuator, SegmentSize, Hd] = CalCR (SCIndex, RFIndex, Fs,
Duration, BW )

SC_Offset      = [    ]; % please add relevant receiver's SC bias factor
RF_Offset      = [    ]; % please add relevant receiver's RF bias factor

SCGain = SCIndex - 12 + SC_Offset ( SCIndex +1 ) ;

   switch RFIndex
     case 0
        RFattenuator = 0;
      case 1
        RFattenuator = 5;
      case 2
        RFattenuator = 10;
      case 3
        RFattenuator = 15;
```

```
        case 4
            RFattenuator = 21;
        case 5
            RFattenuator = 26;
        case 6
            RFattenuator = 31;
    end
RFattenuator = RFattenuator + RF_Offset (RFIndex+1);

if BW == 1

    switch Duration
        case 1  %204.8
            SegmentSize = 2048 * 8;
            Fc2 = 1000 ; % kHz
        case 2
            SegmentSize = 4096 * 8;
            Fc2 = 900 ; %kHz
        case 3
            SegmentSize = 8192 * 8;
            Fc2 = 800 ; %kHz
        case 4  %1.6384
            SegmentSize = 16384 * 8;
            Fc2 = 700 ; %kHz
    end

else  %750 MHz bandwidth

    switch Duration
        case 1  %204.8
            SegmentSize = 2048 * 8;
            Fc2 = 1600 ; % kHz
        case 2
            SegmentSize = 4096 * 8;
            Fc2 = 1400 ; % kHz
        case 3
            SegmentSize = 8192 * 8;
            Fc2 = 1200 ; % kHz
        case 4  %1.6384
            SegmentSize = 16384 * 8;
            Fc2 = 1000 ; % kHz
    end
  end
```

```
%% Filter coefficients
% All frequency values are in kHz.
Fs = Fs / 1000 ; % converting 80000 , as Fs is in kHz i.e. 80000 * 1e3 = 80e6
N     = 200;      % Order
Fc1   = 600;      % First Cutoff Frequency
% Second Cutoff Frequency set by code in above section
flag  = 'scale';  % Sampling Flag
Alpha = 2;        % Window Parameter
% Create the window vector for the design algorithm.
win = gausswin(N+1, Alpha);

% Calculate the coefficients using the FIR1 function.
b  = fir1(N, [Fc1 Fc2]/(Fs/2), 'bandpass', win, flag);
Hd = dfilt.dffir(b);
```

Publications

[1] **A. A. Cheema** and S. Salous, "High resolution temporal occupancy measurements to characterize idle time window in ISM band," in *General Assembly and Scientific Symposium (URSI GASS), 2014 XXXIth URSI*, 2014, pp. 1-4.

[2] S. Salous, **A. Cheema** and X. Raimundo, " Radio channel propagation measurements using a multiband agile chirp sounder," in *General Assembly and Scientific Symposium (URSI GASS), 2014 XXXIth URSI*, 2014, pp. 1-4.

[3] **A. A. Cheema** and S. Salous, "Dual band wideband chirp channel sounder receiver for spectrum occupancy measurements," *(accepted in URSI AT-RASC 2015)*.

[4] S. Salous, S. M. Feeney, **A. A. Cheema,** Y. Nechayaev and C. Constantinou, "Wideband MIMO channel sounder in the 60 GHz band and comparative measurements with VNA for on body networks," *(submitted to IEEE Transactions on Wireless Communications)*.

[5] **A. A. Cheema** and S. Salous, "Wideband sensing engine for cognitive radio networks: implementation and measurements," *(journal paper to be submitted)*.

[6] **A. A. Cheema** and S. Salous, "Dual band wideband chirp channel sounder receiver: Implementation and measurements," *(journal paper to be submitted)*.

Others (Presentations / Reports):

[1] **A. A. Cheema** and S. Salous, "Durham sensing engine for Cognitive Radio," in URSI festival of Radio Science, UK, 2013.

[2] S. Salous, **A. Cheema**, Y. Nechayaev and C. Constantinou, "On body network measurements in the 60 GHz band using a VNA and a custom designed channel sounder," in 8th MCM COST IC1004, Belgium, 2013.

[3] S. Salous, **A. Cheema** and X. Raimundo, "Radio channel propagation measurements and spectrum sensing using an agile chirp sounder," in 9th MCM COST IC1004, Italy, 2014.

[4] S. Salous, X. Raimundo and **A. Cheema**, "Wideband measurements in the 60 GHz band," in 10th MCM COST IC1004, Denmark, 2014.

[5] S. Salous, X. Raimundo and **A. Cheema**, "Small cell wideband measurements in the 60 GHz band," in 11th MCM COST IC1004, Poland, 2014.